pennsylvania
DEPARTMENT OF TRANSPORTATION

Technology Evaluation on Characterization of the Air Void System in Concrete

FINAL REPORT

September 17, 2009

By Maria Lopez de Murphy,
Cliff Lissenden and Chao Xiao

The Thomas D. Larson
Pennsylvania Transportation Institute

PENNSTATE
1855

COMMONWEALTH OF PENNSYLVANIA
DEPARTMENT OF TRANSPORTATION

CONTRACT No. 510602
PROJECT No. PSU 020

DEPARTMENT OF TRANSPORTATION
UNITED STATES OF AMERICA

Technical Report Documentation Page

1. Report No. FHWA-PA-2009-013-PSU 020	**2. Government Accession No.**	**3. Recipient's Catalog No.**
4. Title and Subtitle Technology Evaluation on Characterization of the Air Void System in Concrete		**5. Report Date** September 17, 2009 **6. Performing Organization Code**
7. Author(s) Maria Lopez de Murphy, Ph.D., Cliff Lissenden, Ph.D., Chao Xiao and Sheng Li		**8. Performing Organization Report No.** LTI 2010-02
9. Performing Organization Name and Address The Thomas D. Larson Pennsylvania Transportation Institute The Pennsylvania State University Transportation Research Building University Park, PA 16802-4710		**10. Work Unit No. (TRAIS)** **11. Contract or Grant No.** 510602, PSU 020
12. Sponsoring Agency Name and Address The Pennsylvania Department of Transportation Bureau of Planning and Research Commonwealth Keystone Building 400 North Street, 6th Floor Harrisburg, PA 17120-0064		**13. Type of Report and Period Covered** Final Report: 7/18/08 – 9/17/09 **14. Sponsoring Agency Code**

15. Supplementary Notes
Technical Advisor: Marcella Jo Lucas, MALUCAS@state.pa.us, 717-787-3573

16. Abstract
The objective of this project was to evaluate current technologies that have the capability of characterizing the air void system in concrete within the first several hours of placement. This objective was met by developing a comprehensive technology assessment and literature review, and conducting a laboratory evaluation of two selected technologies: ultrasound and thermography. The literature review presents a comprehensive assessment of research developments in the area of material characterization and structural health monitoring, focusing on technologies that are currently used to characterize air voids in concrete and those that have the capability of characterizing the air void system in concrete within the first 24 hours of placement. Special focus was placed on determining which technologies and equipment development may have a strong potential of being implemented in the field. The laboratory evaluation of the two selected technologies describes results obtained from experiments aimed at demonstrating the feasibility of ultrasound and thermography technologies in characterizing the air void system of fresh concrete, with an eye toward field implementation. Experimental results showed that both technologies can capture physical features that are significantly affected by the air void system in concrete.

17. Key Words Air entrainment, air void characterization, ultrasound, thermography, fresh concrete, field implementation,		**18. Distribution Statement** No restrictions. This document is available from the National Technical Information Service, Springfield, VA 22161	
19. Security Classif. (of this report)	**20. Security Classif. (of this page)**	**21. No. of Pages** 108	**22. Price**

Form DOT F 1700.7 **(8-72)** **Reproduction of completed page authorized**

TABLE OF CONTENTS

LIST OF FIGURES

LIST OF TABLES

EXECUTIVE SUMMARY

This final report incorporates the findings from a research project developed to evaluate technologies that have the capability of characterizing the air void system in concrete within the first several hours of placement. The research work was supported and funded by the Pennsylvania Department of Transportation (PennDOT). Chapter 1 presents the results from a comprehensive technology assessment and literature review. Based on this assessment, two technologies were identified by PennDOT as candidates for a laboratory evaluation: ultrasound and thermography. Results from the laboratory test plan developed are presented in Chapter 2. Both technologies demonstrated the potential to characterize the air void system in concrete within the first several hours of placement. These findings are summarized at the end of this report.

The literature review presents a comprehensive assessment of research developments in the area of material characterization and structural health monitoring, focusing on technologies that are currently used to characterize air voids in concrete and those that have the capability of characterizing the air void system in concrete within the first 24 hours of placement. Special focus was placed on determining which technologies and equipment development may have a strong potential of being implemented in the field. Two technologies were found to be commercially available. Even though one of them was specifically developed as a portable device to measure air void parameters in fresh concrete (Air void Analyzer, AVA), its use in field applications appears to be limited by the capability of reducing the sensitivity to environmental vibration as well as by repeatability. Two other technologies were found to be developed even though no commercial products were available. Between them, the fiber optic airmeter was found to be developed for field application. Even though it has the capability to measure the average air void content of a fresh concrete sample, its existing prototype was not designed to measure more descriptive air void systems parameters. Four technologies were found to be currently under development, and all four have the potential to characterize air void parameters in fresh concrete. Among those, two techniques were found to be well suited for field applications: Nondestructive ultrasound techniques have successfully characterized the air void structure of hardened cement paste; and thermography has been used to characterize concrete defects (cracks).

The laboratory evaluation of two selected technologies (ultrasound and thermography) describes results obtained from experiments aimed at demonstrating the feasibility of ultrasound and thermography technologies in characterizing the air void system of fresh concrete, with an eye toward field implementation. Two different concrete mixtures were used for the analysis: with and without air-entrained admixture. These mixtures were characterized in the fresh and hardened state. Slab specimens were fabricated, and measurements were taken using ultrasound and thermography equipment within the first 24 hours after concrete placement. Results indicate that ultrasound wave features, in particular Rayleigh wave speed and attenuation, are significantly dependent on the air content. It was also found that spatial thermal gradients are affected by the air void system. All of these findings were consistent in both fresh and hardened concrete.

1. TECHNOLOGY ASSESSMENT AND LITERATURE REVIEW

1.1. Introduction

In addition to winter conditions in Pennsylvania, deficient material quality, among other factors, can severely affect the durability of concrete pavements, thus diminishing their service life. A common and well-proven quality control measure has been the determination of air content in fresh concrete using ASTM standard test methods such as ASTM C231, C173, and C138. Reliable indicators of future performance can be obtained from hardened concrete by analyzing the air void system, in particular the air content, spacing factor, and specific surface as defined by ASTM C 457 (2008). The need for obtaining these parameters in the fresh state, thus significantly improving the opportunity for quality control of concrete pavements at an early stage, has moved state and federal agencies, universities, and industry to investigate technologies that can characterize the air void system.

This chapter presents a comprehensive literature review and technology assessment of research developments in the areas of material characterization and structural health monitoring that are currently used to characterize air voids in concrete and those that have the capability of characterizing the air void system in concrete within the first 24 hours of placement. Special focus was placed on determining which methodologies and equipment development may have a strong potential of being implemented in the field.

Sources consulted for the development of this report included the following databases: Compendex, Web of Science, Transportation Research Information System (TRIS), Transportation Research Board (TRB), Transportation Research in Progress (TRIP), National Technical Information System (NTIS), American Society of Civil Engineers (ASCE), Canadian Surface Transportation Research, International Union of Laboratories and Experts in Construction Materials, Systems and Structures (RILEM), and the International Federation for Structural Concrete (CEB-FIB). In addition, various Department of Transportation web sites were surveyed and technical literature was gathered from equipment and sensor manufacturers.

This chapter is organized in six main sections. The objective and organization of this literature review is presented in section 1, Introduction. Section 2 provides background information on the evolution of the cement paste as well as the air void system within the first 24 hours of concrete placement. Background information on the air-void system characteristics and parameters, as well as correlations with concrete durability, are also included in this section. Section 3 presents information on technologies that are currently used to characterize the air void system in concrete (Air Void Analyzer and RapidAir 457). Section 4 discusses technologies currently in development to characterize the air void system in concrete (x-ray CT scanning, ultrasound, flatbed scanner, low-temperature scanning electron microscopy, fiber-optic airmeter and thermography). Discussion of the capabilities and limitations of each technology are included, in particular with respect to its use in “fresh concrete” (see definition in Section 2)

and field applications. Various state DOT efforts to implement each particular technology are noted. Equipment and/or usage fees are included, when available. Section 5 presents a summary of the information gathered in this report, highlighting important aspects of each technology.

1.2. Background Information

1.2.1 Cement Paste Evolution During the First 24 Hours of Placement

Portland cement is mainly composed of C_3S, C_2S, C_3A, C_4AF, and gypsum. Each chemical component has a different contribution to cement paste hydration. When portland cement is mixed with water, its chemical compound constituents undergo a series of chemical reactions that cause it to harden. Each of these reactions caused by different components occurs at a different time and rate. Together, the results of these reactions determine how portland cement hardens and gains strength (Mindess et al., 2003).

Tricalcium silicate (C_3S). Hydrates and hardens rapidly and is largely responsible for initial set and early strength. Portland cements with higher percentages of C_3S will exhibit higher early strength.
Dicalcium silicate (C_2S). Hydrates and hardens slowly and is largely responsible for strength increases beyond one week.
Tricalcium aluminate (C_3A). Hydrates and hardens the quickest. Liberates a large amount of heat almost immediately and contributes somewhat to early strength. Gypsum is added to portland cement to retard C_3A hydration. Without gypsum, C_3A hydration would cause portland cement to set almost immediately after adding water.
Tetracalcium aluminoferrite (C_4AF). Hydrates rapidly but contributes very little to strength. Its use allows lower kiln temperatures in portland cement manufacturing. Most portland cement color effects are due to C_4AF.

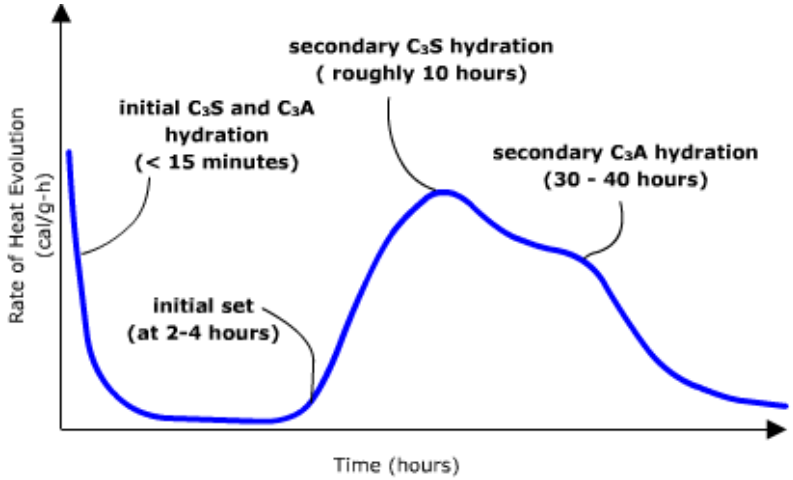

Figure 1.1. Rate of Heat Evolution during Hydration of a Typical Portland Cement (Mindess et al., 2003)

Figure 1.1 shows rates of heat evolution, which give an approximate idea of the hydration process. In the beginning, C_3S and C_3A hydration dominate and contribute to early strength of cement paste. With time, C_2S hydration and secondary C_3S hydration contribute to the increase of strength in the later stage.

With cement paste setting, its flowability is gradually lost. The point at which the paste begins to stiffen considerably is called cement paste's initial set. It usually occurs about 1 hour after mixing. When the cement has hardened to the point at which it can sustain some load, this is called cement paste's final set. At this point the cement paste does not have flowability anymore; it usually happens around 10 hours after mixing, according to ASTM C266. However, it should be noted that the cement paste setting time is affected by a number of factors, including: cement fineness, water-cement ratio, chemical content (especially gypsum content), and admixtures (Kosmatka et al., 2002).

PCA uses the following definition for fresh concrete: “freshly mixed concrete should be plastic or semifluid and generally capable of being molded by hand” (Kosmatka et al., 2002). In this report, fresh concrete will be considered as concrete that is still plastic and workable until its final setting (which usually takes place 10 hours after mixing).

1.2.2 Entrained Air and Entrapped Air

One of the greatest advances in concrete technology was the development of air-entrained concrete in the mid-1930s. Nowadays, air entrainment is recommended for nearly all concretes, primarily to improve freeze-thaw resistance of concrete that is exposed to water and deicing chemicals (Kosmatka et al., 2002).

In air-entrained concrete, many tiny bubbles are intentionally created by using either an air-entraining cement or adding an air-entraining admixture during batching. The air-entraining admixture stabilizes bubbles during the mixing process, enhances the incorporation of bubbles of various sizes by lowering the surface tension of the mixing water, impedes bubble coalescence, and anchors bubbles to cement and aggregate particles.

However, as opposed to “intentionally” entrained air, mechanical processes during the transportation and placement of the concrete can create air bubbles which will inevitably be entrapped into the mixture. These air bubbles are called entrapped air. The characteristics of the two types of air voids in concrete are fundamentally different. Entrained air and entrapped air can be easily distinguished by their sizes. The diameter of entrained air is on the order of 10 to 300 microns whereas the diameter of entrapped air is generally more than 1000 microns. Furthermore, entrained air is more uniformly dispersed than entrapped air. In addition, entrapped air has detrimental effects to the integrity of concrete structures (AASHTO, 2002). PennDOT specifies that “voids 1 mm or more in size are considered entrapped air and voids less than 1 mm in size are considered entrained air. The entrained air in the hardened concrete must be between 3.5% and 7.5%, inclusive” (PennDOT, 2007).

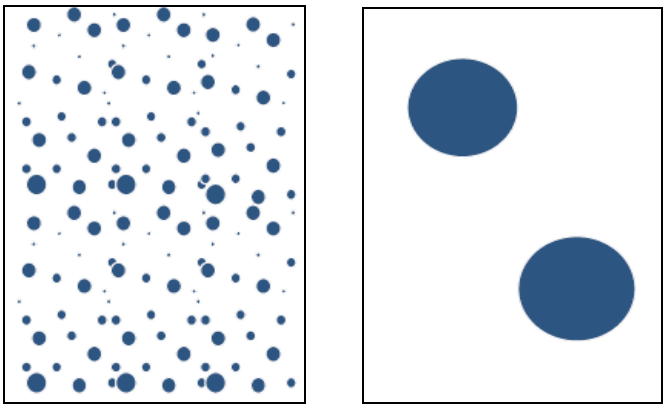

Figure 1.2. Comparison between entrained air (left) and entrapped air (right) (AASHTO, 2002)

1.2.3 Air Void System Characteristics

The advantage of air-entrained concrete as compared to conventional concrete is that it has a protective network of closely spaced air voids in the paste, which can increase the durability of the concrete, especially in climates subjected to freeze-thaw cycles. Litvan (1978) used hydraulic pressure principles to show that the protective mechanism of the air voids can be attributed to the fact that they are larger than the capillary pores, they will rarely be saturated, and thus provide empty spaces within the paste to which excess water can move and freeze without causing damage.

Moreover, entrained air improves concrete workability because the air voids act like fine aggregates in the cement paste, thus reducing the friction between solid aggregates. Entrained air also reduces the chances of bleeding and segregation during handling and transportation of concrete mixes. However, too much entrained air in concrete could lower the strength of the concrete significantly as the mixture loses its integrity under the presence of air voids (Sutter, 2007).

1.2.4 Air Void Parameters

According to ASTM C457, the concrete air void system is characterized by three parameters: air void content, specific surface, and spacing factor. Generally concrete with good freeze-thaw resistance has an acceptable high air content (A), a low enough spacing factor (*L*), and relatively high specific surface (α) (ASTM C457).

Air void content is the total volume fraction of air voids in concrete. In the technical literature, the air void content is sometimes defined in reference to the cement paste instead of the total air void content because the air void system only occurs in cement paste.

Specific surface is defined as the surface area of air voids divided by the volume of air voids. It indicates the void frequency and the mean size of the voids. Smaller bubbles have a higher specific surface.

Spacing factor is defined as “the average distance from any point in the paste to the edge of the nearest void” (Mindess et al., 2003). The spacing factor is considered the most important factor with regard to freeze-thaw resistance, since it is “the spacing of the air voids which determines the maximum distance that freezable water must travel through the cement paste to reach an escape boundary where ice crystals can grow freely without generating disruptive pressures” (Pigeon and Pleau, 1995). Figure 1.3 shows the representation of two cement paste samples with the same air content of 13 percent. Assuming that the thickness of "shells" of protected paste by air voids is 0.254 mm (0.01 inch) (Hover, 2002), the protected area covered by "shells" in the paste to the right is much larger than that in the paste to the left. The paste to the right has a lower spacing factor than the left one even though they have the same air content.

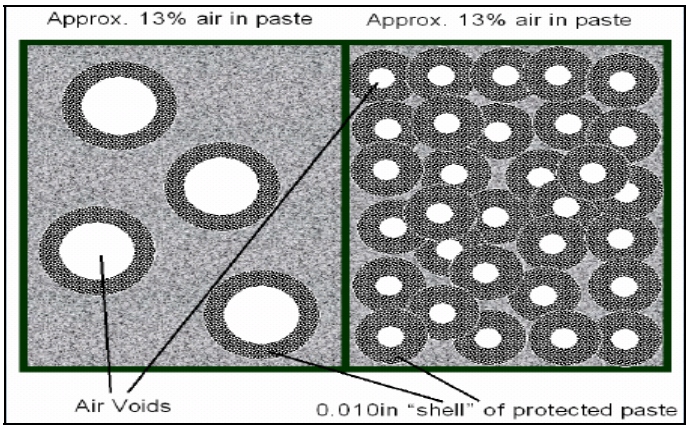

Figure 1.3. Comparison between two pastes which have the same air content and different spacing factor (Hover, 2002)

1.2.5 Correlation between Air Void Parameters and Concrete Durability

Research studies and long-term performance of concrete (Pigeon and Pleau, 1995) have indicated that a concrete air content of 4 to 8 percent by volume provides satisfactory freeze-thaw protection. However, adequate air content is not directly related to an adequate air-void system. High air contents generally indicate larger void size, not necessarily small spacing factors.

Based on research conducted by Kansas DOT (2003), the required maximum spacing factor to ensure freeze-thaw protection was found to be 0.20 mm (0.008 inches) (Mindess et al., 2003). However, Pigeon et al. (1995) stated that although 0.20 mm (0.008 inches) should normally be considered as a safe design value for concretes exposed to severe weathering in northern climates, the critical spacing factor for deicer salt scaling resistance will depend on the type of cement and the duration and intensity of the freezing cycles.

In a protective air void system, specific surface should not be less than 25 mm^2/mm^3 (635 $inch^2/inch^3$). In order to reach this value, entrained air in concrete should dominate in the air void system rather than entrapped air (Mindess et al., 2003).

In addition, recent research by Lane (2006) suggested that the ranges of air content currently used should be reduced to lessen the potential for acceptance problems associated with excessive air content. Moreover, with different air entrainment admixtures, the threshold of air void parameters should be defined accordingly.

1.2.6 Effect of the Concrete Mixture Design on Air Void Characteristics

With the increase of the water-cement ratio, more water is available for the generation of air voids. An increase in the water-cement ratio from 0.4 to 1.0 can lead to a rise in the air content by 4 percentage points. However, air voids will become coarser at such high water-cement ratio. In other words, the spacing factor also increases, which is harmful to the concrete freeze-thaw durability. Increasing the fine aggregate content percentage will cause more air voids in the concrete at a fixed water-cement ratio (Kosmatka et al., 2002). Zhang and Wang (2005) conducted an investigation about the effect of materials and mixing procedures on air void characteristics in fresh concrete. Their results showed that both the replacement of portland cement by fly ash and the addition of a water-reducing agent can reduce the spacing factor and increase the specific surface of air voids in concrete.

1.3. Technologies Currently Used to Characterize the Air Void System in Concrete

1.3.1 Air Void Analyzer (AVA)

1.3.1.1 Description of Technology

The Air Void Analyzer, also known as AVA, is a device that measures the air void parameters of a fresh concrete sample. AVA calculates the size distribution of air voids in concrete by measuring the amount of air as it rises through a glycerol-based solution in a container as a function of time. This technology is based on Stokes' Law. A picture of an Air Void Analyzer is shown in Figure 1.4. AVA was developed by Dansk Beton Teknik Company, which is located in Hellerup, Denmark. It has been adopted by many European countries, including Belgium, Czech Republic, Denmark, Finland, France, Germany, Holland, Hungary, Iceland, Italy, Poland, Sweden, Spain, and Switzerland as a tool to evaluate concrete durability (Germann Instruments, Inc., 2008). In Canada, the Ontario Ministry of Transportation also uses AVA to monitor the freeze-thaw resistance of concrete (AASHTO, 2002).

Figure 1.4. Air Void Analyzer (Germann Instruments, Inc., 2008)

1.3.1.2 Capabilities and Limitations for Fresh Concrete

AVA is designed solely for testing of fresh concrete. The test should be performed within the first 2 hours after placement (per manufacturer's recommendations). It takes less than 30 minutes to complete the test. AVA is capable of calculating all the air void parameters specified by ASTM C457 (Germann Instruments, Inc., 2008). The parameters measured are spacing factor, specific surface, and air content.

1.3.1.3 Capabilities and Limitations for Hardened Concrete

AVA is not intended to be used in hardened concrete.

1.3.1.4 Capabilities and Limitations for Field Application

AVA is very portable and therefore feasible for field application. However, the device is extremely sensitively to the environment where the test is being conducted. Wind or vibration will have negative impact on the accuracy of the test. Iowa State has developed a mobile lab to reduce these environmental effects and to improve AVA's performance in field applications (Grove et al., 2006; Dislehorst and Kurgan, 2007).

Studies have been done to determine the accuracy of AVA in field application. In the round-robin study of AVA conducted by Dislehorst and Kurgan (2007), the discrepancy in results of two AVA tests on the same sample by different operators using different AVA devices was found to be 53 percent. In a previous study conducted at Penn State, it was concluded that AVA

measures consistently higher spacing factor with an average difference of 0.15 mm (0.0059 inches) and lower specific surface with an average difference of 16.82 mm^{-1} (426.5 $inch^{-1}$) as compared to RapirAir 457, which is the standard ASTM testing method (Desai et al., 2007).

1.3.1.5 DOT Efforts to Implement This Technology

FHWA's Mobile Concrete Laboratory purchased AVA in 1993. In 2002, the Kansas State Department of Transportation developed a concrete durability specification based on AVA. To date, 15 state DOTs in the United States own AVA equipment (Dislehorst and Kurgan, 2007). Many of them are currently using AVA on a limited basis. State DOTs that have a record of using AVA in field applications are Arkansas, California, Iowa, Kansas, Kentucky, Louisiana, Minnesota, Missouri, New Mexico, New York State, North Carolina, Pennsylvania, South Dakota, Texas, and Wisconsin (Germann Instruments, Inc., 2008).

1.3.1.6 Manufacturer Information and Associated Equipment Cost

Germann Instruments, Inc. (quote provided in January 2009)

AVA-2000 Air Void Analyzer with laptop computer and installed software, accessories, 2 gallons of AVA release liquid, and aluminum carrying case $28,500.00

AVA-3000 Air Void Analyzer with laptop computer and installed software, base unit with riser column, temperature bath water tank, accessories, 2 gallons of release liquid, and two aluminum carrying cases – Latest Design $37,500.00

Consummable: 1/ea. AVA-2240 AVA Release Liquid: 1 gallon $80.00

1.3.2 RapidAir 457

1.3.2.1 Description of Technology

The RapidAir 457 is an automated image analysis system for determining air void parameters in hardened concrete. Its development originates back to the 1990s when the computer DOS operation system was still dominating. In 2002, a new and updated Windows-based software RapidAir system was developed (Jakobsen et al., 2006). This system automates the ASTM C457 standard test method for determining air void characteristics. RapidAir 457 is capable of performing two ASTM tests – Linear Traverse Analysis and Modified Point Count Analysis. The linear traverse method uses a series of regularly spaced lines to intercept the sample and then sum up the distances traversed across a given component. The modified point count method is based on the frequency with which areas of a given component coincide with a regular grid system of points (ASTM C 457). A standard test to calculate air void parameters can take as long

as 6 hours for an experienced operator, whereas the automated analysis using RapidAir 457 only requires 15 minutes for the Linear Traverse Analysis and 30 minutes for the Modified Point Count analysis. In addition, the Linear Traverse Analysis can be automatically performed by RapidAir based on the color intensity of the image, therefore avoiding human misjudgment (Elson, 2001).

The RapidAir 457 microscopy imaging system is composed of a computerized control unit (PC) with a high-resolution LCD color monitor, a video camera, and a microscope objective mounted on a motorized stage. Along with the hardware, user-friendly image analysis software is designed to help the operator conduct the test and process the image to determine the air void parameters. Figure 1.5 shows the configuration of the RapidAir 457.

Figure 1.5. Basic configuration of RapidAir 457 (Jakobsen et al., 2006)

The test procedure used by RapidAir 457 is essentially the same as ASTM C457. The main difference involves the preparation of the sample for better image quality. Besides the traditional grinding and polishing process required for ASTM C457, a contrast enhancement is applied to obtain a better distinction between air voids and the rest of the sample by filling white powder, such as barium sulfate, in the air voids. Figure 1.6 shows an image of a prepared surface. This process allows for RapidAir to identify air voids, which then leads to an improved precision. After sample treatment, the specimen is mounted on the moving stage, which is placed under the video camera. The stage is controlled by PC to move under the video camera in a fashion that the desired area specified by ASTM C457 is analyzed. After scanning, the air void parameters such as air content, specific surface, and spacing factor are tabulated by RapidAir in an Excel spreadsheet.

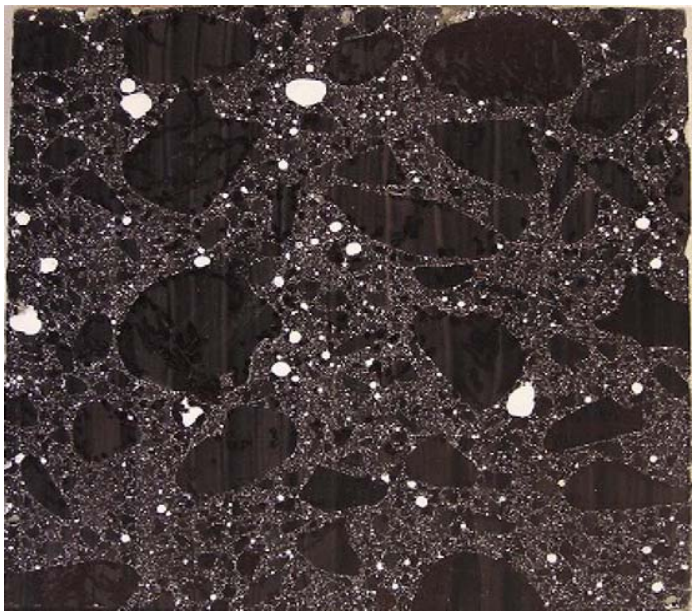

Figure 1.6. Image of specimen surface after contrast enhancement (Jakobsen et al., 2006)

1.3.2.2 Capabilities and Limitations for Hardened Concrete

Performing ASTM C457 manually is time-consuming and prone to errors. The use of RapidAir 457 appears to reduce human error and improve the efficiency of the test while at the same time meeting the requirement specified by ASTM C457. Therefore, RapidAir 457 is widely used to characterize the air void system in hardened concrete around the world.

In order to assess the accuracy and precision of the RapidAir 457 automated imaging system, a round-robin study was conducted for a 2-year period starting in 2005 (Simon, 2005; Jakobsen et al., 2006). This study found RapidAir 457 to be accurate and consistent. Compared to the automatic analysis performed by RapidAir 457, the data obtained manually according to ASTM C457 showed a much higher variation, especially between different laboratories. Therefore, it was concluded that the development of an automated system for performing ASTM C457 measurements, such as RapidAir 457, can provide more consistent and accurate results than those obtained manually.

1.3.2.3 Capabilities and Limitations for Fresh Concrete

No literature record has been found for RapidAir 457 application on fresh concrete. Because RapidAir 457 is an image analysis technique, it can only examine a smooth surface of a concrete specimen, which is extremely difficult to achieve from a fresh concrete sample. Considering this limitation, this technology has little potential for the fresh concrete application.

1.3.2.4 Capabilities and Limitations for Field Application

To use RapidAir 457 in the field, the sample must have a minimum size of approximately 100 cm^2 (16 in^2) and a well-prepared surface. However, in the field it is hard to obtain the appropriate sample size directly from the pavement under study. Surface preparation is also a critical step and will require a laboratory environment. Therefore, the potential of RapidAir 457 for field application is very limited.

1.3.2.5 Manufacturer Information and Associated Equipment Cost

Germann Instruments, Inc. offers the RapidAir system with a cost per unit of approx. $ 48,000.

1.4 Technologies Currently in Development to Characterize the Air Void Systems in Concrete

1.4.1 X-ray CT Scanning

1.4.1.1 Description

X-ray CT scanning is a nondestructive health monitoring technique. The technique is used to visualize the interior of objects in three dimensions. Slices of continuously spaced images are assembled together to form the 3D view of objects. With proper calibration and image processing, the data can be used to compute interior dimensions, surface areas, volume, and other parameters of a specific feature, for example, the map of porosity within the sample. Practical uses of X-rays originate back to the nineteenth century. A significant effort was made to develop this technology in the 1970s. The application of X-ray CT scan in the medical field started in the 1990s. With more understanding of x-ray attenuation effects, this technology has started to be implemented in other fields (e.g., forensic analysis of structures, connections).

X-ray CT scanning is based on the concept of X-ray attenuation. X-ray attenuation in materials is due to two phenomena. One of them (Compton scattering) depends mainly on the bulk density of the material. The other (mass attenuation) depends on the atomic number of the material. The simplest application of X-ray CT scanning is to scan a sample of uniform material with voids inside. The X-ray CT scanning can generate a 3D map of density with respect to location inside the sample. Voids are identified as close-to-zero density. Another simple scanning example is to scan a sample with uniform density but varying composition; X-ray CT scanning can generate a map of material variation. If the sample contains both material and density variations, and the interest is to obtain a porosity map, more steps are involved. First, the sample with porosity is scanned. Then the sample is vacuum saturated and re-scanned. By subtracting the two density maps, the porosity distribution can be obtained. The technique can be extended for applications on samples with different fluids by proper calibration. This could provide a solution

for obtaining air void characteristics in fresh concrete using X-ray CT scanning. Figure 1.7 is the schematics of a general X-ray CT scanner set up.

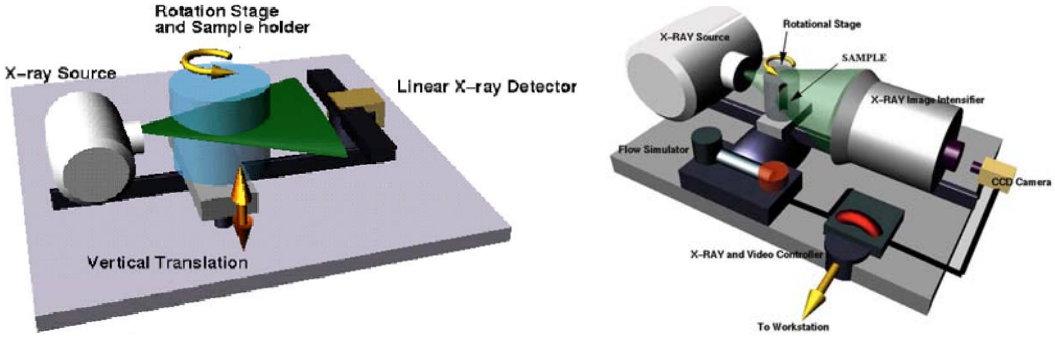

Figure 1.7. X-ray CT scanning (Sutter, 2007)

Contrast and resolution of X-ray CT scanning are important aspects of this technology. “Tuning the scanner is essential for obtaining good quality images. Part of tuning the scanner for optimum results involves selecting the best voltage and current at which to run the X-ray source. As with many other parameters, there are tradeoffs that may require some trial and error to optimize. Higher voltage results in more energetic, more penetrating X-rays. This allows lower power settings, smaller focal spot sizes and higher resolution. However, the difference in attenuation through various materials is less, leading to lower-contrast images” (Penn State University Center for Quantitative X-ray Imaging, 2008).

The resolution of X-ray CT scanning is determined by three factors – voxel size, size of X-ray source, and the amount of detector. Voxel size refers to the physical dimension of a voxel, or a pixel in the entire image. The resolution of the scanner cannot exceed the size of the X-ray source. And to achieve high resolution, a large amount of detectors are required to capture the attenuation effect. A medical scanner usually has a pixel array of 512 x 512, whereas an industrial scanner can reach a pixel array of 4095 x 4095. The industrial scanner also has a very small focal spot size, which in turn lowers the demand of detectors. A typical medical scanner has a resolution of 250 microns and an industrial scanner has a resolution of 5 microns with low power setting. High power requires a larger focal spot size to avoid damage to the anode. However, large focal spot size reduces the resolution of the scanner.

Other factors that affect the capability of X-ray CT scanners are noise reduction and data processing. Noise reduction requires tuning of the parameters of the scanner to optimize the quality of image. Data processing will be discussed further in the next section.

1.4.1.2 Capabilities and Limitations for Hardened Concrete

The use of X-ray CT scanning to characterize air voids in hardened concrete is still being researched and developed. The Wisconsin Department of Transportation sponsored a research project to assess the feasibility of different technologies that could potentially be used for

characterizing air void parameters in concrete (Sutter, 2007). This research report concluded that X-ray CT scanning has the potential to accurately characterize the air void system in fresh concrete. One advantage of this technology was its nondestructive nature. A preliminary scanning of both fresh and hardened concrete under X-ray was obtained in their research. They concluded that the characterization of air voids in both fresh and hardened concrete was very promising. However, a method of processing the image data needs to be developed to compute the air content, spacing factor, and specific surfaces (Sutter, 2007).

Researchers at the University of Maine (Landis and Corr, 2008) have proposed an image analysis methodology by which three-dimensional data can be used to calculate the air void parameter. Figure 1.8 a) shows a top view of a three-dimensional image of a hardened concrete sample from an X-ray CT scanner. Aggregate, cement and air voids are all visible. Since the only interesting information from this image is the air void structure, the data are transformed into an array of binary points. The image using the binary matrix is displayed in Figure 1.8 b). Cement paste and aggregate are both displayed as white; air voids are black in the image. The matrix is transformed further so that each pixel is a number that corresponds to the distance from the closest air void. Figure 1.8 c) is the visualization of the transformed data. With this matrix of distances from air voids, the "true" average spacing factor and spacing factor distribution can be determined. Other air void parameters such as air content and specific surface can be obtained similarly.

a) b) c)

Figure 1.8. a) Raw image, b) Binary image, c) Transformed image
(Landis and Corr, 2008)

The limitation of this technology is closely related to the resolution of the scanner used to obtain the raw image. For example, if there is need to evaluate air voids with a diameter of less than 300 microns, a scanner with resolution in the scale of 10-100 microns should be considered. For this range, only industrial scanners could be used. If a medical scanner were to be used, only air void diameters larger than 250 microns would be detected.

1.4.1.3 Capabilities and Limitations for Fresh Concrete

From the literature review conducted so far, very few reports have been found to show images of fresh concrete under X-ray CT scanning. Figure 1.9 shows an X-ray CT scanning image of a fresh concrete sample (Sutter, 2007). As mentioned above, WisDOT's report concluded that this technology has the potential to be used on fresh concrete; however, further research is

required to develop an efficient technique to obtain finer image details for data processing. It is inferred that a better understanding of the attenuation of x-rays in fresh concrete as well as techniques to reduce data noise will be needed. Similar conclusions have been found by other researchers (Thomas, 2002; Halverson et al., 2005).

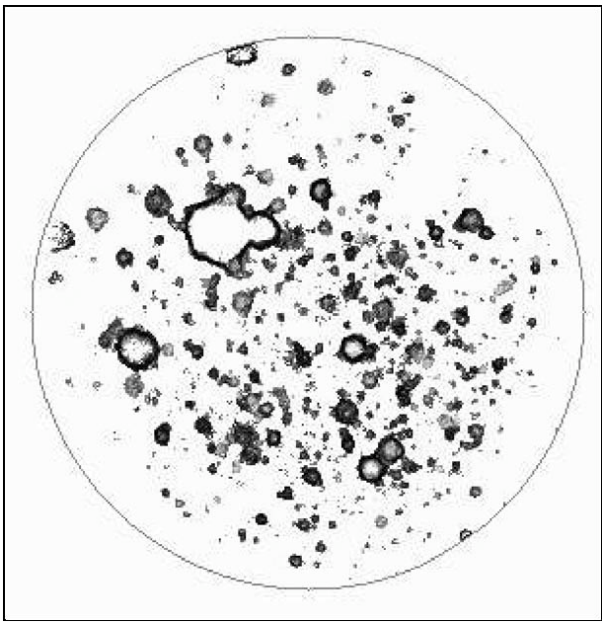

Figure 1.9. X-ray CT scanning image of a fresh concrete sample (Sutter, 2007)

The Center of Quantitative X-ray Image at Penn State possesses transparent core holders covering sample diameters up to 4 inches and lengths up to 24 inches. X-ray CT scanning can be conducted on samples of up to those dimensions. It should be pointed out that one particular concern of using X-ray CT scanning on fresh concrete is time. High-resolution scanning with large sample size could take hours to complete. Air void characteristics could change over this period of time and the time effect on the obtained data should be considered. A laboratory evaluation of the feasibility of using CT scanning on fresh concrete samples should be conducted in order to qualify these statements. Hardened concrete samples have been scanned at the Penn State facility. Very detailed images have been obtained, as shown in Figure 1.10. This three-dimensional image shows a slice of a 4-inch-diameter concrete cylinder (after a splitting tensile test).

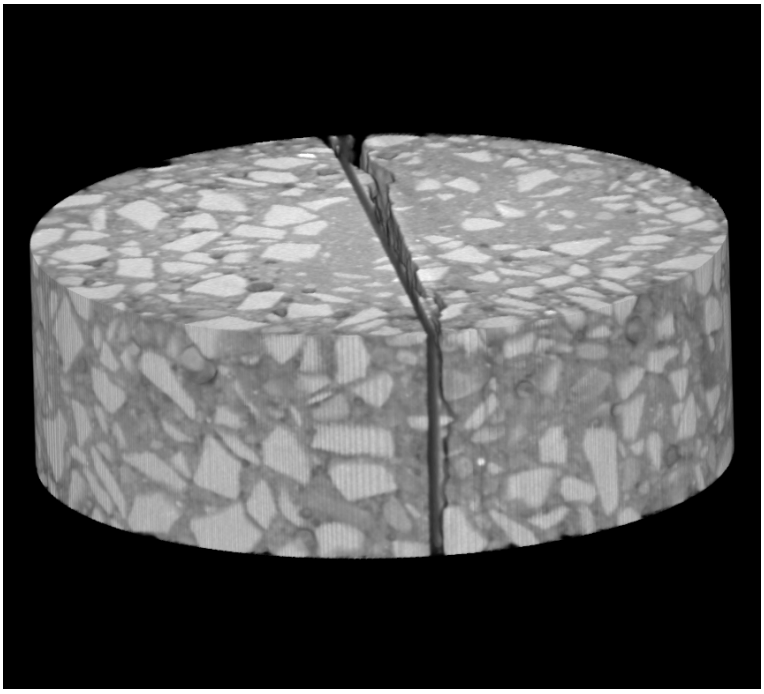

Figure 1.10. X-ray CT scan of a 4-in diameter slice of concrete (Penn State)

1.4.1.4 Capabilities and Limitations for Field Application

Industrial X-ray CT scanners used for research purpose are generally large in size. A possible solution is the use of a portable x-ray device such as the one shown in Figure 1.11, or the development of a mobile laboratory with an x-ray unit. Another challenge with x-ray application is radiation. The amount of x-rays is proportional to the power required for a particular resolution. Resolution, radiation, and portability are the three key factors associated with the field application of X-ray CT scan. Research is needed to find an optimum balance among these three factors. The amount of time required for creating the right size of image is unknown at this moment. Testing is required to develop a standardized procedure to optimize the scanning process. Images obtained with this technology will not be affected by environmental conditions if x-ray CT scan is conducted indoors.

Figure 1.11. Portable X-ray imaging device developed by MinXray, Inc.

1.4.1.5 DOT Efforts to Implement This Technology

The Wisconsin State Department of Transportation has recommended the continuation of research on X-ray CT scan as a technology to characterize air void systems.

1.4.1.6 Manufacturer Information and Associated Equipment Cost

Equipment available at Penn State's Center of Quantitative X-ray Image:

Medical X-ray CT scanner

Figure 1.12. Universal HD-350 medical scanner at Penn State

The Universal HD-350 scanner shown in Figure 1.12 is based on a medical scanner modified to allow tuning to materials other than water and for extraction of raw image data for offline analysis. It allows in-plane pixel sizes from 0.25 to 1 mm on a side on objects from 120 to 480 mm in diameter. Slice thickness can be varied from 1 to 10 mm. It uses excitation voltages from 80 to 140 kV with maximum power of about 13 kw. The images are 512 x 512 pixels.

HD600 (OMNI-X) industrial high-resolution x-ray computed tomography (CT) scanner

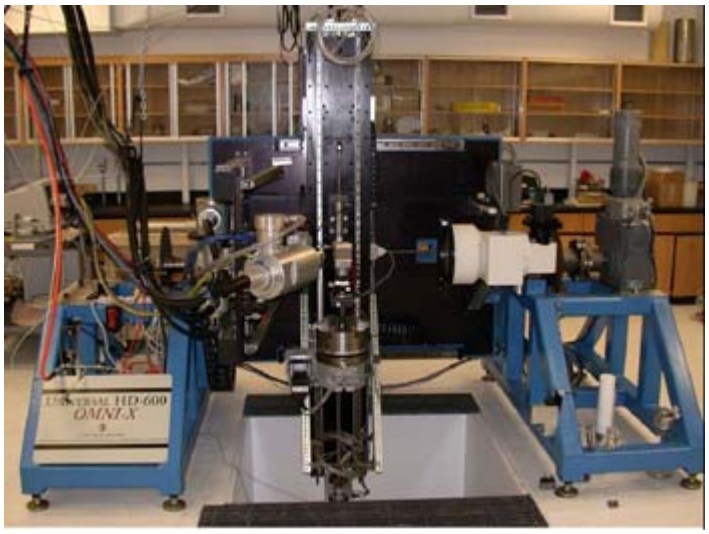

Figure 1.13. Universal HD-600 industrial scanner at Penn State

The Universal HD-600 scanner, shown in Figure 1.13, is a unique system designed for high resolution and maximum flexibility. Its main features include dual X-ray sources, 1024 x 1024-pixel area detector with image intensifier, and a continuously tiltable gantry for horizontal or vertical sample orientation. The micro-focus source is an X-tek 225 kV, 225 watt tube with a minimum focal spot size of about 5 microns at 8 watts. The higher-power source is a Pantak 1600 watt sealed x-ray tube capable of 320 kV with the minimum focal spot of about 100 microns. The HD-600 is capable of continuously variable magnification with pixel sizes approximately 1/1000 of the sample diameter.

Equipment usage fees:
Scanning Power and Labor Cost: estimated at $134/hour
Data Analysis Cost: estimated at $24/hour
Overhead cost: 50%

1.4.2 Ultrasound

1.4.2 1 Description of Technology

Nondestructive ultrasonic techniques are testing techniques that use very short ultrasonic pulse-waves with frequencies ranging from approximately 20 kHz to 1 GHz to penetrate into materials to identify flaws or to characterize materials. A typical ultrasonic setup consists of a pulser, a transducer, a receiver and display devices. A pulser is an electronic device that can produce high-voltage electrical pulses. Driven by the pulser, the transducer generates high-frequency ultrasonic energy. The ultrasonic energy is introduced and propagates through the materials in the form of ultrasonic (or stress) waves. When there is a discontinuity in the wave

propagation path, part of the energy will be reflected back or scattered. For the purpose of characterizing an air void system, the discontinuity is the air void. The change of ultrasonic energy can be detected by the receiver. The signal will be transformed into an electrical current by the receiver and displayed on a screen. The signal strength is directly related to reflections, scattering, and the distance that the signal travelled. Therefore, information about the discontinuity location, size, orientation, and other features can be obtained (Krautkramer and Krautkramer, 1990). Furthermore, data analysis and signal processing of well-chosen features enable characterization of the air void system due to attenuation and scatter. Figure 1.14 shows a schematic of a pulse-echo test setup that relies on reflection from a crack-like defect for detection and characterization.

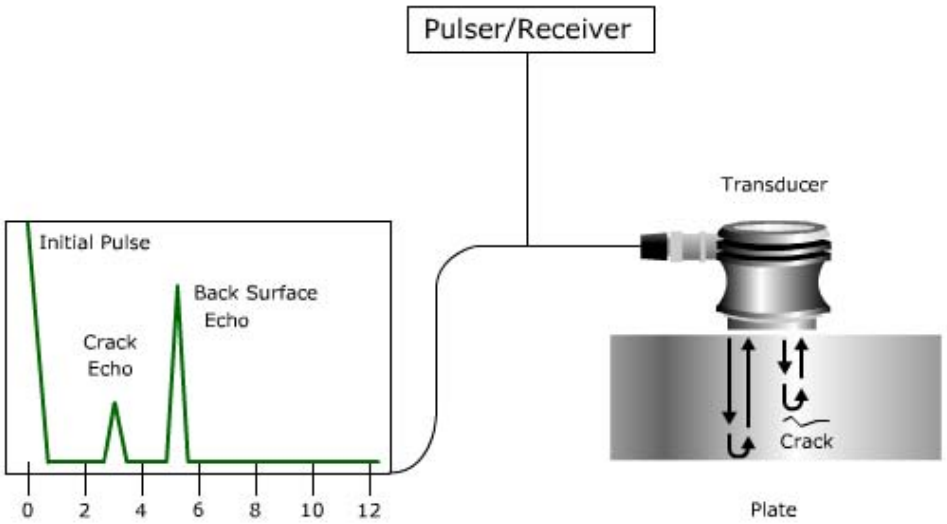

Figure 1.14. Schematic diagram of a pulse-echo ultrasonic test setup (Krautkramer and Krautkramer, 1990)

Researchers at the Georgia Institute of Technology have used the measurement of ultrasonic attenuation to characterize air void parameters in cementitious materials (Punurai, 2006; Punurai et al., 2006; Punurai et al., 2007). When ultrasonic waves travel through materials, their intensity diminishes with distance. There are two basic mechanisms of ultrasonic wave attenuation: geometric attenuation and material attenuation. Geometric attenuation is the phenomenon by which the amplitude of an ultrasonic wave decreases as the wavefront spreads out over a wider area. Material attenuation can be classified as either absorption or scattering. One source of absorption losses is internal friction in a viscoelastic material. Scattering losses are highly complex, and are dependent upon the intrinsic length scale of the scatterer, the volume and distribution of scatterers, and the acoustic properties of these scatterers in relationship to the matrix material. Since these two mechanisms (absorption and scattering) are coupled, any attenuation measurements will inevitably include both contributions (Punurai et al., 2007). Figure 1.15 shows a diagram of the Punurai et al. (2007) through-transmission test setup with transmitter and receiver on opposite surfaces of the specimen. Clearly this setup is

not conducive to field application for pavements where only one surface is accessible, but a modified setup is tractable.

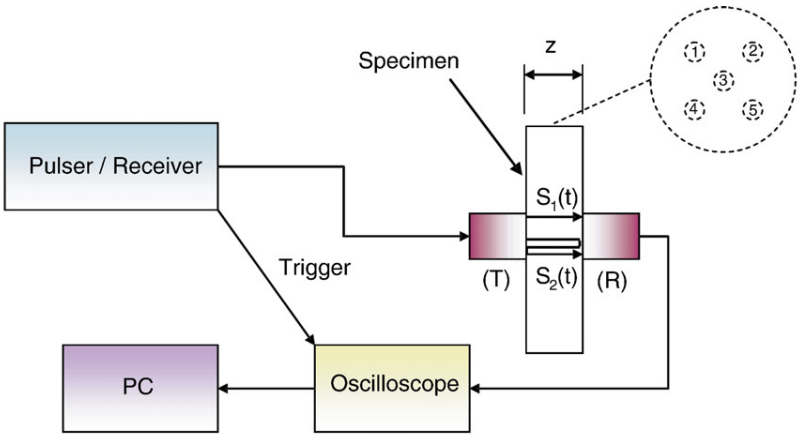

Figure 1.15. Schematic diagram of the experimental setup for the attenuation measurements (Punurai et al., 2007)

1.4.2.2 Capabilities and Limitations for Hardened Concrete

Biwa (2001) conducted research on the theoretical relationship between ultrasonic attenuation and the size and volume fraction of entrained air voids. The total ultrasonic attenuation that can be measured is mainly determined by two contributions: one is material absorption that occurs when ultrasound travels through the cement paste because of the intrinsic viscoelasticity of the cement paste matrix; the other is scattering that happens when ultrasound is reflected at the interface between the paste and air voids. Since both scattering and material absorption are related to the number and geometry of the air voids, a model based on this principle was constructed by Biwa to determine some of the air void parameters.

Note that the absorption attenuation is due to the intrinsic viscoelasticity of the cement paste matrix, and its contribution is reduced by the "missing" volume fraction which is occupied by the entrained air voids. For this simple spherical scatterer geometry, the number of scatterers, n_s, is related to the volume fraction, $(4/3)\,\pi a^3 n_s$, where 'a' is the radius of the spherical air void. Since the entrained air voids have a (relatively) low volume fraction (under 15 percent), this model assumes there is no acoustic interaction between the scattered acoustic wave fields from each individual entrained air void. In addition, this model assumes that all scatterers have the same size (i.e., all have the same radius, a). Finally, the scattering cross section is defined as the ratio of the scattered power divided by the intensity of the incident wave on a single scatterer, and accounts for differences in geometry and elastic properties of the scatterer.

Punurai et al. (2007) used the direct model built by Biwa as part of an inversion procedure to predict the entrained air void size and volume fraction of cement paste from the attenuation results. The absorption contribution can be removed from the total attenuation by subtracting the measured attenuation in the cement paste without entrained air at the same water content. Then the remaining attenuation is the contribution from entrained air voids.

Therefore, the air void size and volume fraction can be predicted according to the direct model. In this research, very good agreement was found between predictions of entrained air content, obtained from the inversion procedure (based on the theoretical attenuation model and using the ultrasonic measurements), and measurements of entrained air content by standard petrographic methods and by gravimetric analysis. The results demonstrate the accuracy of using attenuation to measure the size and volume fraction of entrained air voids in hardened cement paste. The attenuation measurements were then used to detect the existence of additional, larger entrapped air voids in the cement paste.

The work by Punurai (2006), Punurai et al. (2006, 2007), and Biwa (2001) applies ultrasonic techniques to hardened cement paste. More research needs to be conducted if ultrasound is to be used for concrete with aggregate. This extension will be complicated because the heterogeneous composition of concrete causes more ultrasonic scattering.

1.4.2.3 Capabilities and Limitations for Fresh Concrete

Aggelis and Philippidis (2004) studied wave propagation in fresh mortar to define the dispersive and attenuative nature of fresh mortar. The results revealed that the sand content in fresh mortar has the dominant effect on wave velocity and attenuation. Coarser grains result in higher attenuation. However, the contribution from other sources such as heterogeneity due to entrapped air voids, which are always present in fresh mortar, should not be neglected. This research is a qualitative study. How to quantify the air void parameters of fresh mortar accurately needs further study. Moreover, the effect of aggregate size in concrete must be dealt with because normal concrete aggregates are significantly larger than sands. Aggelis and Philippidis (2004) suggested that in order to apply ultrasound technique to fresh concrete, alternative testing methods could be adopted in the assessment of mortar sieved from the given concrete.

Shin et al. (2007) developed an improved method for measuring the surface wave velocity of early-age concrete to enable determination of elastic properties and strength predictions. Advantages of this method are that it applies to fresh concrete and that it is a single-surface measurement technique. Analysis of signal features in addition to wave velocity could enable determination of the air-void system parameters.

The Review of Progress in Quantitative NDE is an annual forum organized by the Center for Nondestructive Evaluation at Iowa State University. This year the forum was held at the University of Rhode Island on July 26-31, 2009. Two research groups presented their current work on characterization of the air void system in fresh concrete. The group at Georgia Tech (Natalie Darrough, Kim Kurtis, and Laurence Jacobs) is using an immersion technique whereby ultrasonic transducers (transmitter and receiver) are immersed in the fresh cement paste. The principle is that attenuation is sensitive to the air void distribution and that attenuation variance can be correlated to air size and spacing. One of the researchers stated that they had difficulty with moving the receiver in order to get measurements over two distances, which is required to determine attenuation. One issue is that fresh cement paste attenuates the

ultrasonic signal very rapidly; another is physically moving the receiver in the fresh cement paste. A group at Northwestern University (Ningli Yan, Oluwaseyi Balogun, Sridhar Krishnaswamy, and Jeffrey Thomas) is attempting to use wide-band ultrasonic pulses generated by a laser to characterize the porosity, tortuosity, and permeability of fresh cement paste. Fast and slow compression waves, consistent with Biot's theory, are generated and are thought to be capable of characterizing both porosity and tortuosity based upon wave speeds. Note that both groups are researching fresh cement paste, not fresh concrete with coarse aggregate.

1.4.2.4 Capabilities and Limitations for Field Implementation

Ultrasonic techniques are very feasible for field application because ultrasound instrumentation for nondestructive evaluation is designed to be portable. The time to take measurements is short. Therefore, it is efficient in terms of testing speed. Ultrasonic tranducers need to be coupled to the surface of the material to be characterized. Often gel or water is used as couplant, but air coupling technology is improving and should be considered.

1.4.2.5 Manufacturer Information and Associated Equipment Cost

There are several companies that manufacture ultrasonic equipment in Pennsylvania: GE Sensing and Inspection Technology in Lewistown; Olympus division R/D Tech in State College; Ultran Group in State College.

1.4.3 Flatbed Scanner

1.4.3.1 Description of Technology

The flatbed scanner was the first technology developed to characterize air void systems in hardened concrete. A flatbed scanner is mainly composed of two parts: a glass pane and a moving optical light source. The use of a flatbed scanner was studied previously for application to air void systems in concrete. However, results were not satisfying because of the low resolution of conventional scanners. Recently, advances in high-resolution flatbed scanners make the characterization of air void systems in concrete possible with sufficient accuracy. The image obtained from this new technique can achieve a maximum point-to-point resolution of 8 microns (Zalocha and Kasperkiewicz, 2005).

In order to enhance the contrast rate between air voids and other components in concrete, the specimen is polished and then painted similarly to the methods specified in ASTM C457. After treatment, the specimen is placed on the glass pane of the flatbed scanner and an opaque cover is used to cover it to eliminate ambient light. By moving the sensor and light source across the pane, the entire specimen is scanned using a high-resolution scanner. Image processing software is then used to distinguish each pixel and group them into cement paste, aggregate, or air void. After the image is acquired, a standard linear traverse or point count can be automatically conducted according to the ASTM C457.

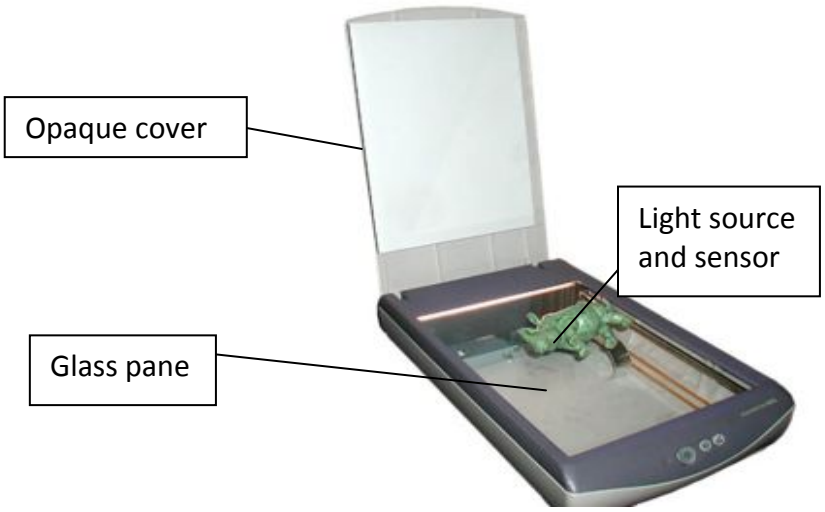

Figure 1.16. Configuration of a flatbed scanner (Freedom Scientific, Inc., 2009)

Compared with a microscope-based system, a significant advantage of the flatbed scanner is its lower equipment cost as well as its capability for scanning an entire surface rather than constructing it point by point. Another advantage of using the scanner is the use of a very steady light source, which in microscopic observations may cause problems due to interference.

1.4.3.2 Capabilities and Limitations for Hardened Concrete

The flatbed scanner has been a very popular technology for characterizing air void system in hardened concrete due to improvements in resolution and reduction in cost of equipment. By using flatbed scanners properly, good-quality images of the whole analyzed surface of concrete specimens with air void systems can be obtained in a relatively short time. Image processing software can then be used to calculate the air void parameters automatically.

Researchers at Michigan Tech (Carlson et al., 2006) have developed a computer script program to calculate the standard air void system parameters in hardened concrete from ASTM C 457. They pointed out that selecting a threshold value for the gray-scale image is the most important step. Each pixel in the gray-scale image will fall within the 0~256 scale between pure white and pure black. The threshold value is a dividing line between what is and what is not classified as air by the scanner. Figure 1.17 shows the comparison among different threshold values. Figure 1.18 shows how the pixels in the grayscale image are converted from 0~256 scale to binary values according to the selected threshold value of 150. The value of 0 is considered as air and 255 is considered as non-air. Once the data are collected, the calculations for air content, specific surface, and spacing factor are performed.

Figure 1.17. Example of threshold value comparison (Carlson, 2006)

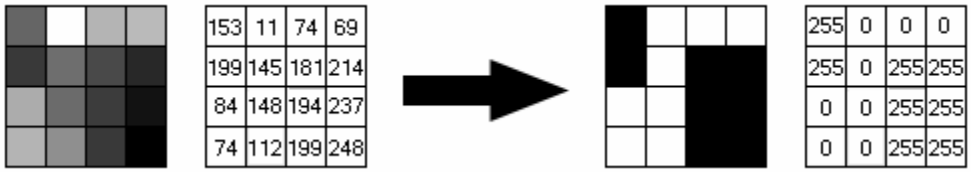

Figure 1.18. Example of threshold conversion from scanned to binary pixel intensities (Sutter, 2007)

Carlson et al. (2006) conducted a research study comparing the performance of a flatbed scanner versus the RapidAir 457 system to determine air void system parameters of hardened concrete. The results showed that the flatbed scanner tends to report approximately 9 percent lower air content than that determined by RapidAir 457. In general, the results of air void system parameters obtained by the flatbed scanner correlate well with the results acquired with RapidAir 457.

1.4.3.3 Capabilities and Limitations for Fresh Concrete

So far, the flatbed scanner has never been used in visualizing fresh concrete. The configuration of the flatbed scanner limits the application for fresh concrete. Because fresh concrete has flowability it cannot be appropriately placed on the glass pane (unless it is confined by a clear container). It should also be pointed out that the heat released by the hydration process over time may influence the quality of the image obtained by the flatbed scanner.

1.4.3.4 Capabilities and Limitations for Field Implementation

This technology requires complex and precise sample preparation steps. The flatbed scanner may not be appropriate for field implementation.

1.4.3.5 Manufacturer Information and Associated Equipment Cost

As mentioned previously, the low cost is an important advantage of flatbed scanner. Many manufacturers produce a variety of flatbed scanners, such as HP, Canon, Epson, and so on. HP's Scanjet 8300 Professional Image Scanner is taken as an example here because it is a popular image scanner model in the market. Specific information from the HP website is listed as follows:

Figure 1.19. HP Scanjet 8300 Professional Image Scanner (HP, Inc., 2009)

Equipment price: $499.99
Optical Resolution: 4800 x 4800 dpi (~ 5.3 x 5.3 microns)
Maximum Scan Size: 8.5 inches x 14 inches
Environments: PC and Mac Compatible

1.4.4 Low-temperature Scanning Electron Microscopy

1.4.4.1 Description of Technology

The low-temperature scanning electron microscope (LTSEM) is a new technique that was developed based on the conventional scanning electron microscope that has been widely used to image the sample surface. The LTSEM is different from the standard SEM by its imaging environment, in which the specimen is kept at a cryogenic (-190 degree Celsius) temperature by using liquid nitrogen during imaging. At low temperature, the water in the cement paste is transformed into ice, the vapor pressure drops and water evaporation is minimal. Therefore, the hydration reaction between cement and water can be quenched and the specimen can be viewed in the LTSEM at a "stable" hydration state (Corr et al., 2004).

The LTSEM equipment can be mainly divided into two parts, which are the cryogenic chamber and the microscope chamber. A diagram of the cryogenic chamber is given in Figure 1.20. The cryochamber has a dedicated vacuum system and employs an airlock system which allows for specimen manipulation while keeping the vacuum in the cryochamber. The sample preparation is a key component of the entire process. First, the specimen is quenched in the liquid nitrogen and mounted on the holder while still immersed in the liquid nitrogen. Then the holder is transferred into the cryochamber through the airlock system. A knife is used to slice the sample so that the interior of the specimen can be observed by LTSEM. Finally, a layer of conductive material is used to coat the fractured specimen in order to prevent surface charging. After preparation, the specimen is moved into the microscope chamber where a Joule-Thomason refrigerator is used to maintain the cryogenic temperature of the specimen during imaging.

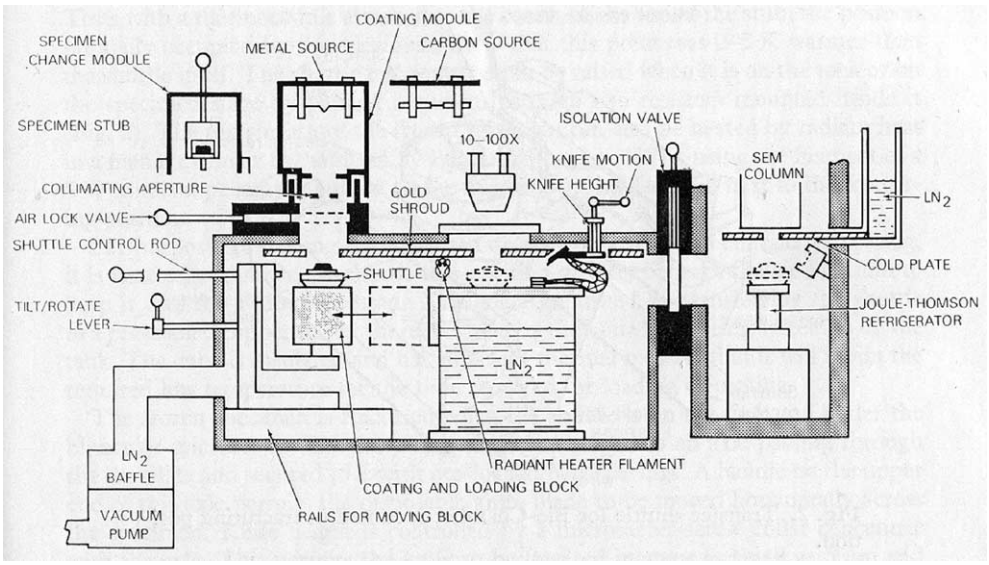

Figure 1.20. LTSEM cryochamber (Corr et al., 2004)

1.4.4.2 Capabilities and Limitations for Hardened Concrete

The main advantage of LTSEM is its ability to quench the hydration in fresh concrete. However, the quenching process does not benefit the application in hardened concrete. Since the resolution of SEM can be on the order of a nanometer, the quality of the image obtained by SEM is very high; using LTSEM will provide similar image resolution. By using an image processing software similar to the software currently employed by the RapidAir 457, air void parameters in hardened concrete can be analyzed using LTSEM.

The conventional scanning electron microscopy can be used to image a well-prepared surface of hardened concrete at a sufficient level of resolution in a similar way as the other imaging techniques. However, due to the expensive cost and unnecessarily high resolution compared with other imaging systems, SEM is not widely used as an imaging analysis technique to characterize the air void system in hardened concrete.

1.4.4.3 Capabilities and Limitations for Fresh Concrete

Corr et al. (2004) conducted a research study on the application of LTSEM for fresh concrete cement paste. The objective of this study was to image ice formation in air voids and study the progress of hydration in cement paste. The main focus was on the morphology of the air voids. By comparing the images of the air voids at the different stages, the hydration process can be studied microscopically. Figure 1.21 shows the images of fresh cement paste before and after sublimation (e.g., transition from the solid to gas phase with no intermediate liquid stage).

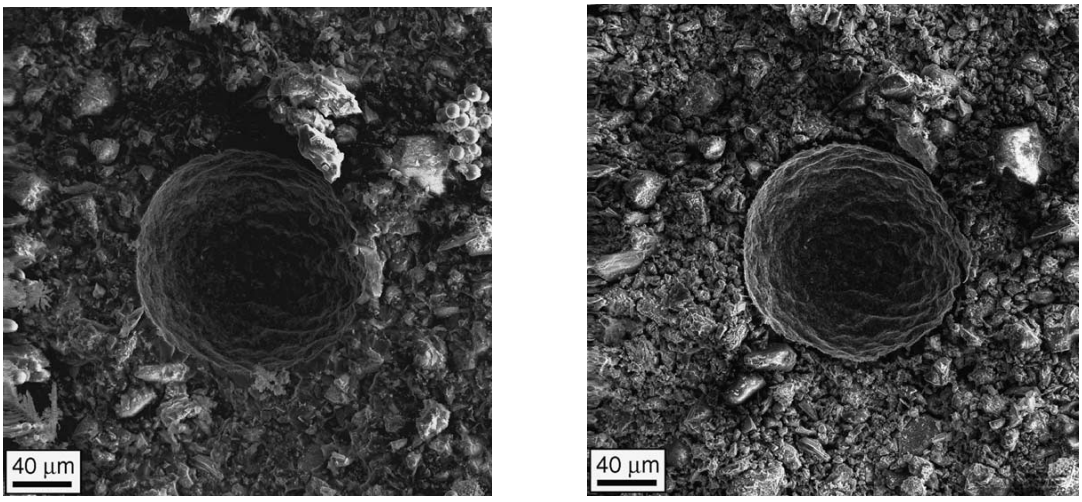

a) b)

Figure 1.21. Fresh cement paste specimen a) before and b) after sublimation (Corr et al., 2004)

Using LTSEM technology, microscopic images of the air voids in the fresh cement paste can be obtained. However, there are still unknown questions that should be resolved before air void parameters in the fresh concrete can be quantitatively calculated. Can the quality of image be maintained with the addition of aggregates? There is need to develop an image analysis software with the capability to distinguish air voids from other components in the fresh concrete. It should be noted that due to the low temperature, the size of the air voids undergoes shrinkage to some extent (Corr et al., 2002). In order to measure the true size of the air voids in the fresh concrete, the correlation between the sizes of the air voids at the normal temperature and the cryogenic temperature should be built.

1.4.4.4 Capabilities and Limitations for Field Application

When using low-temperature scanning electron microscope, a sample can be directly obtained from the fresh concrete placed in the field. Since LTSEM requires a vacuum and a cryogenic environment for imaging, an indoor laboratory is necessary for analyzing field samples.

1.4.4.5 Manufacturer Information and Associated Equipment Cost

The LTSEM system is available in the Huck Institutes of the Life Sciences at Penn State. The usage fee is $100 per hour (including 75 L of liquid nitrogen, supports for the Vacuum Transfer Device, and cryo-sputter coating).

1.4.5 Fiber-optic Airmeter

1.4.5.1 Description of Technology

The fiber-optic airmeter is a device for the assessment of air void systems in fresh concrete, developed by Dr. Farhad Ansari at the New Jersey Institute of Technology in 1990. The principle

of this system is based on the phenomenon of reflection and refraction. According to Snell's law, when light travels through the interface between two different mediums, the amount of reflected and refracted light is determined by the ratio of refractive indices of each medium. If a light travels from one medium with a high refractive index to another medium with a low refractive index, the reflected light will contribute more to the received light signal. Otherwise, most of the light will be refracted. In fresh concrete, an air void has the lowest index among all the components. When a light is transmitted into the concrete by a glass optical fiber, the fiber sensors can detect the intensity of the reflected light. As a result, air voids are detected in concrete (such as cement paste, aggregates) because the intensity of the reflective light will be greatly changed when the head of the optical fiber encounters air voids.

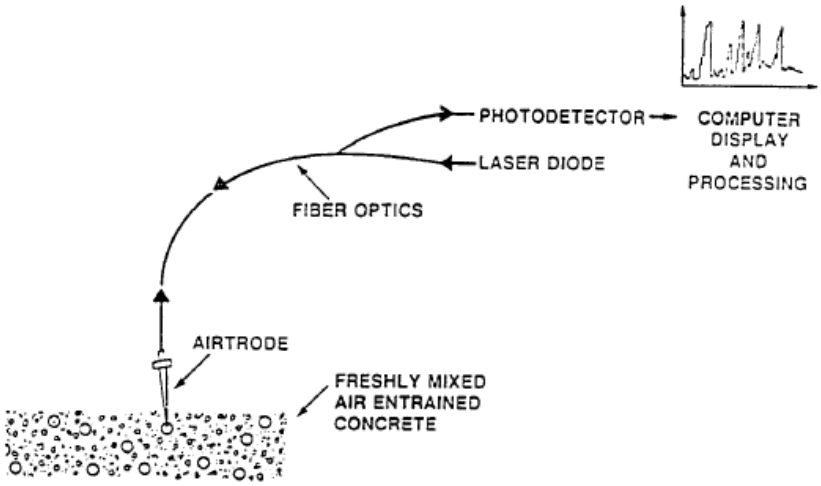

Figure 1.22. Configuration of the fiber-optic airmeter for detection of air voids in fresh concrete (Ansari, 1990)

Figure 1.22 shows the configuration of the fiber-optic airmeter system used for determining the entrained air in fresh concrete. A visible light at 670 nm wavelength is emitted by a laser diode. The optical fiber delivers the emitted light to concrete. After encountering air voids, the light is reflected back to a photodetector through the optical fiber. Then, the reflective light signal is transformed into an electrical current in the photodetector and converted to a digital signal by a digital converter. Finally, real-time data can be put into a computer for data processing and analysis (Ansari, 1990).

1.4.5.2 Capabilities and Limitations for Hardened Concrete

Since the fiber-optic airmeter was solely designed for fresh concrete, it is not capable of measuring air void characteristics in hardened concrete.

1.4.5.3 Capabilities and Limitations for Fresh Concrete

The main feature of the fiber-optic airmeter is that it can determine air void characteristics in fresh concrete in the field. However, it should be noted that this technology was only

developed to estimate the air content in fresh concrete. A standardized procedure must be developed to obtain other air void characteristics such as distribution and size of air voids. This technology may not have the accuracy needed to characterize parameters such as specific surface and spacing factor.

Using Snell's law, the reflective signal intensity from air voids is much greater than the light intensity reflected by other components in the concrete. In other words, an increase in the amount of air voids will lead to an increase in the amplitude of reflective signal intensity. The threshold value of signal intensity beyond which the intensity amplitude represents the air voids is set. Therefore, the sum of absolute signal levels above the threshold value represents total air (A) and the sum of all the signal levels represent total value in concrete (T). After that, air content can be calculated by dividing A over T.

Ansari (1994) conducted research on the accuracy of the fiber-optic airmeter by comparing the results of air content in fresh concrete obtained by this technology with volumetric and pressure methods, which are standards specified by ASTM. The comparison showed a good agreement in accuracy. It can be concluded that the fiber-optic airmeter is capable of measuring air content in fresh concrete. However, considering its limitations in determining the distribution of air voids in fresh concrete, the fiber-optic airmeter cannot be considered as a ready device to characterize the air void systems in fresh concrete.

1.4.5.4 Capabilities and Limitations for Field Application

In-situ application is the main advantage of the fiber-optic airmeter. As mentioned previously, this technology only requires the operator to insert the fiber optic probe into the concrete. Additionally, the time required for the test is fairly short. Therefore, this technology is very suitable for field application.

However, there are some limitations to the implementation of this technology in field applications. Due to the composition of fresh concrete, the quartz-based optical fiber can easily be scratched and even damaged. Therefore, consistent measurements may be difficult to obtain and will influence the accuracy of results. To avoid this problem, Ansari (1994) suggested strengthening the optical fiber with abrasion-resistant materials.

1.4.5.5 Manufacturer Information and Associated Equipment Cost

Research prototype. Not commercially available.

1.4.6 Thermography

1.4.6.1 Description of Technology

Thermography is a commonly used non-destructive testing technique in mechanical engineering. This technique is based on heat transfer and infrared imaging science. The key component of the technology is an infrared camera that captures the infrared radiation in the range of 0.9~14 microns. According to the Black Body Radiation Law, the amount of radiation from an object is a function of the surface temperature and material of the object. The temperature variation within the object can be observed by the camera. The advancement of infrared camera technology made it possible to detect temperature change to 0.08 degree Celsius (Clark et al., 2003).

Different thermography techniques have been developed for various applications. For example, the sonic infrared imaging technique, which combines ultrasonic/sonic excitation with infrared imaging, is usually used in defect detection in materials and structures (Han et al., 2005). Lock-in thermography, which measures the near-tip singular temperature field, is used to identify fatigue cracks (Sakagami et al., 2000). The technique of thermography has also been successfully applied in the field of civil engineering. To monitor the health of structural repairs, thermography is used to investigate the delamination of FRP reinforcement on concrete bridges and buildings.

Maihofer et al. (2003), at the Federal Institute for Materials Research and Testing Center in Germany, applied impulse thermography to detect shallow voids in concrete structures. Figure 1.23 shows the experimental set-up of the impulse thermography. It consists of a heating device, an infrared camera, and a computer system that collects and processes the experimental data. After heating the sample with the heating device for a period of time, the heat variation of the sample surface is observed by the infrared camera as it cools down. Due to the fact that the rate of cooling within the voids is slower than the rate elsewhere, the voids can be mapped according to temperature variation. In addition, the maximum temperature difference and the time of its occurrence are a function of the void size and its depth below the surface. Thus, the distribution of air voids can be characterized using this technique.

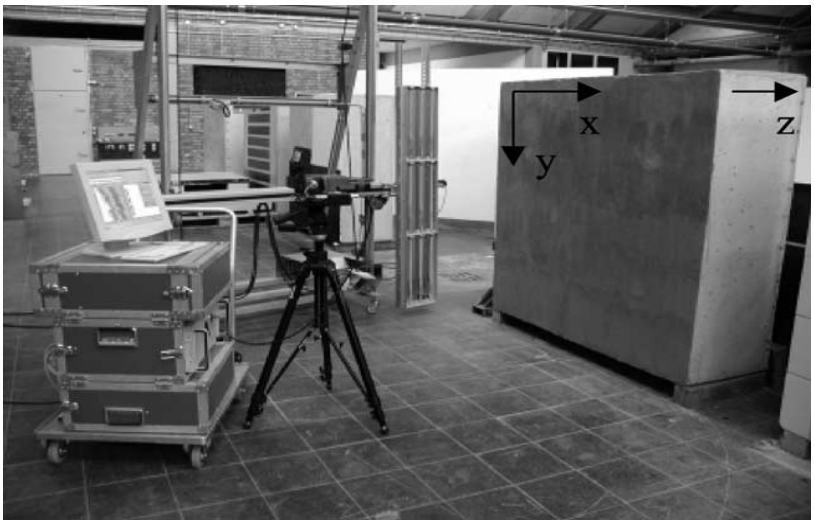

Figure 1.23. Experimental set-up for the measurement of impulse-thermography (Maihofer et al., 2003)

Researchers at the City University of Hong Kong applied flash thermography to detect surface cracks on concrete (Sham et al., 2008). First, the inspected surface is excited by a flash light emitted from a flash lamp. Then, the reflected radiation is recorded using an infrared camera. Computer tomography of the concrete sample is generated eventually. The incident light bounces against the walls several times inside the surface crack; the crack, as a result, is heated up to some extent. This phenomenon causes a difference in heating emission between cracks and the intact region. Therefore, surface cracks can be distinguished in the infrared image.

1.4.6.2 Capabilities and Limitations for Hardened Concrete

In Maihofer's research on impulse-thermography (2003), the result showed this technique is very feasible for the detection of shallow voids in concrete structures. However, it can only detect voids that can be defined as defects. The voids with a size of more than 10 cm and a depth of less than 10 cm from the surface can be detected using impulse-thermography. For our purpose of characterizing the air void system in hardened concrete, a large depth of concrete can still be examined by cutting the sample into small pieces. However, the sizes of air voids in concrete are much smaller than 10 cm, which is the maximum resolution the technique can achieve. If the resolution of this technique can be further improved, impulse-thermography can be a competitive candidate for characterizing the air void system in hardened concrete.

The study of flash thermography conducted by Sham et al. (2008) represented a better solution of surface crack detection. The results showed the capacity to successfully detect surface cracks with 0.5 mm to 1 mm crack width and to detect micro cracks with widths of 0.1 to 0.5 mm by using water as stimulus. However, only surface cracks on concrete were discussed in this study. Its capability to measure the air voids deeper within concrete is not clear at this point.

1.4.6.3 Capabilities and Limitations for Fresh Concrete

The hydration process in fresh concrete releases a significant amount of heat. It is directly related to the amount of water and type of cement used. Due to the different hydration level, the surrounding temperature of an air void is different from the temperature in the area of paste cement and aggregates. The air void system is expected to leave its signature on the surface radiation measured by the infrared camera because it affects heat transfer through the concrete. If the heat of hydration is insufficient to characterize the air void system parameters, then flash thermography using a heat lamp can be employed. The air void system signature within the measured surface radiation will need to be interpreted through heat transfer modeling as a function of air void system parameters. If enough precision and accuracy can be achieved, thermography can be a technique to characterize the air voids in fresh concrete.

1.4.6.4 Capabilities and Limitations for Field Application

Thermography is extremely well suited for field application because the equipment is lightweight and very portable. However, environmental absorption of radiation will affect the thermography measurements and will have to be minimized.

1.4.6.5 Manufacturer Information and Associated Equipment Cost

Infrared Cameras, Inc., located in Texas, is a leading manufacturer of thermal imaging and infrared camera systems. It designs and manufactures infrared cameras. Toughcam EL Infrared Camera, shown in Figure 1.24, is the latest portable infrared camera for structure inspection work.

Figure 1.24. Toughcam EL camera (Infrared Cameras, Inc., 2009)

"The ICI Toughcam EL camera is equipped with single point temperature measurement. The camera has a resolution of 160 x 120 and a temperature measurement range of -20° to 250° C (-4° to 482° F). Its lithium ion battery supplies 3 hours of continuous operations per charge. *ICI Reporter* software provides quick accessibility to a full range of tools for analyzing Toughcam images." (Infrared Cameras, Inc.). Price: $ 4995.00

1.5 Summary of Technologies Evaluated

This chapter presents a comprehensive literature review and technology assessment of research developments in the areas of material characterization and structural health monitoring that are currently used to characterize air voids in concrete and those that have the capability of characterizing the air void system in concrete within the first 24 hours of placement. Special focus was placed on determining which methodologies and equipment development may have a strong potential of being implemented in the field.

Two technologies were found to be commercially available; both are currently being provided by the same manufacturer (Germann Instruments, Inc., 2008).The *RapidAir 457* was developed as an automated image analysis system for determining air void parameters (air content, spacing factor, and specific surface) in hardened concrete. Due to its configuration for image analysis, it has very little potential for application in fresh concrete. The second commercially available technology, *Air void analyzer (AVA)*, was developed as a portable device that can calculate the air void parameters of fresh concrete. It has been adopted by several state transportation agencies in the United States and abroad as a tool to evaluate concrete durability. Transition to approved specifications based on this technology is currently under development by many of these agencies. Use of this technology in field applications appears to be limited by the capability of reducing the sensitivity to environmental vibration as well as repeatability.

Two technologies were found to be developed even though no commercial products were available. Advances in *high-resolution flatbed scanners* have made this technology able to accurately characterize the air void systems in hardened concrete. Flatbed scanners could be used for fresh concrete if a polished surface could be obtained for analysis. Field application is also very unlikely, unless laboratory conditions are present. The *fiber-optic airmeter* was developed in 1990 to assess the air void content of fresh concrete. Although a prototype exists, no commercially available product has been developed. This technology was developed for field application. Since it was only developed to obtain the average air void content of a concrete sample, research needs to be conducted to determine the capability of obtaining more precise air-void parameters such as specific surface and spacing factor.

Four technologies were found to be currently under development. They all have a potential to be used to characterize air void parameters in fresh concrete. *X-Ray CT scanning* has the capability of visualizing the air void system in concrete (both in hardened and fresh state). Research is currently underway to develop image analysis methodologies to process the information needed to compute air void parameters. The potential for field application of this technology is based on the current availability of a portable x-ray device with the appropriate resolution and accuracy. Nondestructive *ultrasound* techniques have been developed to identify flaws or to characterize materials. Ultrasonic techniques have successfully characterized the air void structure of hardened cement paste. Research will need to be conducted to evaluate its potential in fresh concrete. A qualitative study in fresh mortar has indicated promising results. Ultrasound techniques are very feasible for field application

because ultrasound instrumentation for nondestructive evaluation is designed to be portable. *Low-temperature scanning microscopy (LTSEM)* uses the capabilities of scanning electron microscopy (SEM) on a concrete sample that has been kept at very low temperatures to stop the hydration process. This technology has been used to study the air void structure in fresh cement paste. Research will need to be conducted to evaluate its potential in fresh concrete samples. Even though fresh samples can be obtained from the field, indoor laboratory conditions are needed to perform an LTSEM analysis. *Thermography* uses heat-transfer and infrared imaging science to capture temperature variations in an object. Concrete cracks have been able to be detected using this technology. It could be envisioned that detection of shallow voids in hardened concrete is within the capabilities of this technology. In order to be implemented in fresh concrete, development of a correlation between surface radiation and air void parameters needs to be developed. Thermography is very well suited for field applications.

Table 1.1 can be used as a quick reference to the key aspects of the literature review.

Table 1.1. Summary of technologies evaluated in literature review

Technology	Resolution limit	Air void characteristics within detection limit	State of Development	Potential for fresh concrete	Potential for field application
Air Void Analyzer-AVA *Section1. 3.1 Page 7*	Can detect air void with diameter less than 300 microns	Air content Spacing factor Specific surface	Commercialized	Very likely	Likely
RapidAir 457 *Section 1.3.2 Page 9*	Can detect air void with diameter less than 300 microns Max = 2.1 microns	Air content Spacing factor Specific surface	Commercialized	Very unlikely	Very limited
X-ray CT Scanning *Section 1.4.1 Page 12*	Can detect air void with diameter less than 300 microns Max = 1 micron	Air content Possible to measure Spacing factor and Specific surface	Under development	Very likely	Likely
Ultrasound *Section1. 4.2 Page 18*	Can detect air void with diameter less than 300 microns	Air content Possible to measure Spacing factor and Specific surface	Under development	Likely	Very likely
Flatbed Scanner *Section 1.4.3 Page 22*	Can detect air void with diameter less than 300 microns Max = 5.3 microns	Air content Spacing factor Specific surface	Developed	Very unlikely	Very unlikely
Low-temperature SEM *Section 1.4.4 Page 25*	Can detect air void with diameter less than 300 microns Max = less than 1 micron	Possible to measure Air content, Spacing factor and Specific surface	Under development	Likely	Unlikely
Fiber-optic Airmeter *Section 1.4.5 Page 27*	Can detect air void with diameter less than 300 microns	Air content	Developed	Very likely	Very likely
Thermography *Section 1.4.6 Page 30*	Can detect air void with diameter on the order of 1 centimeter	Air content and size of large voids Possible to measure smaller air void characteristics	Under development	Likely	Very likely

2. LABORATORY EVALUATION OF SELECTED TECHNOLOGIES

2.1. Introduction

Penn State's research team conducted a laboratory evaluation of two selected technologies , ultrasound and thermography, to ascertain their capabilities to characterize the air void system in fresh concrete (concrete within the first several hours of placement). These two technologies were selected by PennDOT based on the findings from a literature review developed in Task 1 of this project. In the laboratory evaluation developed for Task 3, experiments aimed at demonstrating the feasibility of ultrasound and thermography technologies were conducted at Penn State with an eye toward field implementation.

This chapter presents results from this laboratory investigation. It is organized in five main sections. Section 1 provides an introduction. Section 2, Concrete Mixtures Investigated, describes the design, preparation, and characterization of the different concrete mixtures evaluated. Section 3 describes the results from the evaluation of the ultrasound technology. Section 4 presents findings from the evaluation of the thermography technology, including results from finite element simulations.

All experiments described in this report were performed at the Civil Infrastructure Testing and Evaluation Laboratory (CITEL) at Penn State. This laboratory is affiliated with the Department of Civil and Environmental Engineering and the College of Engineering at Penn State.

2.2. Concrete Mixtures Investigated

2.2.1. Mixture Design

Based on the approved laboratory test plan, two different concrete mixtures were investigated: The first one is a concrete mixture with air-entrained admixture meeting PennDOT's criteria on composition, strength, and air content (AA paving mixture); the second one is a concrete mixture without air-entrained admixture. PennDOT's specifications for an AA paving mixture were extracted from section 704.1 (PennDOT Specification Manual, 2007) and are listed in Table 2.1. In addition, the PCA technical bulletin for the design and control of concrete mixtures (Kosmatka et al., 2002) was also consulted to determine the final mixture composition for a typical laboratory batch (with an approximate volume of 3.5 cubic feet).

Table 2.1. PennDOT design criteria for an AA paving mixture

Cement Factor (lbs/cu.yd)		Maximum Water Cement Ratio (lbs/lbs)	Minimum Mix Design Compressive Strength (psi)		Proportions Coarse Aggregate Solid Volume (cu.ft/cu.yd)	28-Day Structural Design Compressive Strength (psi)
Min.	Max.		7 days	28 days		
587.5	752	0.47	3000	3750	9.93-13.10	3500

Trial mixtures were conducted to determine the appropriate quantities of water-reducing and air-entraining admixtures. Two commercially available products (CATEXOL 1000N and CATEXOL AE260 from Axim Italcementi Group, 2008) were selected from a list of PennDOT-approved chemical admixtures (PennDOT Publication 35/Bulletin 15, 2009). Target values of 4 (4 $\pm$ 1) inches of slump and an average 6 percent (6 $\pm$ 1.5%) entrained air were used. Table 2.2 shows the final mixture composition for the concrete with air entrained.

Table 2.2. Weights of component materials per cubic feet of concrete with air entrained

Material	Type	Specific Gravity	Weight (lbs/cubic feet)
Cement	I	3.15	21.7
Pozzolan	F	2.14	3.81
Coarse aggregate	#57	2.82	72.0
Fine aggregate	A	2.59	36.9
Water	-	1.00	1.02
Water reducer	Normal range	-	17.1 * (ml/cubic feet)
Air entrainer	Synthetic	-	12.9 * (ml/cubic feet)

*The units of chemical admixtures are in milliliters.

The concrete without air-entrained admixture had the same composition as listed in Table 2.2, with the exception that the air-entrained admixture was omitted. Water reducer quantities were kept at the same ratio as for the mixture with air-entrained admixture. From each mixture, three different mixture compositions were studied: concrete, sieved-concrete (same as concrete mixture with the coarse aggregate larger than ¾ inch diameter sieved, thus

removing the effect of larger particles); and mortar (same composition of the cement paste used in the concrete mixture).

The following notation will be used in this report to refer to the six different types of concrete mixture compositions evaluated: XX#. The first letter refers to the type of mixture (N, normal concrete; S, sieved-concrete; M, mortar). The second letter indicates if the mixture has air entrained admixture (A) or not (N). These two letters are followed by a number if more than one batch was made for each concrete mixture (e.g., NA2 is the second batch of the normal concrete with air entrained). Table 2.3 summarizes the notation used for the six different mixtures.

Table 2.3. Mixture shorthand notation

Concrete Type	With air entrainment	Without air entrainment
Normal concrete	NA	NN
Sieved concrete	SA	SN
Mortar	MA	MN

2.2.2. Materials

Material sources used to create the laboratory concrete mixtures are provided in Table 2.4. Two concrete mixtures (SA2 and NA3) were provided by a local ready-mix plant (Centre Concrete); all other concrete mixtures were produced on site. The same materials, including admixtures, were used for the two ready-mix batches.

Table 2.4. Material source information

Material	Product name	Manufacturer name
Cement	Saylor's	Essroc Italcementi Group
Pozzolan	Type F	Sinew Incorporated
Coarse aggregate	#57	New Enterprise
Fine aggregate	Type A	Glen O.Hawbaker
Water	Tap water	State College Municipal water supply
Water reducer	1000N	Axim Italcementi Group
Air entrainer	AE260	Axim Italcementi Group

As indicated in Table 2.4, the coarse aggregate used was classified as AASHTO #57. The absorption percentage for this aggregate was found to be 0.54 percent (PennDOT requires a maximum absorption = 3.0 percent). Table 2.5 presents the gradation values of this coarse aggregate along with the gradation requirements specified by PennDOT in Section 703.2 (PennDOT Specifications Manual, 2007).

Table 2.5. Coarse aggregate gradation

# 57 Sample	Sample weight:15.00 lbs				PennDOT's Specifications
Sieve	Retained (lbs)	% Retained (lbs)	Cum. % Retained	Cum. % Passing	Cum. % Passing
2 inch	0.00	0.00	0.00	100.00	
1-1/2 inch	0.00	0.00	0.00	100.00	100
1 inch	0.45	3.03	3.03	96.97	95-100
3/4 inch	4.60	30.93	33.96	66.04	
1/2 inch	5.40	36.31	70.28	29.72	25-60
3/8 inch	2.60	17.48	87.76	12.24	
# 4	1.60	10.76	98.52	1.48	0-10
# 8	0.22	1.48	100.00	0.00	0-5
Pan	0.00	0.00	100.00	0.00	
Total	14.87				
% Loss	0.87				

The fine aggregate used was classified as Type A. It had a fine modulus of 2.86 (PennDOT specification's limits = 2.30-3.15) and an absorption of 1.67 percent. Table 2.6 presents the gradation values of the fine aggregate along with the gradation requirements specified by PennDOT in Section 703.1 (PennDOT Specifications Manual, 2007).

Table 2.6. Fine aggregate gradation

Sand Sample	Weight (lbs) 4.40				PennDOT's Specification
Sieve	Retained	% Retained	cum. % Retained	% Passing	% Passing
3/8 inch	0.00	0.00	0.00	100.00	100
# 4	0.03	0.56	0.56	99.44	95-100
# 8	0.92	20.61	21.17	78.83	70-100
# 16	0.72	16.10	37.27	62.73	45-85
# 30	0.71	15.99	53.27	46.73	25-65
# 50	1.17	26.24	79.50	20.50	10-30
# 100	0.64	14.41	93.92	6.08	0-10
# 200	0.20	4.39	98.31	1.69	
Pan	0.08	1.69	100.00	0.00	less than 3
Total	4.44				
% Loss	-0.91				

2.2.3. Concrete Mixing Procedure

A portable concrete mixer, made by Construction Equipment Inc., with a maximum capacity of 4 cubic feet was used to produce the laboratory concrete mixtures, Figure 2.1. Moisture

contents of coarse and fine aggregates were checked in order to adjust their weights. Then, the mixture design amount of each component material was weighted out. The water reducer and air entrainer were measured using graduated cylinders. Both admixtures were added into mixing water and stirred until well dispersed.

Figure 2.1. Portable concrete mixer

The mixing procedure followed is described below:

1) The inside of the concrete mixer was properly buttered by a cement mortar with a similar water/cement ratio as the mixture to be made. After the inside surface of the mixer was appropriately buttered, the excess mortar was removed and discarded.
2) The entire amount of the coarse aggregate and 2/3 of the fine aggregate were first added into the mixer. Half of the water was added and blended for 20 seconds. Then, ¼ of the water was added and blended for another 20 seconds.
3) All of the cement and fly ash were added, followed by the remaining fine aggregate and then blended for 30 seconds.
4) The remaining water was added and blended for 30 seconds.
5) The mixture was mixed for 3 minutes.
6) The mixture was allowed to charge for 2 minutes. During this time, the concrete mixer was covered.
7) The mixture was mixed for another 3 minutes to finish mixing.

2.2.4. Characterization of Fresh Concrete

Characterization of all fresh concrete batches used for this laboratory investigation included determining the total air content using pressure air tests (ASTM C 231) and its workability using slump tests (ASTM C 143). These tests were conducted immediately after finishing mixing (or

upon arrival of the concrete truck from the batching plant). A total of 13 mixtures were tested. Table 2.7 presents dates of mixing, total air content and slump for each mixture. It should be noted that SA2 mixture was used as a trial batch from the ready-mix plant to adjust the admixture quantities to such a large concrete volume. NA3 was the final concrete batch used for the production of two large concrete slabs, as defined in the proposed laboratory test plan.

Table 2.7. Fresh concrete characterization

Batch Date	Mixture Type	Concrete volume (cubic feet)	Slump (inches)	Total air content (%)
5/11/09	NA1	3.5	4.7	7.0
5/13/09	SA1	3.5	4.8	7.4
5/15/09	MA1	3.5	10	6.5
5/19/09	NN1	3.5	2.0	1.4
5/21/09	SN1	3.5	1.2	1.4
5/22/09	MN1	3.5	9.0	1.2
6/23/09	NA2	3.5	3.5	5.3
6/24/09	SA2 *	81	6.0	9.5
6/25/09	MA2	3.5	9.5	6.2
6/26/09	NN2	3.5	2.5	1.1
6/27/09	SN2	3.5	2.0	1.0
6/28/09	MN2	3.5	8.6	0.8
7/1/09	NA3 *	81	6.0	6.6

* These mixtures were ready mixes from Centre Concrete.

2.2.5. Characterization of Hardened Concrete

Compression tests were conducted using a Boart Longyear Compression Machine produced by Calibration Service Inc. Compression strengths of all the mixtures were tested at 3, 7, and 28 curing days. Two cylinders (6 inch diameter x 12 inch height) were tested for each mixture, following ASTM C 39 (2005). The compression loading rate was set as 35 $\pm$ 7 psi/sec. Results were recorded and then averaged to obtain a representative compressive strength for each mixture. Compression test results are presented in Table 2.8.

The air void system of the hardened concrete was determined using a RapidAir 457 device manufactured by Concrete Expert International Inc., shown in Figure 2.2a), which follows ASTM C 457 linear traverse method (2008). Results are presented in this section.

Sample preparation. Samples from cylinders (4 in diameter x 8 in height) were cut following instructions provided by Mr. Seth Pelepko, petrographer from PennDOT. A section of approximately 4 in x 4 in (area) x 1 in (thickness) was cut perpendicularly to the top surface using a diamond blade saw. The schematic of the sample location is shown in Figure 2.2b.

Table 2.8. Summary compression tests

Mixture type	Compression strength (psi)		
	3 days	7 days	28 days
NA1	2984	3200	3906
SA1	-	3348	3888
MA1	-	4662	5680
NN1	4697	5581	6144
SN1	-	4927	6537
MN1	-	5947	7446
NA2	3460	4006	4582
SA2	2241	2793	3336
MA2	3971	4710	-
NN2	4618	5074	6119
SN2	4648	5000	5754
MN2	4800	5318	6227
NA3	2840	3335	4264

Figure 2.2a. RapidAir 457

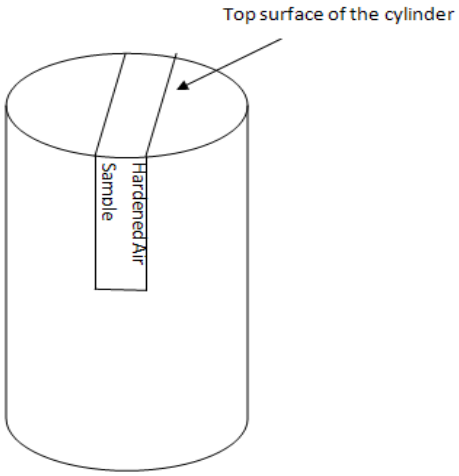

Figure 2.2b. Schematic of the sample location

The sample was cleaned with a soft brush under running tap water in a gentle manner and the surface to be polished was dried using compressed air. Then, a solution of lacquer and acetone with a ratio of 1:10 was applied to the surface with a soft brush. The prepared surface was dried one more time (using compressed air). After that, the sample was placed on a vibro lap machine for polishing, as shown in Figure 2.3. The surface of the vibro lap was filled with a solution of water and superplasticizer with a ratio of 1:1 and an appropriate quantity of grit material. The sample was polished using different grit sizes (80, 220, 320, 600 and 800). The time of running the vibro lap for each grit ranged from 20 to 30 minutes depending on different mixture types. Every time after lapping, the sample was observed under the microscope to check if the polished surface showed the appropriate sharpness of the edges of air voids. When the appropriate sharpness was obtained, the next grit size was used. After a satisfactory polished surface was obtained, the sample was put into a closed container containing lacquer thinner in order to remove the lacquer left on the surface. After 24 hours of soaking, the

sample was cleaned and dried. Then a black marker with a broad nib was used to cover the entire prepared surface. After that, barium sulfate (BaSO4) powder was sprinkled over the entire surface. A rubber stopper was used to tamp the powder into the voids. Finally, the residual powder was removed from the surface and the surface was cleaned using the palm of the hand.

Figure 2.3. Vibro lap polishing machine

The Linear Traverse Method described in ASTM C 457 was used to characterize the air void system in hardened concrete using RapidAir 457 manufactured by Concrete Expert International Inc. For each mixture, two samples were analyzed. For these analyses, the threshold value was set to 188 and the traversed length was 2413.5 mm. The paste content of each mixture was calculated theoretically and then input to the controlling software. The reports of the results were automatically generated by the software. Results for six different mixtures are presented in Table 2.9. It should be noted that for all concrete mixtures (N or S mixtures), results for total air content were very consistent with the ones obtained in the fresh state (Table 2.7). Differences of less than 0.5 percent were found. In the case of the mortar specimens, larger differences on the order of 2 percent were observed.

Table 2.9. Results of linear traverse analysis on air void system of hardened concrete samples

Sample Type	Paste content (%)	Air content (%)	Specific surface (mm^2/mm^3)	Spacing factor (mm)
NA2_1	30.2	4.89	64.52	0.079
NA2_2	30.2	5.15	67.21	0.074
SA2_1	35.1	9.04	70.93	0.055
SA2_2	35.1	9.39	73.35	0.051
MA2_1	51.2	7.58	75.39	0.071
MA2_2	51.2	8.16	74.88	0.069
NN2_1	32.2	1.28	56.11	0.169
NN2_2	32.2	1.47	46.42	0.192
SN2_1	37.7	1.19	50.39	0.207
SN2_2	37.7	1.49	40.04	0.237
MN2_1	56.9	1.31	50.20	0.237
MN2_2	56.9	1.64	51.82	0.209

2.3. Ultrasound

2.3.1 Basis

Ultrasonic waves have a wide variety of uses ranging from medical imaging to nondestructive evaluation and testing. The essence of ultrasonic nondestructive testing is that a pressure wave having a frequency in the ultrasonic domain is emitted into the subject material at one point and, after propagating through the material, is received at another point or back at the point of origin. The received signal is then processed in order to characterize the material properties, detect and classify defects, or measure geometric features. The two features of ultrasonic wave propagation that are expected to be most valuable for this project are wave speed and attenuation. Wave speed measurements enable determination of elastic properties, which depend on the material composition, including porosity associated with air voids. Attenuation measurements are indicative of internal damping, for example, by wave scattering from air voids. The combination of wave speed and attenuation measurements (and possibly others) into a multifaceted feature vector may enable characterization of the air void system in freshly placed concrete. There are many excellent books on ultrasonic nondestructive evaluation; the one most germane to this project is by Rose (1999).

The authors' laboratory plan mentioned three possible ultrasound methodologies. Two of the three (Rayleigh waves, nonlinear acoustics, pitch-catch with high frequency bulk waves) were eliminated from further consideration early in the program, in order to focus on Rayleigh waves. Nonlinear acoustics is a powerful method for characterization of microstructure and detection of damage, but the laboratory setup is much more complex than that for Rayleigh waves. Nonlinear acoustics methods for characterization of the air void system in hardened mortar have been developed by Georgia Tech researchers (Punurai, 2006; Punurai et al., 2006; Punurai et al., 2007). However, application to fresh concrete significantly complicates the

problem due to the high attenuation. Given the short period of time for the laboratory investigation and the inherent complexity of the nonlinear acoustics instrumentation, the authors opted to focus on the simpler method. The pitch-catch with high-frequency bulk waves method suffers two drawbacks: high attenuation due to the high frequency requires that the transducers be very close together, and a suitable fixture to hold the transducers in place and embed them in the concrete was not readily conceived. The ultrasound section of this report focuses exclusively on Rayleigh waves.

Rayleigh waves can propagate long distances along the surface of a thick material (assumed to be a half space). Here, the term 'thick' is relative to the wavelength of the traveling wave (Rose, 1999). The Rayleigh wave velocity equation is:

$$\eta^6 - 8\eta^4 + 8\eta^2\left(3 - 2\varsigma^2\right) + 16\left(\varsigma^2 - 1\right) = 0 \qquad \text{Eq. 1}$$

where $\eta = \frac{c_R}{c_T}$ and $\varsigma = \frac{c_T}{c_L} = \sqrt{\frac{1-2\nu}{2(1-\nu)}}$

c_R = Rayleigh surface wave velocity
c_T = transverse (shear) wave velocity
c_L = longitudinal wave velocity
ν = Poisson's ratio

Shear and longitudinal wave speeds are related to material properties:

$$c_T^2 = \frac{\mu}{\rho} \text{ and } c_L^2 = \frac{\lambda_L + 2\mu}{\rho} \qquad \text{Eq. 2,3}$$

where ρ = mass density
μ = shear modulus
λ_L = Lame's constant

The parameter η, which enables direct computation of the Rayleigh wave speed, depends only on Poisson's ratio, and therefore Rayleigh waves are nondispersive (i.e., do not depend on the frequency). Thus, changes in the Rayleigh wave speed reflect changes in the material properties. Most of the energy travels within one wavelength $\left(\lambda = c_R / f\right)$ of the surface, which ranges from 10-1.4 mm for a 1 km/s wave speed (typical for fresh concrete) and frequencies in the 100-700 kHz range.

Interaction of ultrasonic waves with air voids in concrete causes scattering that decreases the wave's amplitude, which is attenuation. Relative attenuation, $\alpha(f)$, is generally frequency-dependent and can be quantified, in decibels/meter (dB/m), by comparing the amplitudes for different travel distances:

$$\alpha(f) = -\frac{20}{d}\log\left(\frac{A_2(f)}{A_1(f)}\right) \qquad \text{Eq. 4}$$

where A_1 = amplitude for frequency f at point 1
A_2 = amplitude for frequency f at point 2
d = distance traveled between points 1 and 2

2.3.2 Equipment

The experimental evaluation relied on the use of a high-voltage (1000 V) pulser-receiver from Matec Instruments (Explorer II) with built-in oscilloscope and data acquisition. The high-voltage output is needed to penetrate the attenuative fresh concrete. The test setup is shown in Figure 2.4. Two broadbanded 1-inch, 500-kHz center-frequency transducers from Panametrics were used as transmitter and receiver in through-transmission mode. The transducers enabled a broad bandwidth of frequencies (100-700 kHz) to be employed. The transducers were mounted on Plexiglas wedges bonded to steel mediators. The angle of the wedge is selected to be the third critical angle to ensure a dominant surface wave is generated in the mediator. The angle is calculated using Snell's law (Rose, 1999) to be 23 degrees from the normal surface for Plexiglas and steel. The design drawings for the mediator and wedges are presented in Figures 2.5 and 2.6, respectively. The mediators are supported above the concrete surface with only the tip touching the concrete, as shown in Figure 2.7. Note that the angle the mediator makes with the concrete surface is not critical. The ultrasonic wave is transferred from the mediator tip to the concrete surface by Hertzian contact. Thus, the contact area of the mediator tip on the concrete surface is important to the amplitude of the generated wave in the concrete and needs to be controlled as much as possible.

Figure 2.4. Rayleigh wave test setup on fresh concrete

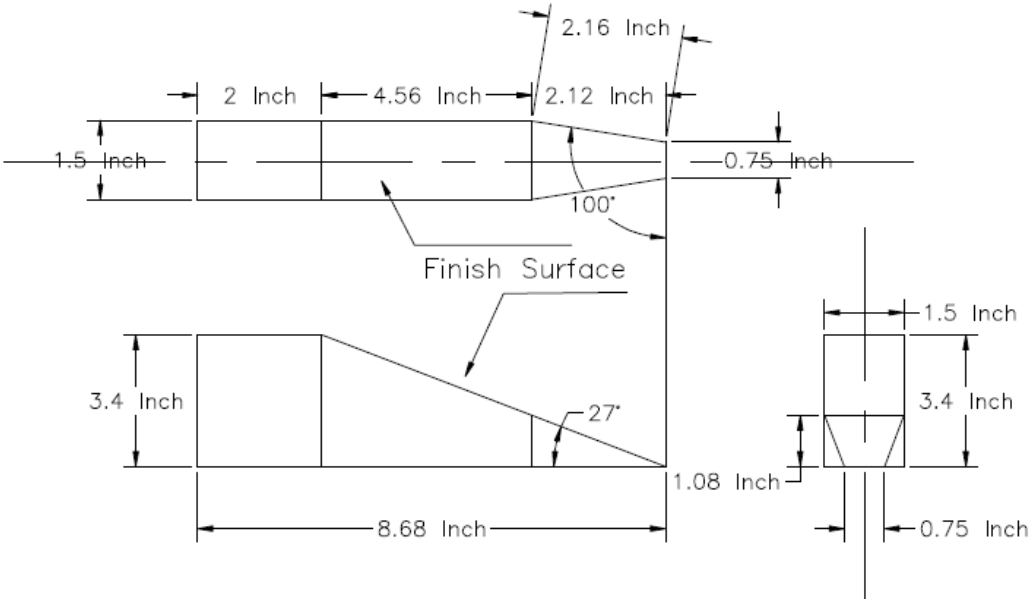

Figure 2.5. Steel mediator design

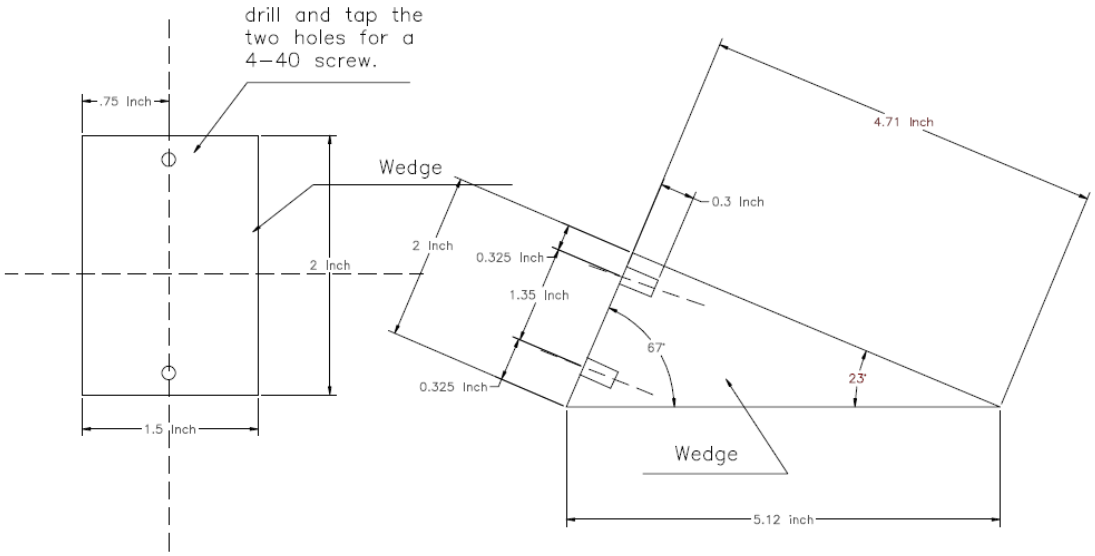

Figure 2.6. Plexiglas wedge design

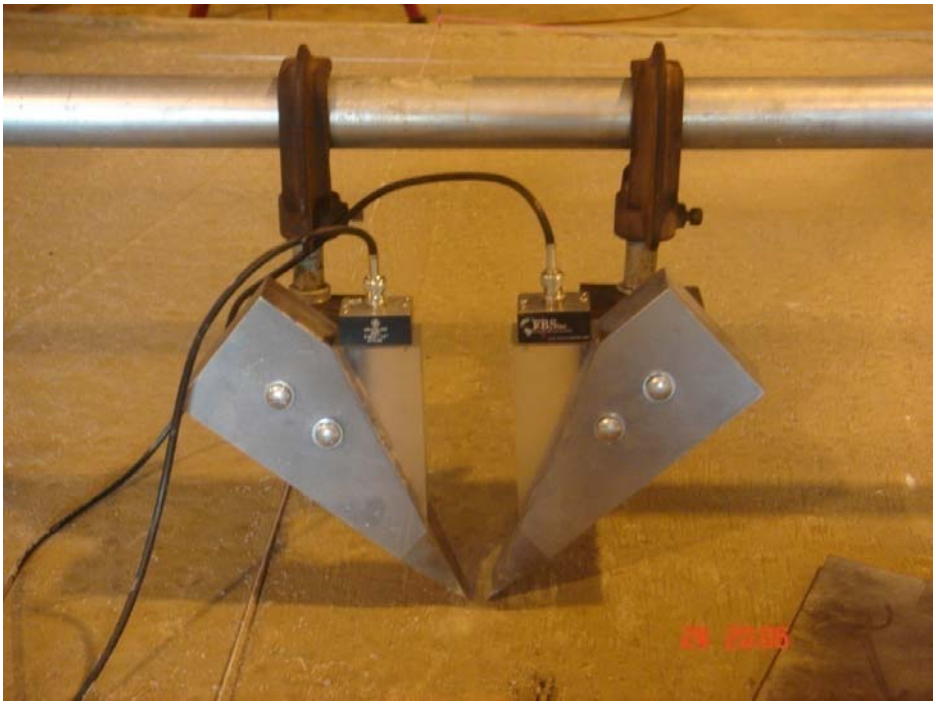

Figure 2.7. Mediator apparatus mounted on a beam

2.3.3 Methods

Impact-echo techniques generate longitudinal, shear, and Rayleigh waves (e.g., Shin et al., 2007). The intent here was to generate only Rayleigh waves, so mediators were used. The pre-test setup follows. Concrete was placed and the surface finished. In order to represent field conditions, no special surface finish was applied, as shown in Figure 2.8. As experience was acquired, the test methods were improved. The best practices are described herein, but since they were developed over time, they were not all used at the beginning of the program.

Figure 2.8. Concrete surface finish

The transducers are screwed to the Plexiglas wedges and coupled with gel. The mediator assemblies are mounted to a pipe with clamps. The pipe spans the concrete slab as a beam and is supported by a scissors jack at each end to simplify leveling and provide a nominal means to control the contact pressure of the mediator tip onto the concrete. The distance between the mediator tips is measured with calipers. This measurement is relatively difficult to make accurately, so multiple readings were taken and averaged together. Cables connect the pulser to the transmitting transducer and the receiver to the receiving transducer. A Hanning windowed 5-cycle toneburst excitation is set, along with the excitation voltage (1000 V), gain (50-70 dB), number of averages (30-60), and data acquisition rate (100 MHz). It is first necessary to measure the travel time for the waves to propagate through the mediator apparatus (126.58 us for 200 kHz) in order to calculate travel times in the concrete between the mediator tips.

The test itself consists of sending an electronic pulse to the transmitter (repeatedly), which is transformed into a longitudinal wave in the Plexiglas wedge by the piezoelectric material in the transducer, then refracted into a surface wave in the mediator, into the concrete, where it travels into the receiving mediator, and finally is converted back into an electrical pulse by the receiving transducer. The A-scan (received signal in the time domain) is observed on the oscilloscope. Selected waveforms are saved for signal processing and analysis. In Figure 2.9 an A-scan can be seen on the oscilloscope for a test on a 6 ft x 6 ft (1.83 m x 1.83 m) slab. In order to measure travel time the oscilloscope curser is moved to the start of the received waveform and the time in microseconds is read. The Rayleigh wave speed is calculated as the distance between the mediator tips divided by the difference in the total travel time and the travel time through the mediator apparatus. Two of the smaller 2 ft x 2 ft (0.61 m x 0.61 m) slabs are shown in Figure 2.10.

Figure 2.9. Rayleigh wave test setup on hardened concrete

Figure 2.10. 2 ft x 2 ft NA and NN concrete placed in forms

2.3.4 Analysis and Results

Concrete is placed in liquid form containing both solids (aggregate and sand) and air voids. Over time, the concrete hardens and then cures to high strength. In its solid state concrete exhibits attenuation due to its heterogeneity, but in its liquid state as a suspension that contains isolated particles and air voids, attenuation is greatly increased, making it very difficult for ultrasonic waves to penetrate (Popovics and Popovics, 1998). The first and foremost issue to address in this laboratory evaluation was how soon after concrete placement can an ultrasonic wave penetrate far enough to be detected by a receiver. After a number of trials and improvements in procedures, the authors were able to **receive a signal four hours after placement**. The received signals are shown in Figure 2.11 for excitation frequencies from 100-600 kHz and a travel distance through the concrete of 3.3 mm. The concrete was a normal mix without air entrainment (NN), and the authors believe that a similar result could be achieved for concrete with air entrainment (NA). As this result was not obtained until the end of the laboratory evaluation period, the remainder of the results presented and analyzed are for times after placement of 5, 6, 7, and 8 hours. These times are approximate and the data acquisition was not instantaneous. However, having learned from the laboratory evaluation, the authors believe that a much improved mediator apparatus could be designed to streamline data acquisition and improve the accuracy of the results.

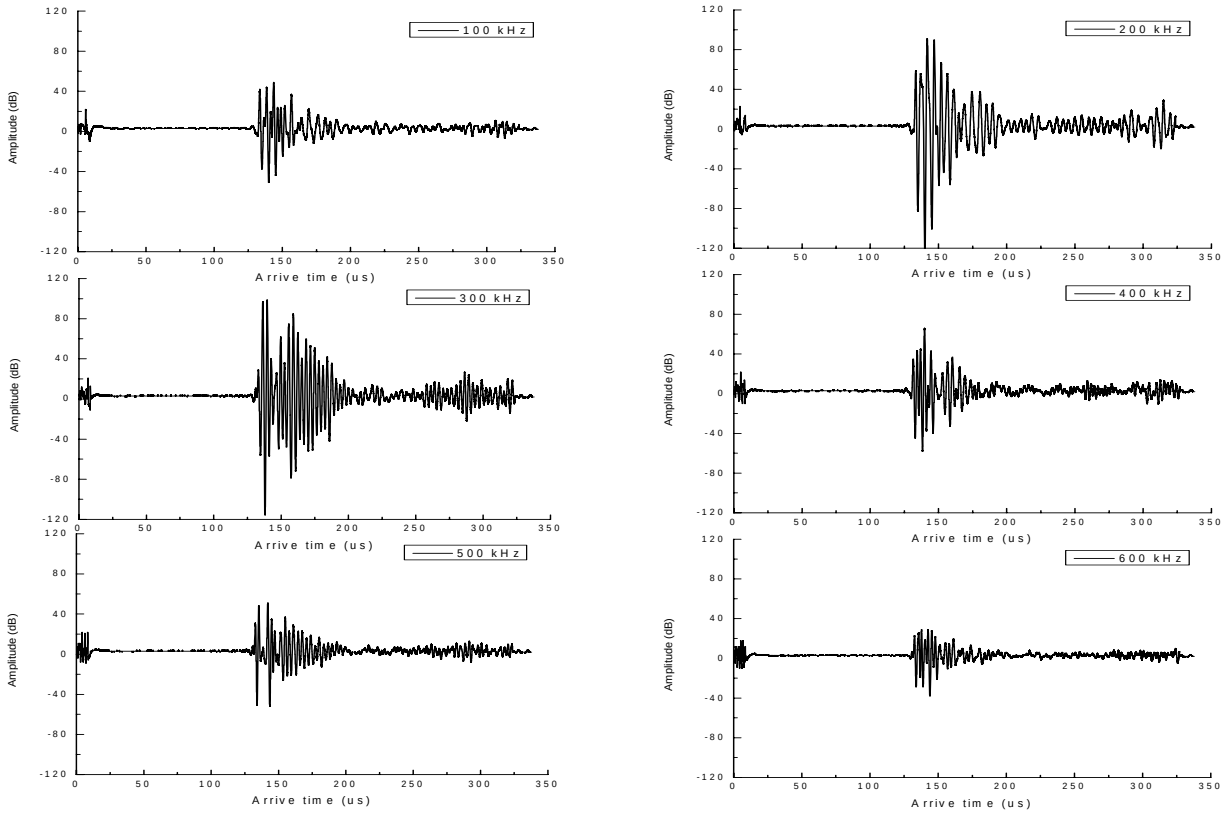

Figure 2.11. Signals received 4 hours after placement of NN, 3.3 mm travel distance, 100-600 kHz excitation frequencies

Signals received 5 hr after concrete placement are shown in Figure 2.12 for excitation frequencies of 100-700 kHz for both NA and NN mixes. The A-scans from the other mixes are similar and therefore are not shown here. Fast Fourier Transforms (FFTs) of the time domain signals shown in Figure 2.12 are computed and shown in Figure 2.13 to illustrate the frequency content in the Rayleigh wave. By noting the travel distance and identifying the time of flight, the Rayleigh wave speed can be calculated.

The calculated Rayleigh wave speeds are shown as a function of time, frequency, and air content in Figure 2.14 for fresh, normal-mix concrete. The results are in excellent agreement with qualitative expectations; namely, that the wave speed increases as the concrete sets up, and that since Rayleigh waves are nondispersive, the frequency does not depend upon frequency. More interestingly, and potentially very useful, is that there is a significant dependence of Rayleigh wave speed on air content. This is evident in all plots shown in Figure 2.14, but really stands out in Fig. 2.14e and 2.14f. Analogous results for sieved concrete and mortar are shown in Figures 2.15 and 2.16, respectively, and demonstrate the same trends. The wave speeds are also plotted as a function of measured air content in Figure 2.17 for 5, 6, 7, and 24 hr.

Figure 2.18 shows that 1-day-old concrete also exhibits an air content dependence for wave speed. Scatter in the wave speed results is shown in Figure 2.19 because the wave speed should be independent of both travel distance and excitation frequency. Finally, wave speed measurements are averaged for all frequencies and travel distances and the results presented in Table 2.10. The percent decrease in wave speed from concrete without air entrainment and concrete with air entrainment is also given in the table.

The finding that the air void system has a significant effect on Rayleigh wave speed is a very encouraging result.

Preceding the laboratory evaluation, the authors expected attenuation to provide the most useful data for characterizing the air void system (content, spacing factor, and specific surface). Much effort was devoted to receiving a signal as soon as possible after concrete placement and obtaining high-quality wave speed measurements. This did not leave sufficient time to adequately explore attenuation features for characterization of the air void system. Attenuation was calculated using EQN (3.1) by applying a Hilbert transform to determine the peak amplitude of the time domain envelope for each excitation frequency and for different travel distances. The Hilbert transform provides a positive envelope to the time domain signal, which oscillates between positive and negative values. Example time domain signals and their associated Hilbert transforms are shown in Figures 2.20 and 2.21 for hardened NA2 and NN2 concrete, respectively. Excitation frequencies from 100-700 kHz and two travel distances are shown in each figure. The attenuation calculated from these data is shown in Figure 2.22, which compares hardened NA2 and NN2 concrete. As expected, the attenuation for concrete with air entrainment is higher than for concrete without air entrainment.

Attenuation was also calculated for fresh NA2 and NN2 mixes. The scatter is significant, thus figures are not included. The primary issue in the scatter is believed to be limited control of the contact pressure between the mediator tip and the concrete surface. Recommendations for improvements to the mediator apparatus are given in the Discussion section to address this shortcoming. The authors believe a practical solution exists, but there was insufficient time to implement it during the laboratory evaluation.

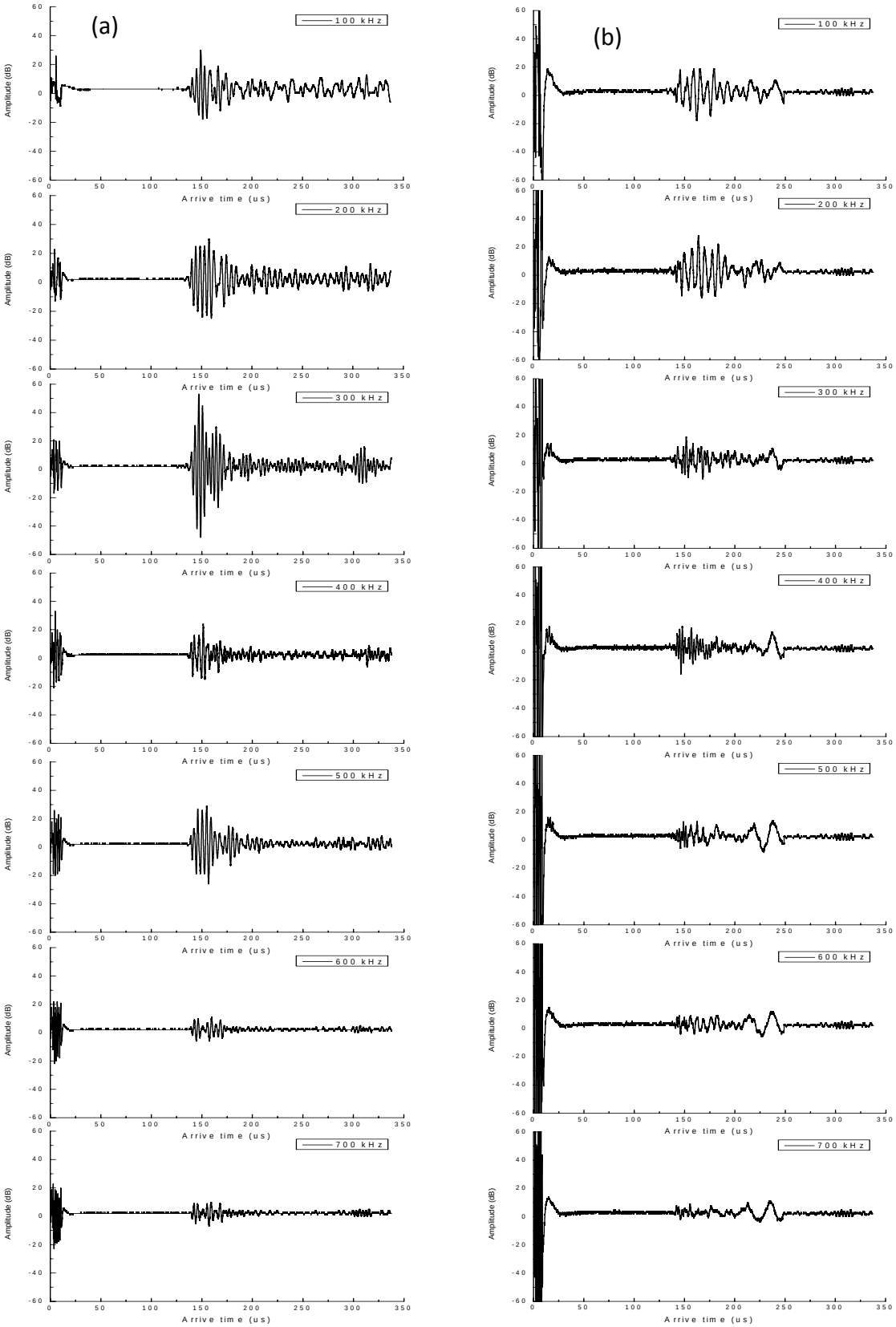

Figure 2.12. Signals received from 100-700 kHz excitation frequencies 5 hr after placement of (a) NA2 with 10.8 mm travel distance, (b) NN2 with 22.3 mm travel distance

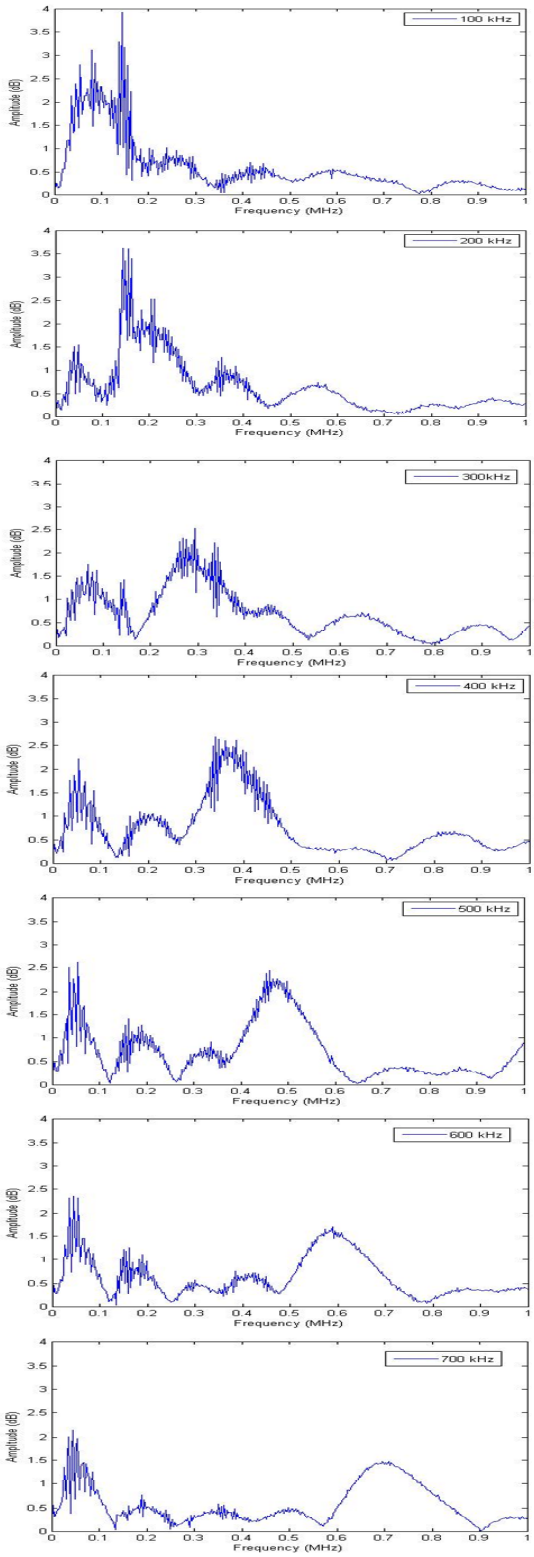

Figure 2.13. Frequency spectrums for 100-700 kHz excitation frequencies 5 hr after placement of NN2 with 22.3 mm travel distance

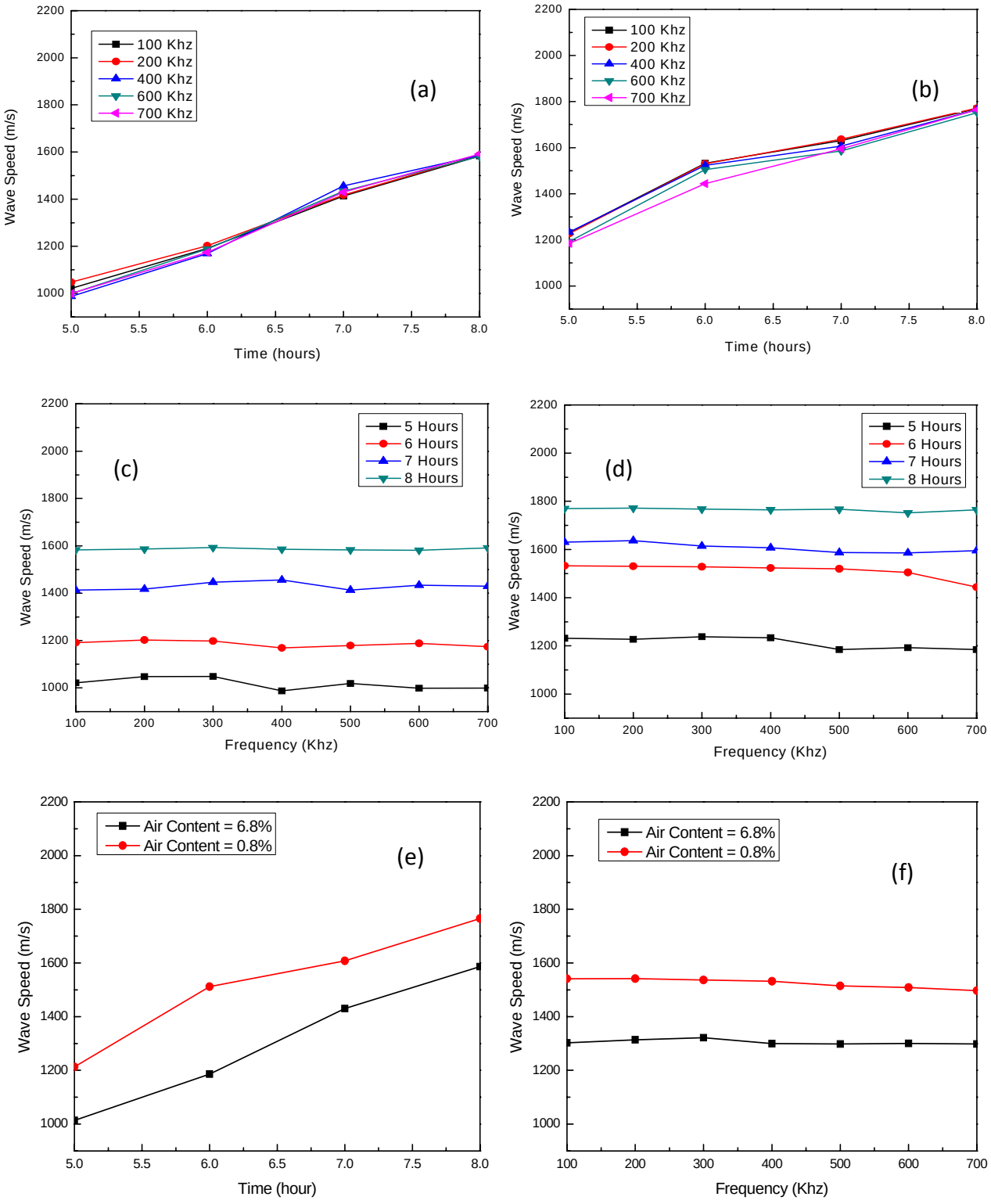

Figure 2.14. Dependence of wave speed in fresh normal-mix concrete on: time after placement, (a) NA2, (b) NN2; excitation frequency, (c) NA2, (d) NN2; and air content, (e) time, (f) frequency

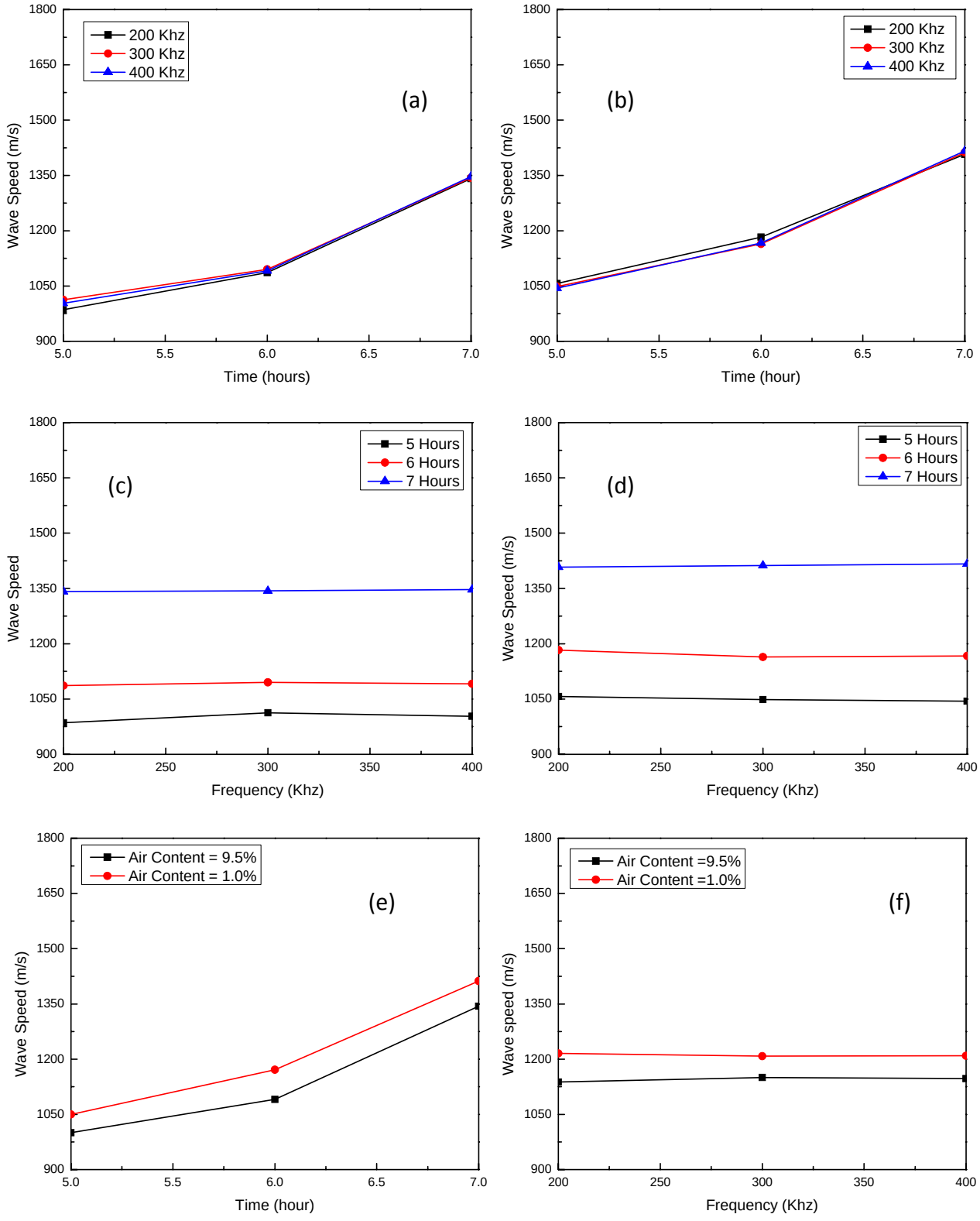

Figure 2.15. Dependence of wave speed in fresh sieved concrete on: time after placement, (a) SA2, (b) SN2; excitation frequency, (c) SA2, (d) SN2; and air content, (e) SA2, (f) SN2

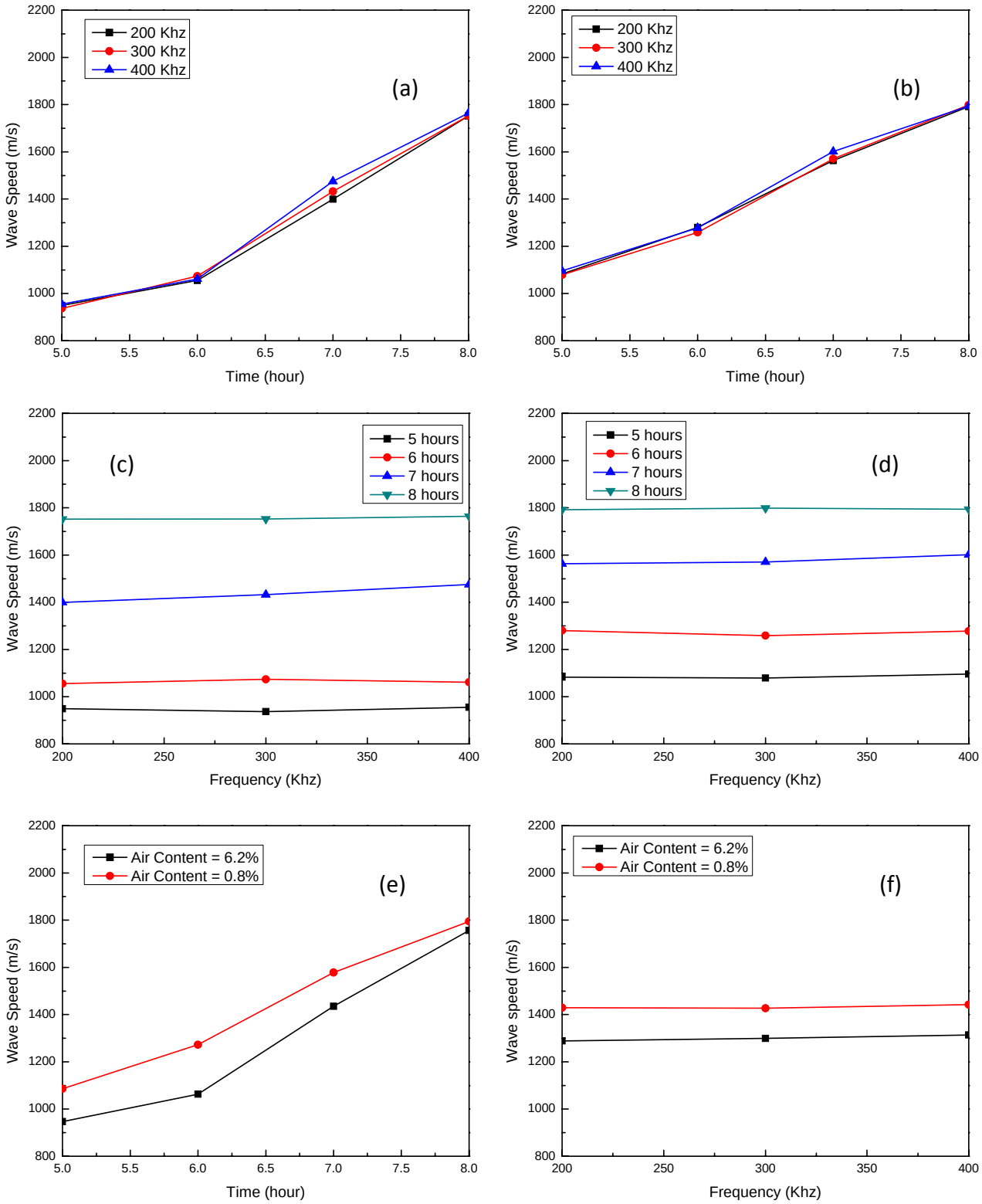

Figure 2.16. Dependence of wave speed in fresh mortar on: time after placement, (a) MA2, (b) MN2; excitation frequency, (c) MA2, (d) MN2; and air content, (e) MA2, (f) MN2

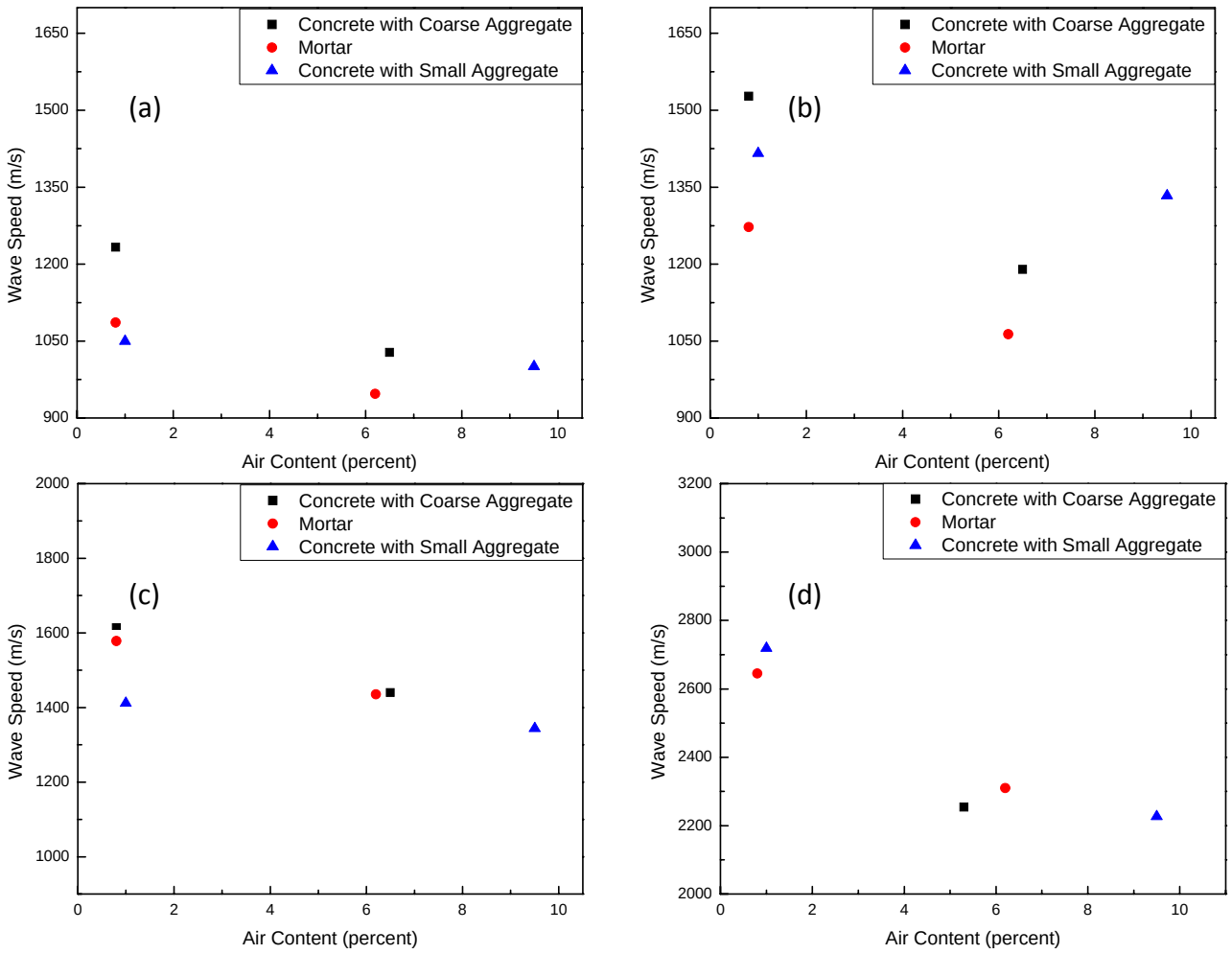

Figure 2.17. Wave speed dependence on air content for normal-mix concrete, sieved concrete, and mortar: (a) 5 hr, (b) 6 hr, (c) 7 hr, (d) 24 hr after placement

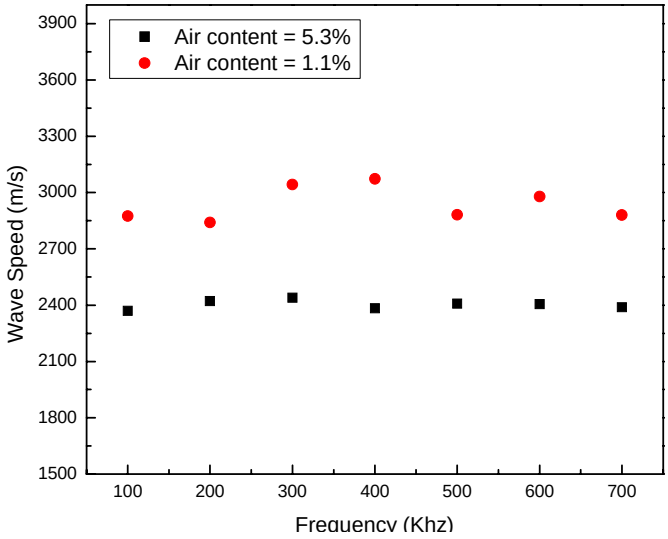

Figure 2.18. Wave speed as a function of excitation frequency for normal mix after 24 hr

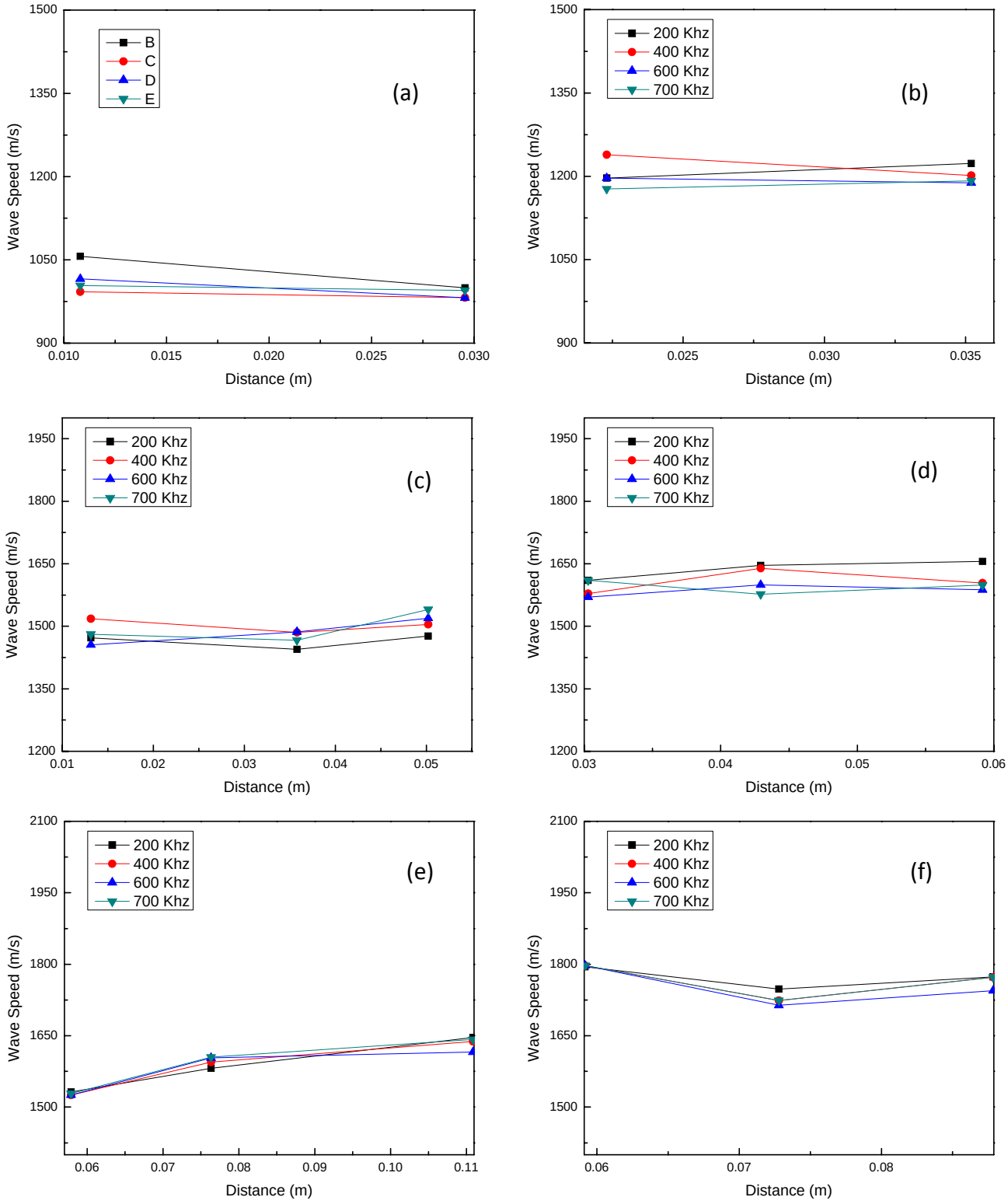

Figure 2.19. Wave speed as a function of travel distance in fresh concrete with air admixture (left side) and without air admixture (right side): (a) NA2 at 5 hr, (b) NN2 at 5 hr, (c) NA2 at 7 hr, (d) NN2 after 7 hr, (e) NA2 after 8 hr, (f) NN2 after 8 hr

Table 2.10. Wave speed in meters/second (m/s) for normal-mix concrete, sieved concrete, and mortar with and without air admixtures as a function of time after placement

Time after placement (hr)	NA2 Normal mix with air	NN2 Normal mix without air	SA2 Sieved concrete with air	SN2 Sieved concrete without air	MA2 Mortar with air	MN2 Mortar without air
5	1017 (-16%)	1213	1000 (-5%)	1050	947 (-13%)	1086
6	1186 (-22%)	1512	1091 (-7%)	1172	1063 (-16%)	1272
7	1430 (-11%)	1608	1344 (-5%)	1412	1436 (-9%)	1578
8	1586 (-10%)	1765	-	-	1756 (-2%)	1795
24	2402 (-18%)	2939	-	-	-	-

Note: percent decrease in wave speed due to air void system is shown in parenthesis.

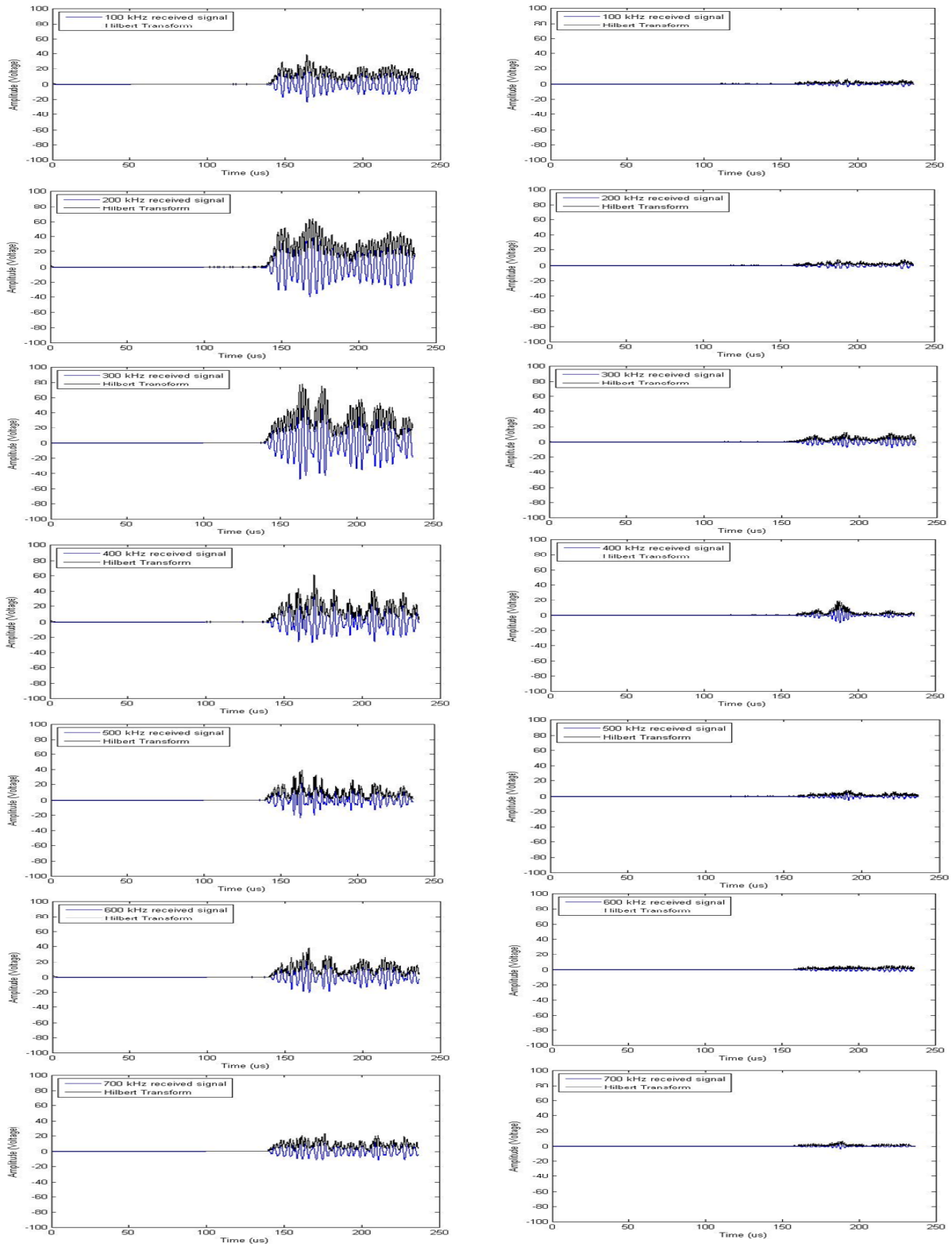

Figure 2.20. Time domain signal and Hilbert transform for hardened NA2 concrete; travel distances of 27.22 mm (left side) and 55.78 mm (right side)

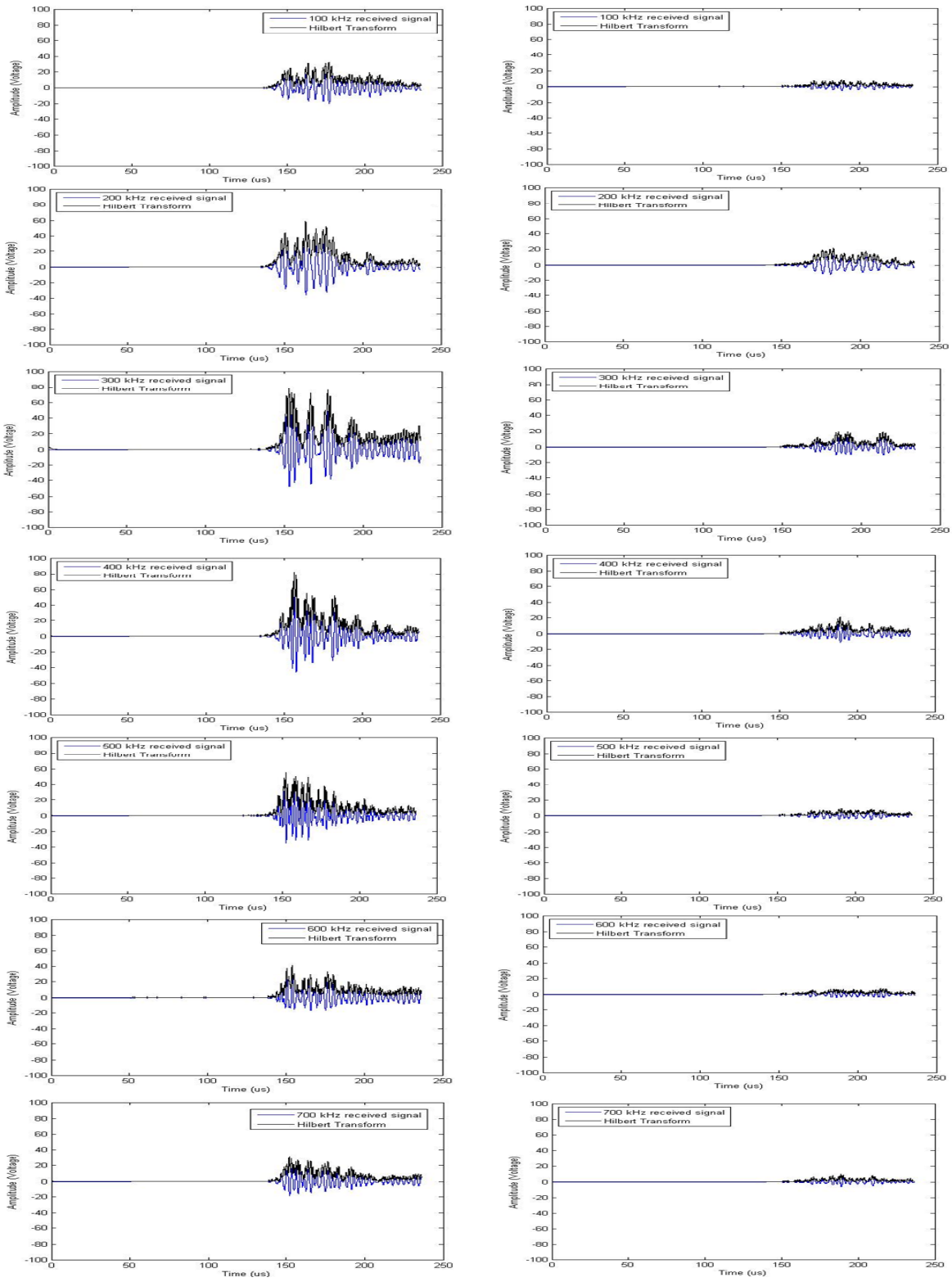

Figure 2.21. Time domain signal and Hilbert transform for hardened NN2 concrete; travel distances of 27.37 mm (left side) and 56.38 mm (right side)

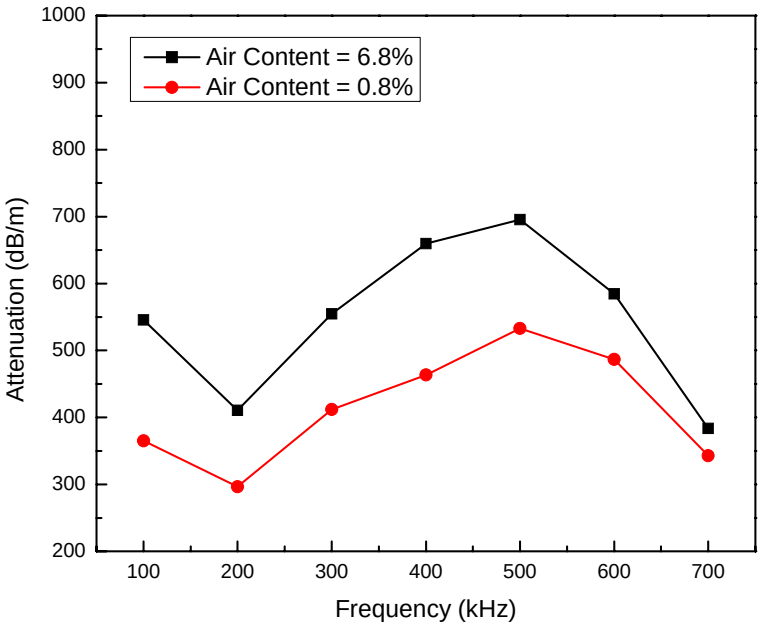

Figure 2.22. Attenuation calculated for hardened NA2 and NN2 concrete mixes

2.3.5 Discussion

An ultrasonic signal is able to penetrate the fresh concrete as early as 4 hr after placement. Both the Rayleigh wave speed and attenuation are influenced by the air void system. Additionally, it is possible to identify through-thickness gradients in material properties (possibly due to the air void system) near the surface by propagation of Rayleigh waves having different excitation frequencies because the effective material thickness characterized is frequency dependent.

The mediator apparatus used here is a fairly crude device. Recommendations for improvement are listed in descending priority:
1. Spring load the mediator mounts to facilitate control over the contact force between the mediator tip and the concrete surface.
2. Mount the mediators on a rail with the capability to accurately measure the distance between the mediator tips on a dial gage.
3. Make the two rail supports easily adjustable for setup on uneven ground with leveling capability. Place a bubble level on the rail.

2.4. Thermography

2.4.1 Basis

Thermographic imaging with an infrared camera has the potential to be a user-friendly, field-friendly technology for characterizing the air void system in fresh concrete. Thermal imaging is an excellent method for detecting defects in all sorts of materials. Defects, such as fatigue cracks, are discontinuities that interrupt the heat flow through a material and often result in hot spots or cold spots on the surface that is being imaged. The application to characterize the air void system in fresh concrete, however, is different; the goal is not to image individual discontinuities (the air voids are too small for the current imaging technology), but to compare the thermal emissivity associated with the air void system. Specifically, features of the surface temperature signature need to be connected to the air content, spacing factor, and specific surface. This connection will be made through experiments in conjunction with heat conduction finite-element simulations to determine the relationship between surface temperature and the heterogeneous concrete composition (air voids, aggregate, etc.). In this section, results from thermographic imaging of fresh and hardened concrete are presented.

2.4.2 Equipment

2.4.2.1 Infrared Camera

The infrared camera (Figure 2.23) used for this project is model P660 manufactured by FLIR Systems Inc. This infrared camera is equipped with a 45-degree wide angle lens. Some technical specifications of the camera are:

- Minimum focus distance = 0.3 m
- Thermal sensitivity < 0.045 °C
- Resolution = 480x640 pixels

The infrared camera is mounted to a movable steel frame as shown in Figure 2.24. The infrared camera is placed perpendicular to the concrete slab. The distance from the lens to the slab surface is approximately 0.46 m (18 in).

Figure 2.23. FLIR P660 infrared camera (FLIR Systems Inc.)

Figure 2.24. Infrared camera mounted on frame above concrete slab

2.4.2.2 Halogen Lamps

Halogen lamps (800 W) were used to heat the surface of the concrete slab. Figure 2.25 shows the setup for the lamps. The halogen lamps were mounted by clamps to the same steel frame as the camera. The light from the halogen lamps was perpendicular to the concrete slab. The distance between the halogen lamps and concrete slab surface was approximately 0.34 m (13.5 in).

Figure 2.25. Setup for halogen lamp heating

2.4.3 Methods

Concrete slabs used for thermography tests were approximately 2 ft square and 6 inches thick (0.6 x 0.6 x 0.15 m). Two 6-ft-square and 6-inch-thick slabs were fabricated for demonstration purposes on July 1. However, better correlations were found from the 2-ft-square slabs. First, the concrete slab was heated by the halogen lamp. The heating duration was 40 minutes. After the heating process, the lamp was switched off and the cooling-down process of the slab surface was observed and recorded using the infrared camera. The images were taken every 30 seconds until 10 minutes after removing the heat source, every 1 minute from 10 minutes to 20 minutes, every 2 minutes from 20 minutes to 30 minutes, every 5 minutes from 30 minutes to 60 minutes. In total, 41 images were saved for each test.

A spot in the hottest zone of the infrared image was chosen to be analyzed. The temperatures of this spot during the cooldown process are plotted as a function of time. In addition, a horizontal line crossing the hottest zone of the infrared image was selected for analysis. The temperatures along this line are also plotted. The results from slabs with and without air entrainment are compared.

2.4.4 Analysis and Results for Fresh Concrete

Surface temperature data acquired by the infrared camera for concrete with and without air entrainment are shown in Figures 4.4 and 4.5, respectively. These thermal images were taken 2 hr after concrete placement and 1 minute after removing the halogen lamp heat source. Thermocouple wires are clearly visible. These images were analyzed by tracking temperature as a function of time at the spots marked by cross-hairs. A comparison of surface cooldown at two spots is shown for slabs NA2 and NN2 in Figure 4.6, where it is observed that the slab with air entrainment reached a higher temperature given the same thermal loading. These data show, however, that cooldown measurements over time at a single point are insufficient for air void system characterization. Thus, the main feature of the infrared camera will be used – i.e., the camera provides the temperature field over a distinct surface area. This enables determination of spatial thermal gradients on the surface when discreet spots are use for reference.

The spatial thermal gradient along line 1 is shown in Figure 2.29 and along line 2 is shown in Figure 2.30 for cooldown times of 1, 5, 10, 30, and 60 minutes. Each data point represents one pixel from the thermal image. There is an observable difference in the thermal gradients, which appears to be attributable to the air void system. Not only is it visible here, but also in the results for hardened concrete. Spatial gradients for NA and NN concrete appear skewed, thus an effort is made to quantify the differences. First, the average temperature gradient is calculated by dividing the overall temperature change along a line by half the length of the line (approximately the distance between maximum and minimum temperature). The results for lines 1 and 2 are presented in Table 2.11. The gradients for NA2 are larger than the gradients for NN2 after 1 minute and 5 minutes, but the reverse is true after 10, 30, and 60 minutes. More data would be needed to explain this. Next, a quadratic polynomial was curve fit to the gradients, which correlated well to the data, as shown in Table 2.12. The fit coefficients for the first- and second-order terms of the quadratic polynomial are shown in Tables 2.13 and 2.14, respectively. In general, both first- and second-order coefficients are higher for air-entrained concrete than concrete without air entrainment. Since the coefficient of the quadratic term represents the curvature, the air-entrained concrete exhibits faster change in the thermal gradient. Perhaps the skewness between the NA and NN samples is better represented by the zero-th order coefficient. Further analysis of these data in conjunction with the finite element simulations is expected to be fruitful.

The use of thermography for this application is dependent upon identification of surface thermal field features that are strongly dependent on air void system characteristics (content, size, spacing). The authors have selected the most obvious feature, but there may be others found to be more effective after further study.

2.4.5 Analysis and Results for Hardened Concrete

Thermography was conducted on hardened normal-mix concrete, sieved concrete, and mortar. For normal-mix concrete, thermal images are shown in Figures 2.31 and 2.32, while cooldown

at spot 1 is shown in Figure 2.33 and the spatial thermal gradient along line 1 is shown in Figure 2.34. For sieved concrete, thermal images are shown in Figures 2.35 and 2.36, while cooldown at spot 1 is shown in Figure 2.37 and the spatial thermal gradient along line 1 is shown in Figure 2.38. For mortar, thermal images are shown in Figures 2.39 and 2.40, cooldown at spot 1 is shown in Figure 2.41, and the spatial thermal gradient along line 1 is shown in Figure 2.42. Figure 2.39 shows a hot spot to the right and below center, which is probably associated with a lump on the surface of the mortar.

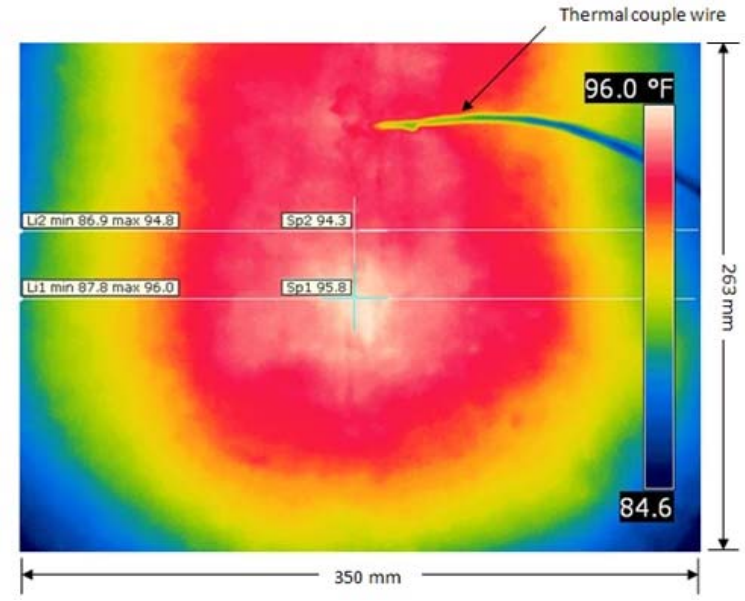

Figure 2.26. Thermal image for NA2 (2 hr after placement, 1 min after removal of heat source)

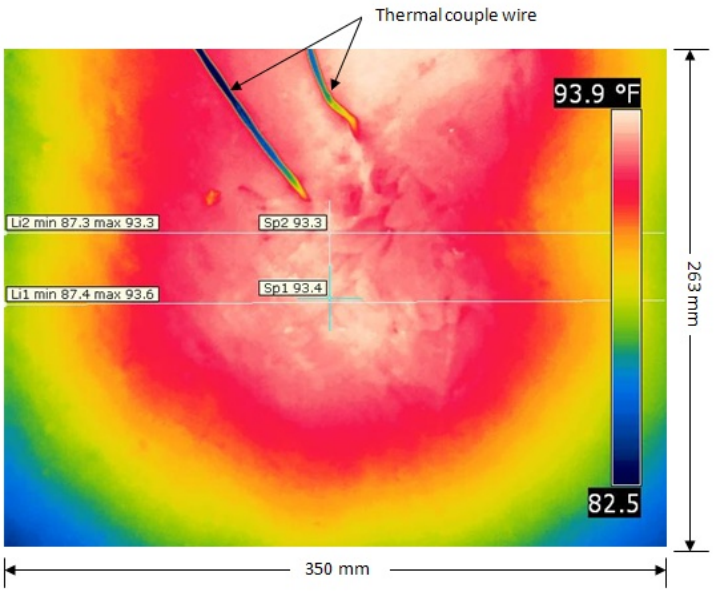

Figure 2.27. Thermal image for NN2 (2 hr after placement, 1 min after removal of heat source)

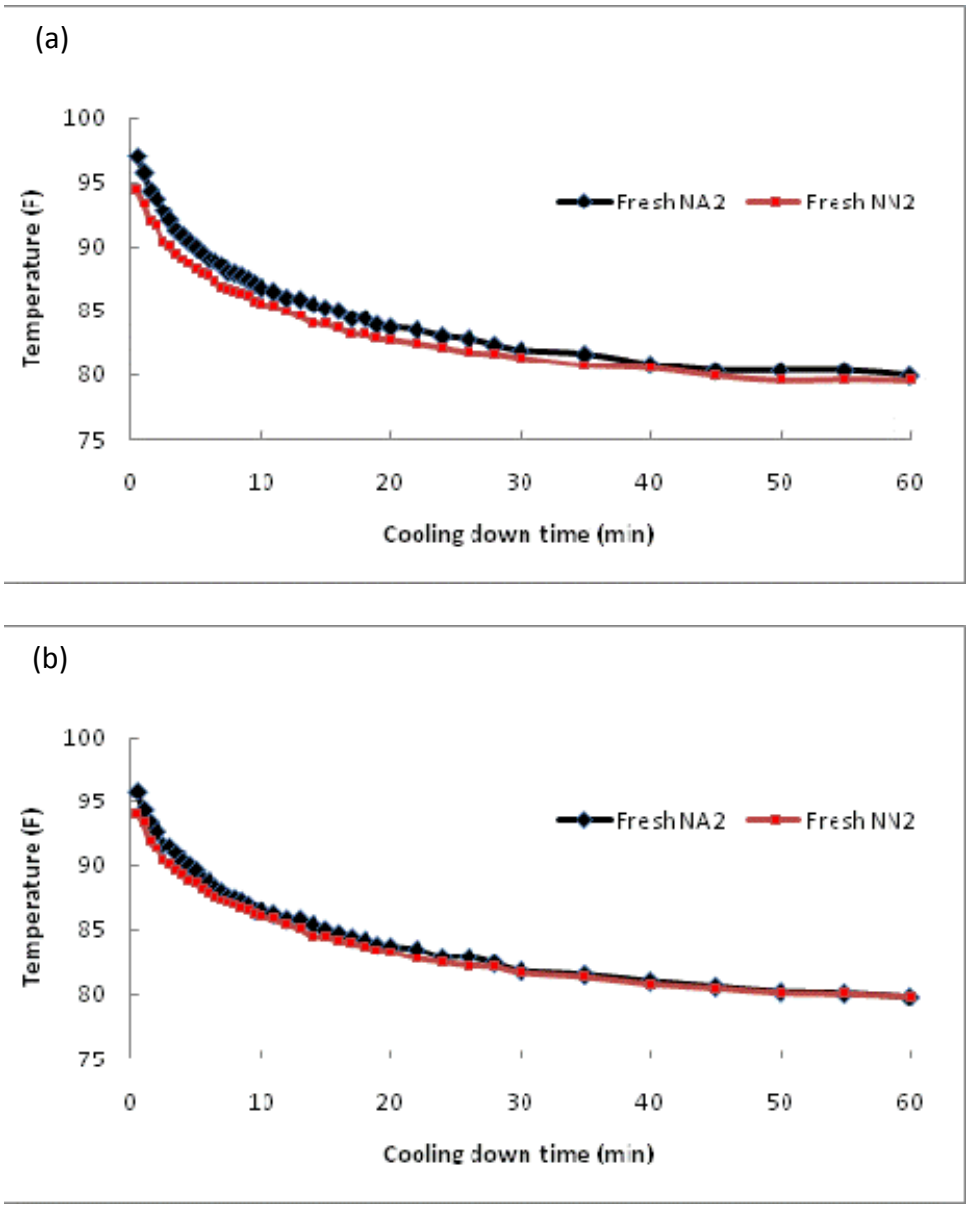

Figure 2.28. Slab surface cooldown at (a) spot 1 and (b) spot 2 for concrete with and without air entrainment

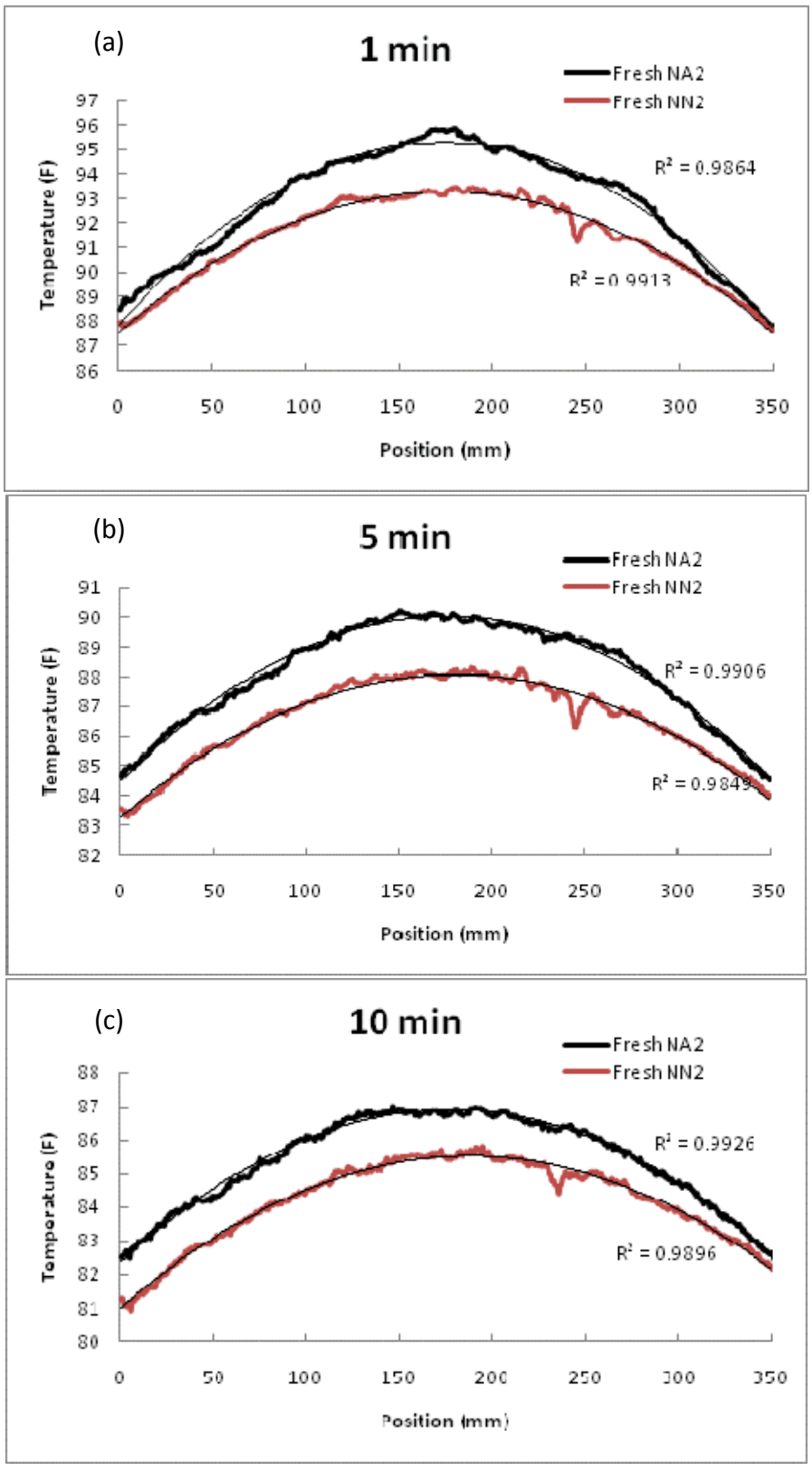

Figure 2.29. Spatial thermal gradient along line 1 for NA2 and NN2 concrete after heat source was removed for (a) 1 min, (b) 5 min, (c) 10 min, (d) 30 min, (e) 60 min

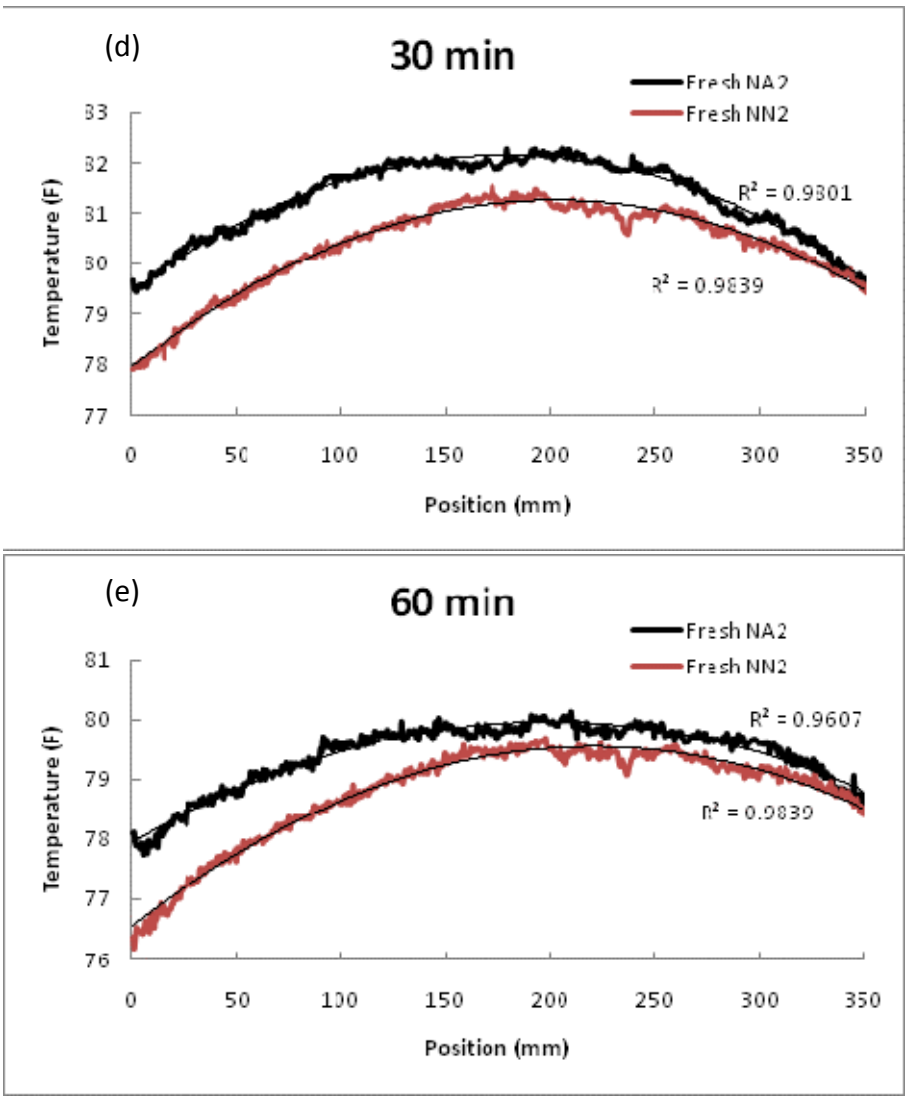

Figure 2.29 (continued). Spatial thermal gradient along line 1 for NA2 and NN2 concrete after heat source was removed for (a) 1 min, (b) 5 min, (c) 10 min, (d) 30 min, (e) 60 min

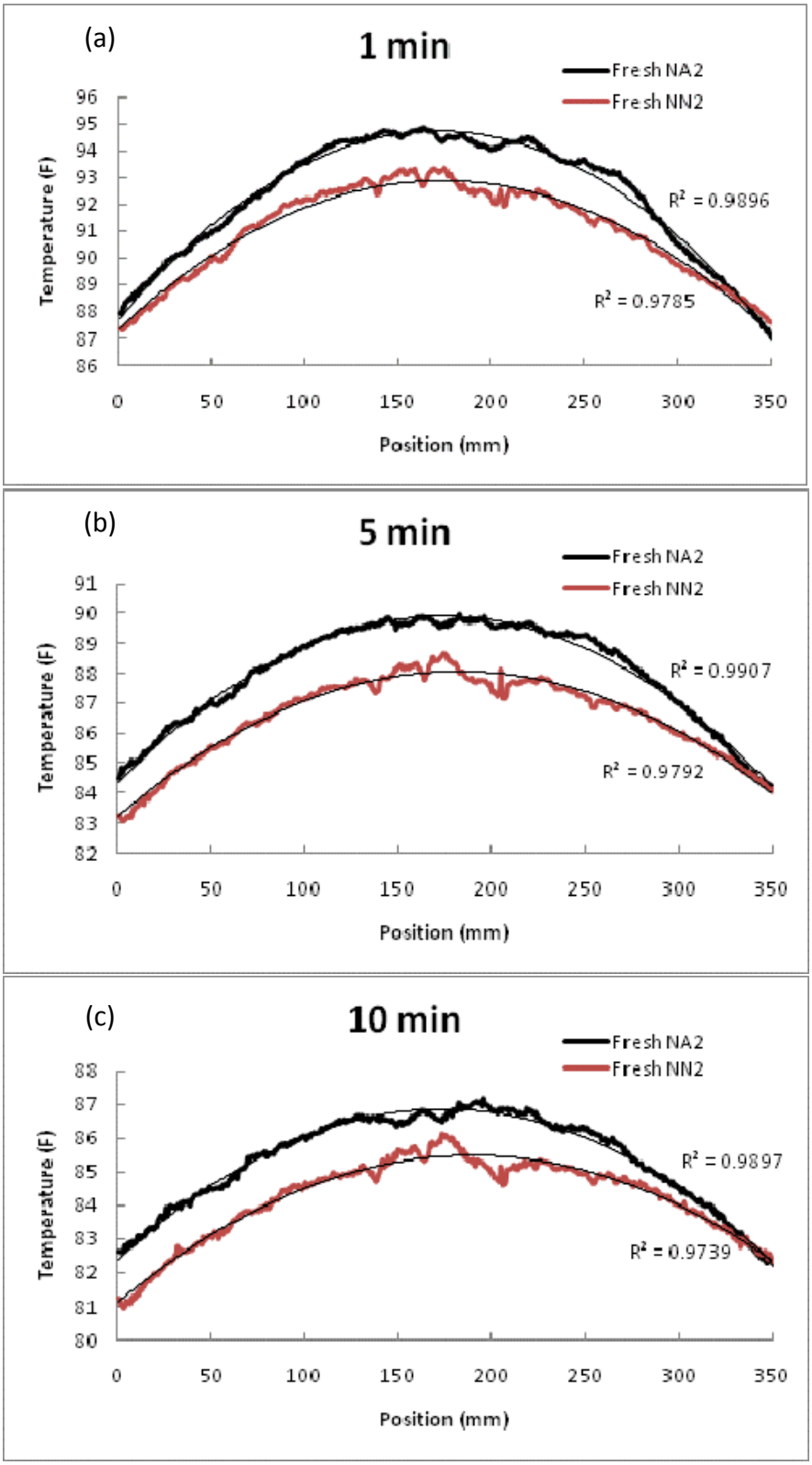

Figure 2.30. Spatial thermal gradient along line 2 for NA2 and NN2 concrete after heat source was removed for (a) 1 min, (b) 5 min, (c) 10 min, (d) 30 min, (e) 60 min

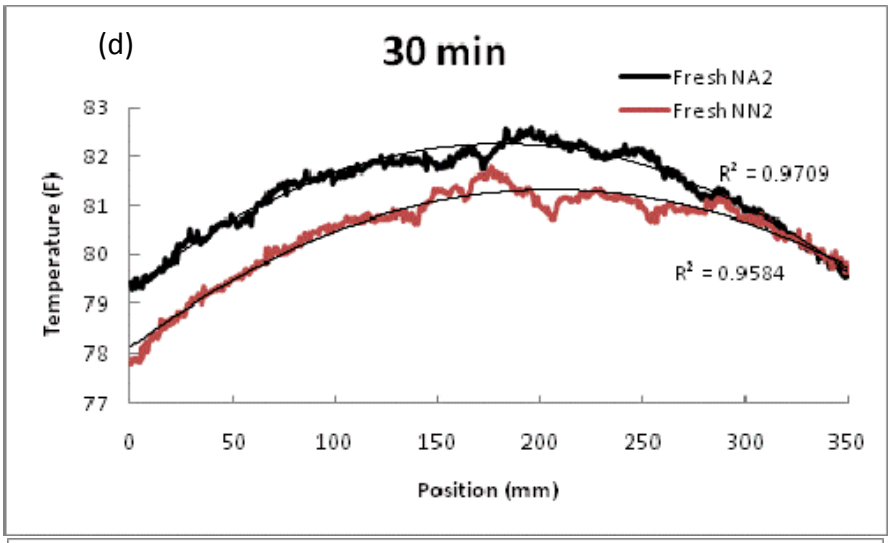

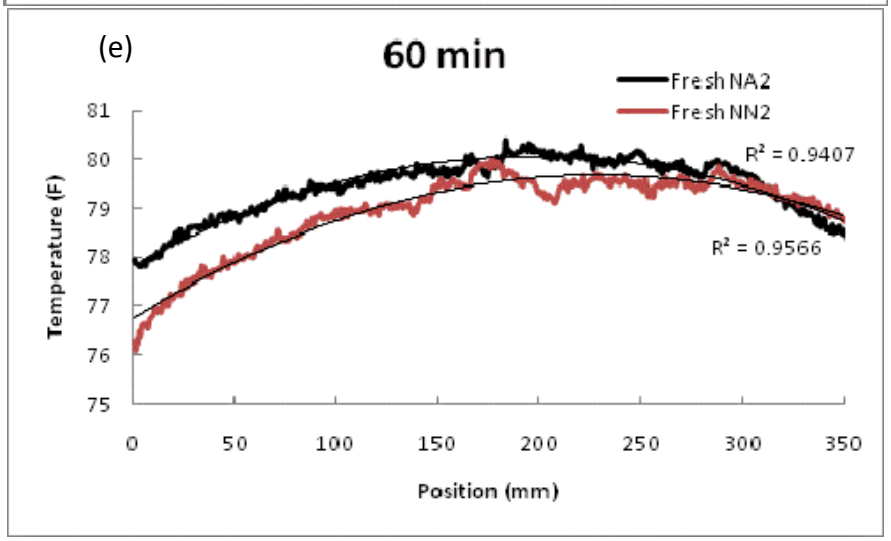

Figure 2.30 (continued). Spatial thermal gradient along line 2 for NA2 and NN2 concrete after heat source was removed for (a) 1 min, (b) 5 min, (c) 10 min, (d) 30 min, (e) 60 min

Table 2.11. Spatial thermal gradient for fresh concrete

Cooldown time (min)	$\frac{\Delta T}{d/2}$ (°F/mm)			
	Line 1		Line 2	
	NA2	NN2	NA2	NN2
1	0.0470	0.0345	0.0459	0.0344
5	0.0326	0.0288	0.0337	0.0321
10	0.0261	0.0281	0.0287	0.0294
30	0.0165	0.0209	0.0188	0.0229
60	0.0135	0.0199	0.0149	0.0223

Table 2.12. Quadratic polynomial curve fit to thermal gradient for fresh concrete

Cooldown time (min)	Fit coefficient, R^2			
	Line 1		Line 2	
	NA2	NN2	NA2	NN2
1	0.9864	0.9913	0.9896	0.9785
5	0.9906	0.9849	0.9907	0.9792
10	0.9926	0.9896	0.9897	0.9739
30	0.9801	0.9839	0.9709	0.9584
60	0.9607	0.9839	0.9407	0.9566

Table 2.13. Spatial gradient first-order fit coefficients for fresh concrete

Cooldown time (min)	Fit coefficient for 1st order term			
	Line 1		Line 2	
	NA2	NN2	NA2	NN2
1	0.0857	0.0654	0.0817	0.0636
5	0.0633	0.0532	0.0638	0.0532
10	0.0513	0.0483	0.0513	0.0460
30	0.0303	0.0328	0.0329	0.0314
60	0.0202	0.0271	0.0227	0.0257

Table 2.14. Spatial gradient second-order fit coefficients for fresh concrete

Cooldown time (min)	Fit coefficient for 2nd order term			
	Line 1		Line 2	
	NA2	NN2	NA2	NN2
1	-0.000246	-0.000246	-0.000238	-0.000183
5	-0.000180	-0.000147	-0.000183	-0.000146
10	-0.000144	-0.000128	-0.000147	-0.000121
30	-0.0000847	-0.0000811	-0.0000910	-0.0000762
60	-0.0000508	-0.0000613	-0.0000574	-0.0000562

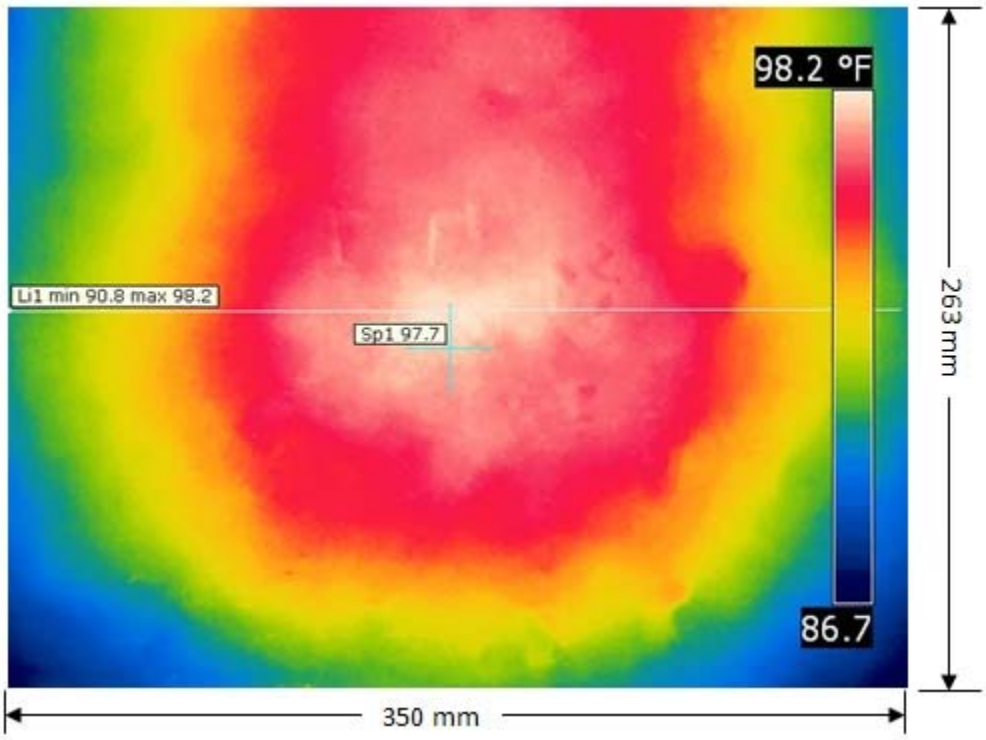

Figure 2.31. Thermal image for hardened NA2 (1 min after removal of heat source)

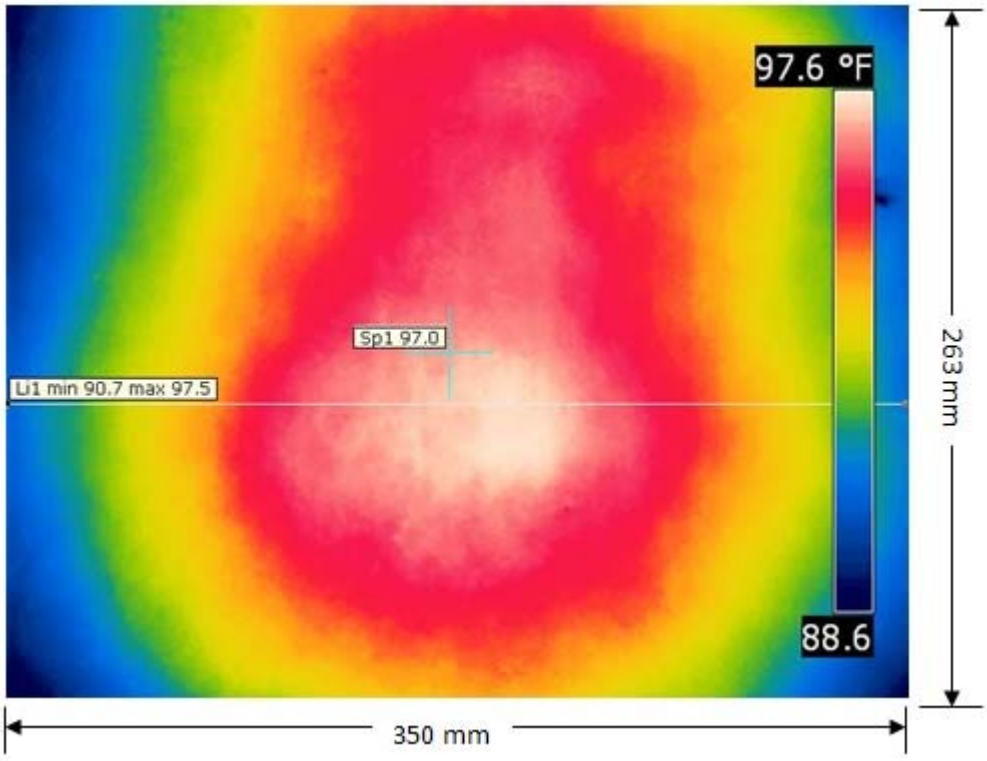

Figure 2.32. Thermal image for hardened NN2 (1 min after removal of heat source)

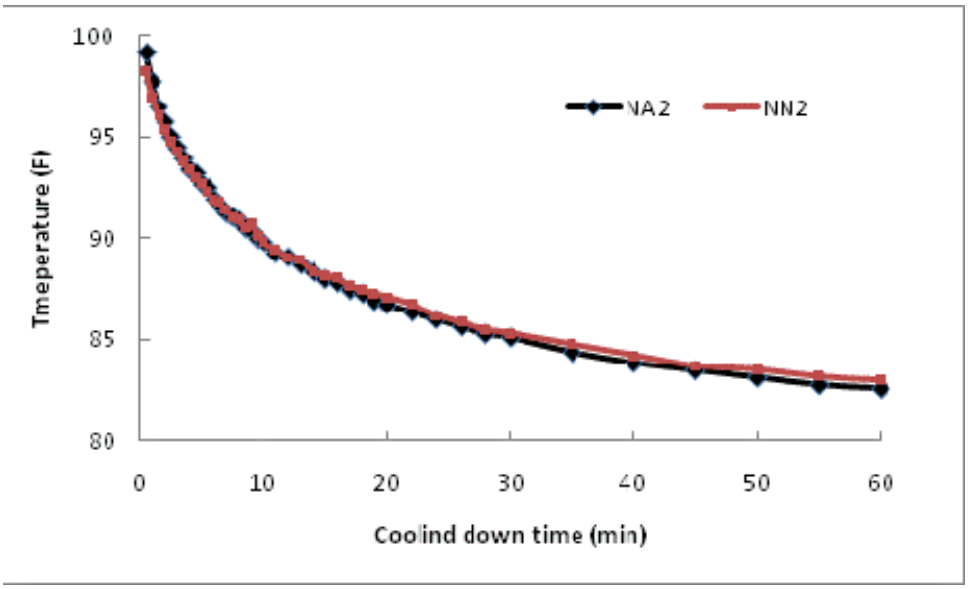

Figure 2.33. Slab surface cooldown at spot 1 for hardened normal concrete with and without air entrainment

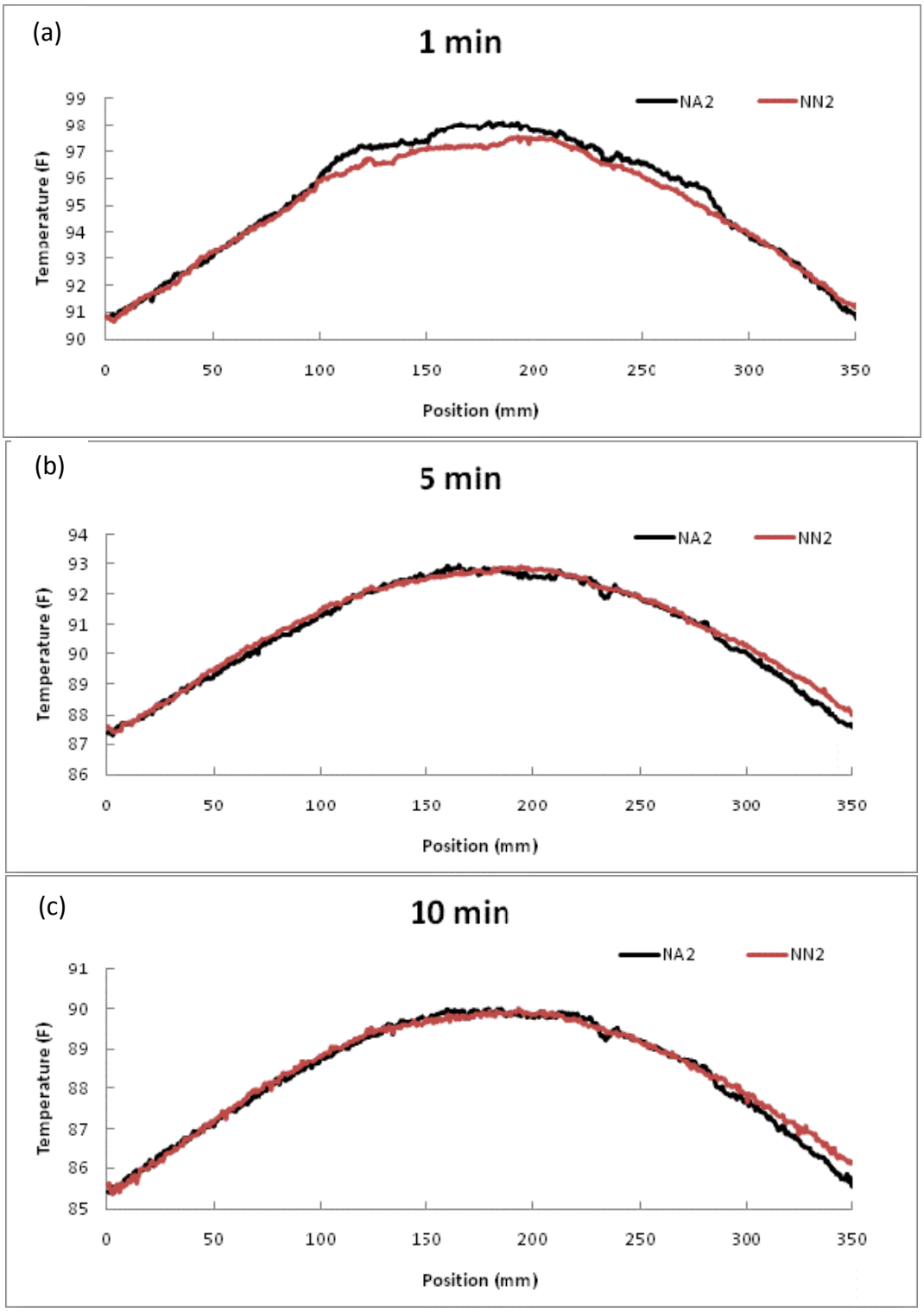

Figure 2.34. Spatial thermal gradient along line 1 for hardened NA2 and NN2 concrete after heat source was removed for (a) 1 min, (b) 5 min, (c) 10 min, (d) 30 min, (e) 60 min

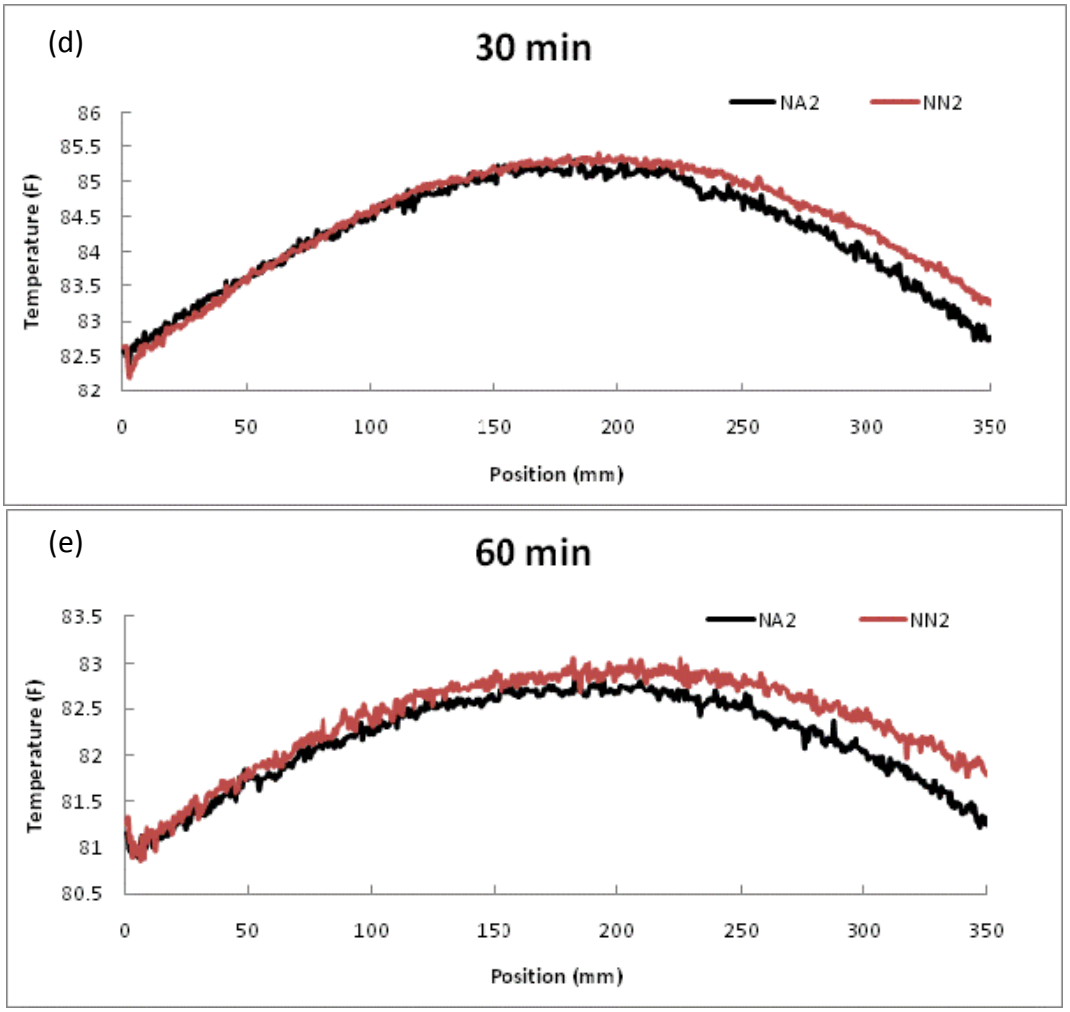

Figure 2.34 (continued). Spatial thermal gradient along line 1 for hardened NA2 and NN2 concrete after heat source was removed for (a) 1 min, (b) 5 min, (c) 10 min, (d) 30 min, (e) 60 min

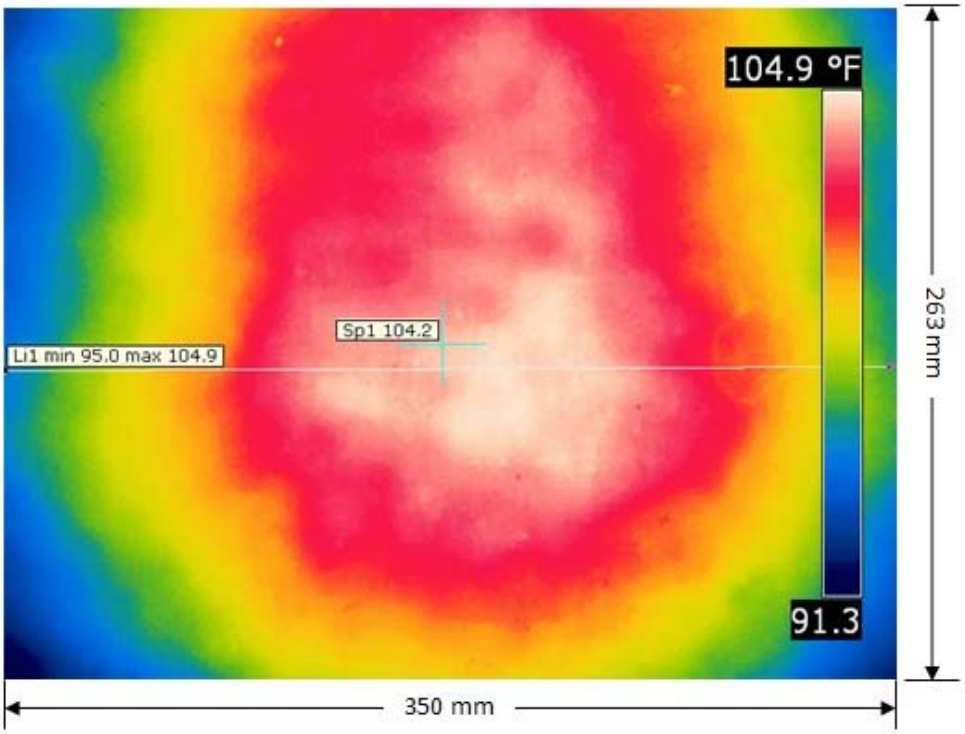

Figure 2.35. Thermal image for hardened SA2 (1 min after removal of heat source)

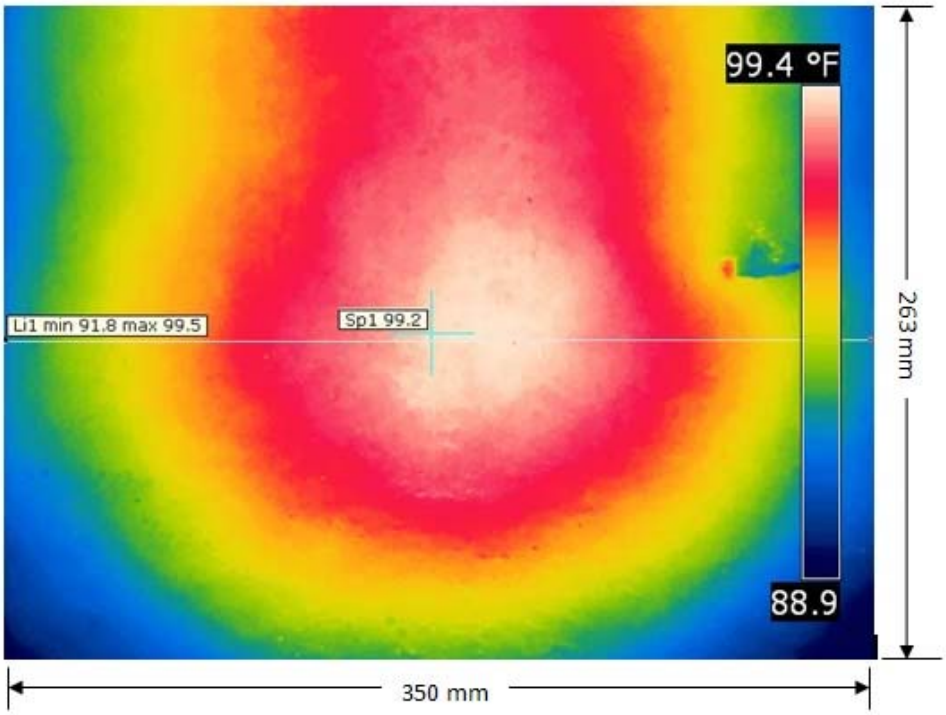

Figure 2.36. Thermal image for hardened SN2 (1 min after removal of heat source)

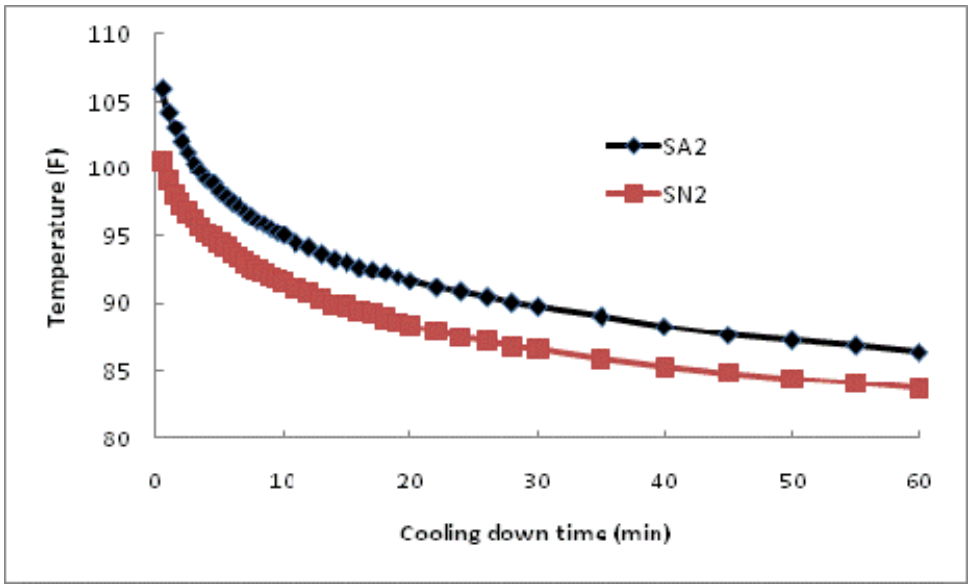

Figure 2.37. Slab surface cooldown at spot 1 for hardened sieved concrete with and without air entrainment

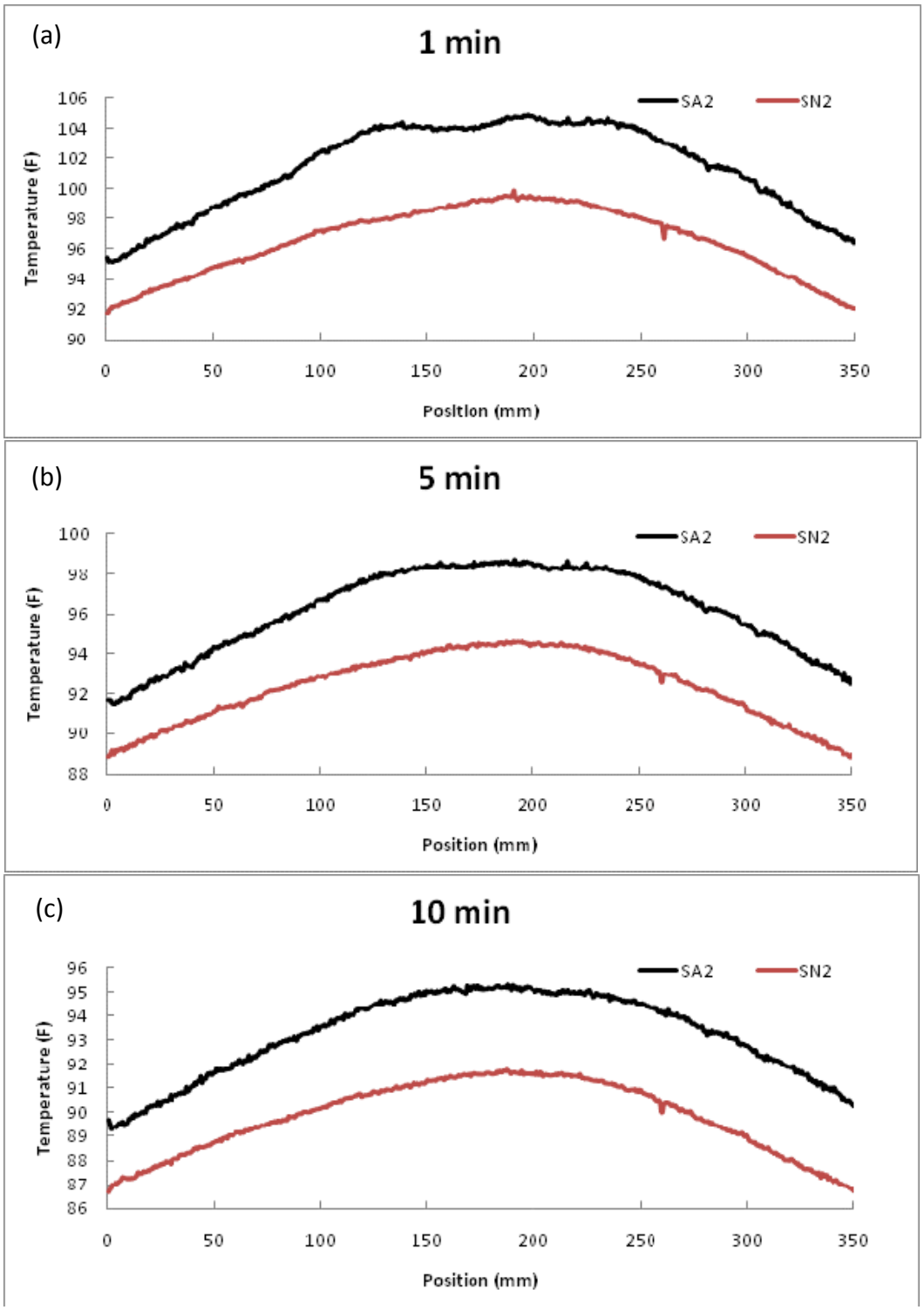

Figure 2.38. Spatial thermal gradient along line 1 for hardened SA2 and SN2 concrete after heat source was removed for (a) 1 min, (b) 5 min, (c) 10 min, (d) 30 min, (e) 60 min

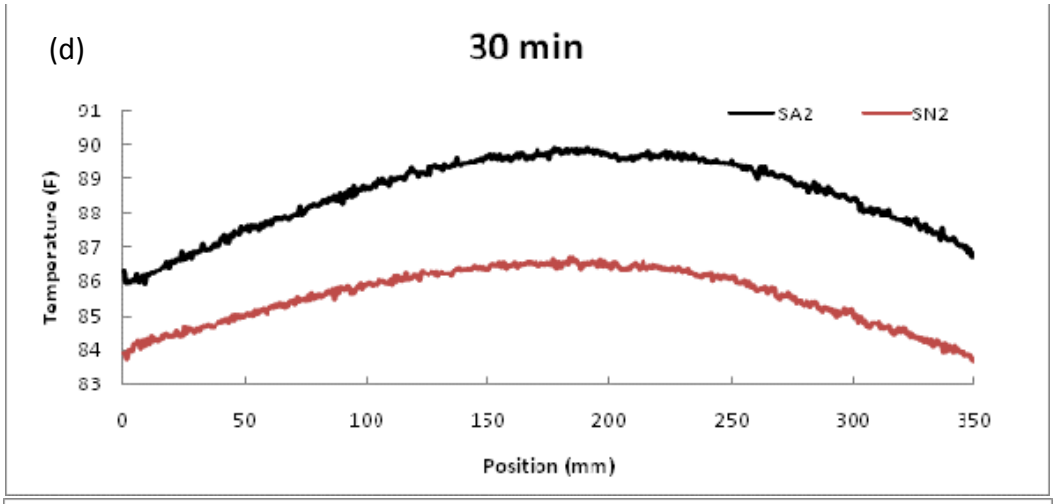

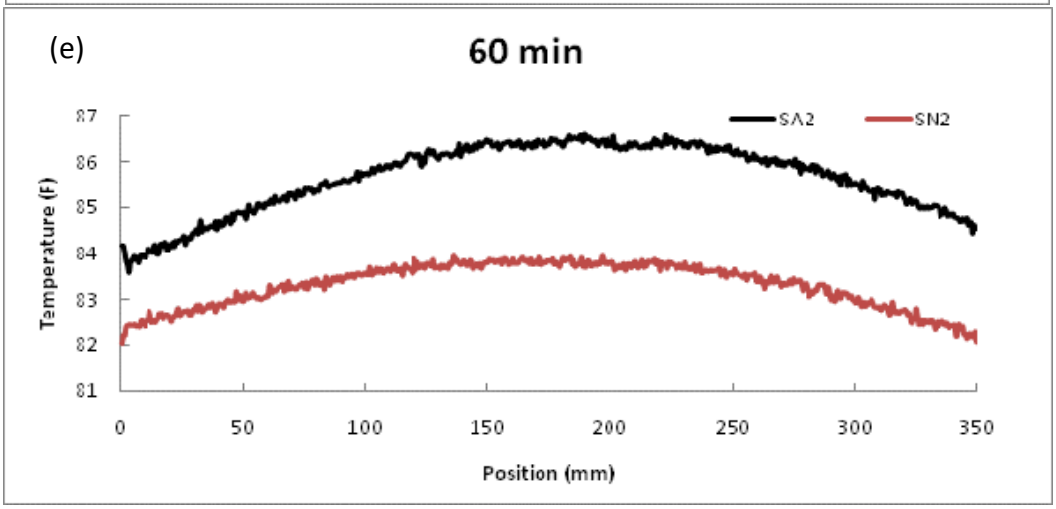

Figure 2.38 (continued). Spatial thermal gradient along line 1 for hardened SA2 and SN2 concrete after heat source was removed for (a) 1 min, (b) 5 min, (c) 10 min, (d) 30 min, (e) 60 min

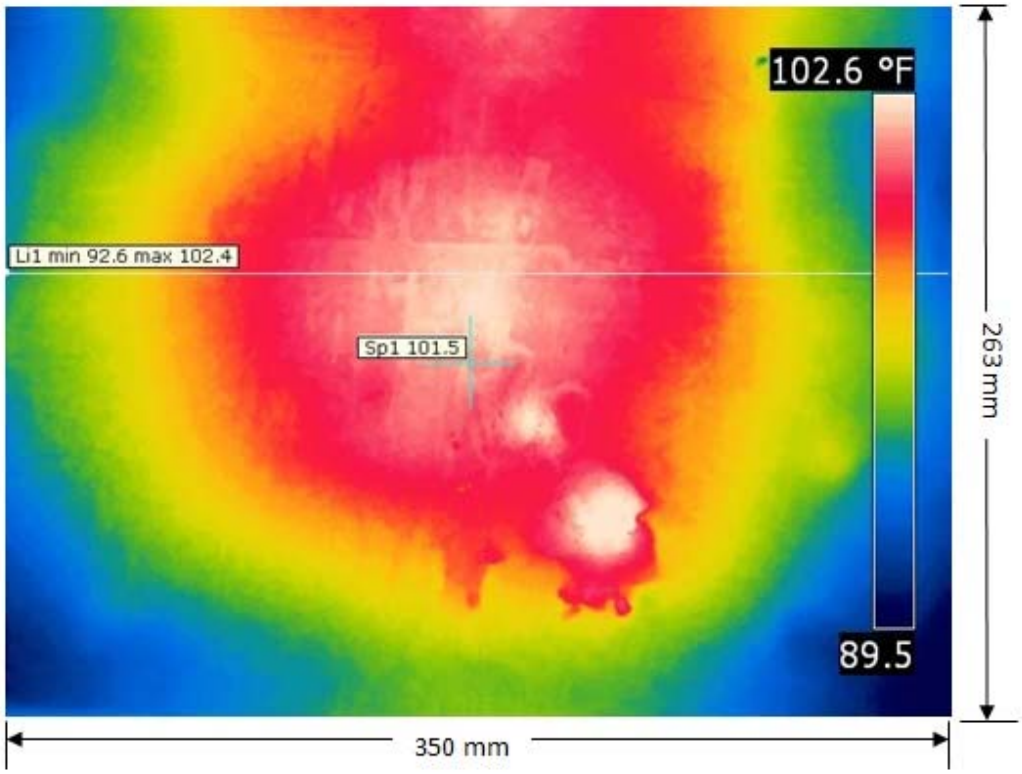

Figure 2.39. Thermal image for hardened MA2 (1 min after removal of heat source)

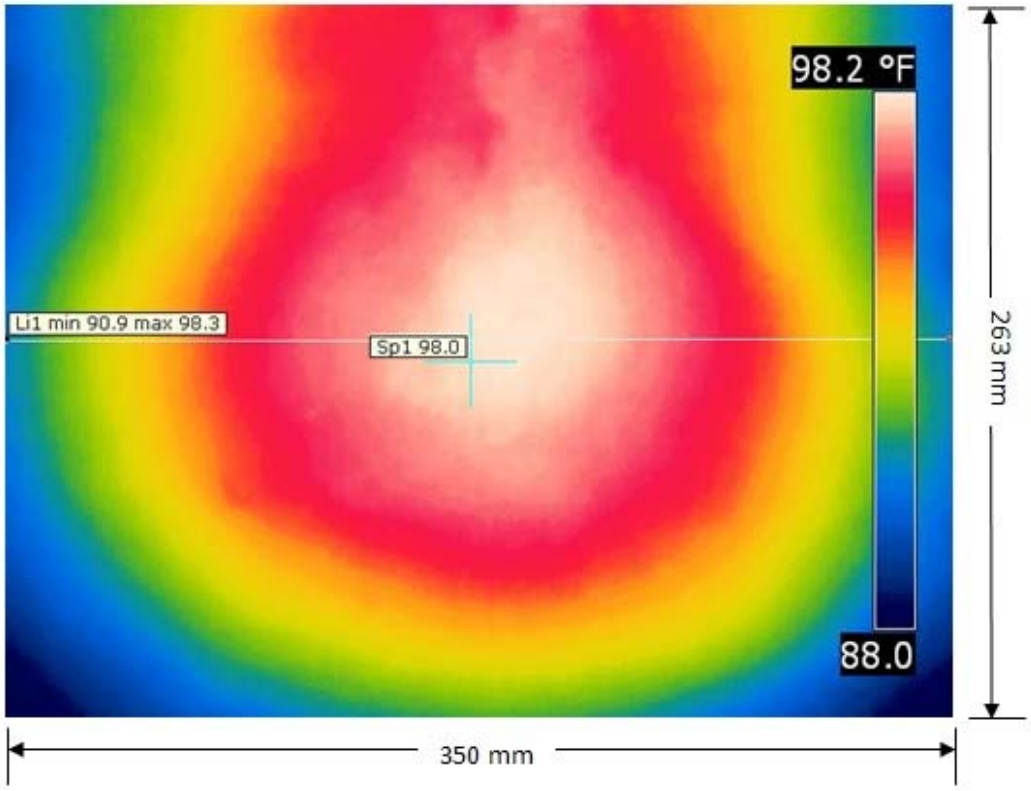

Figure 2.40. Thermal image for hardened MN2 (1 min after removal of heat source)

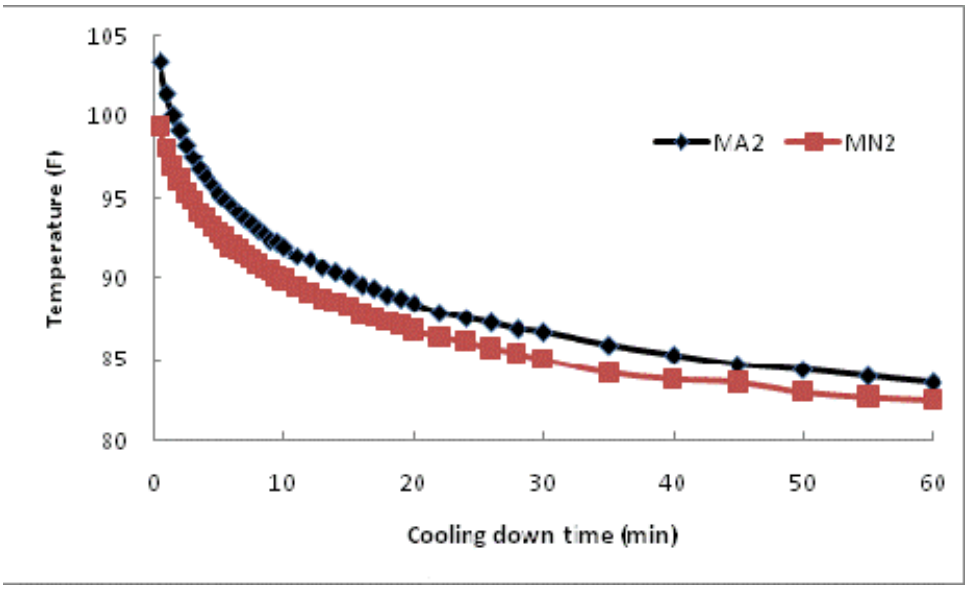

Figure 2.41. Slab surface cooldown at spot 1 for hardened mortar with and without air entrainment

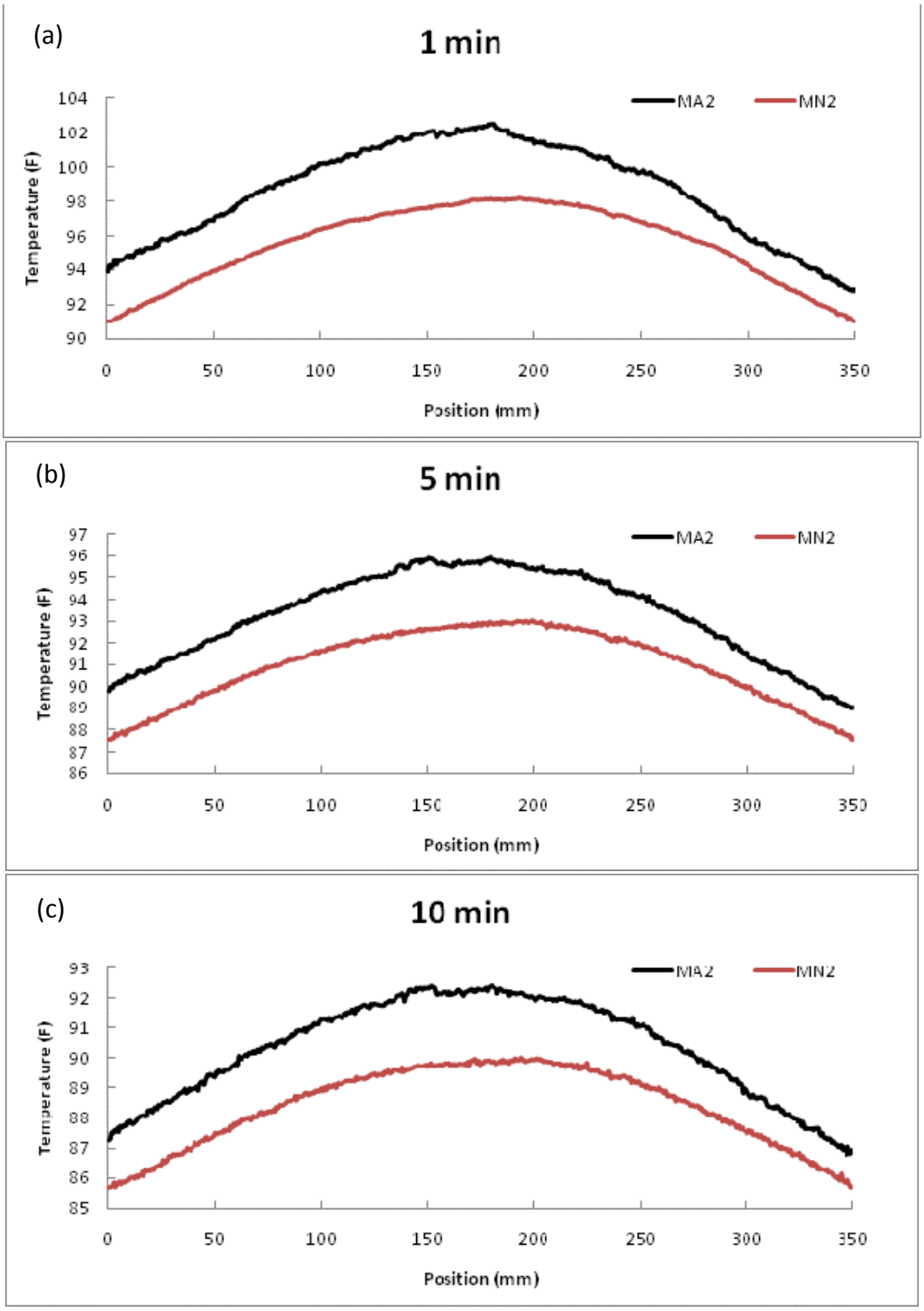

Figure 2.42. Spatial thermal gradient along line 1 for hardened MA2 and MN2 concrete after heat source was removed for (a) 1 min, (b) 5 min, (c) 10 min, (d) 30 min, (e) 60 min

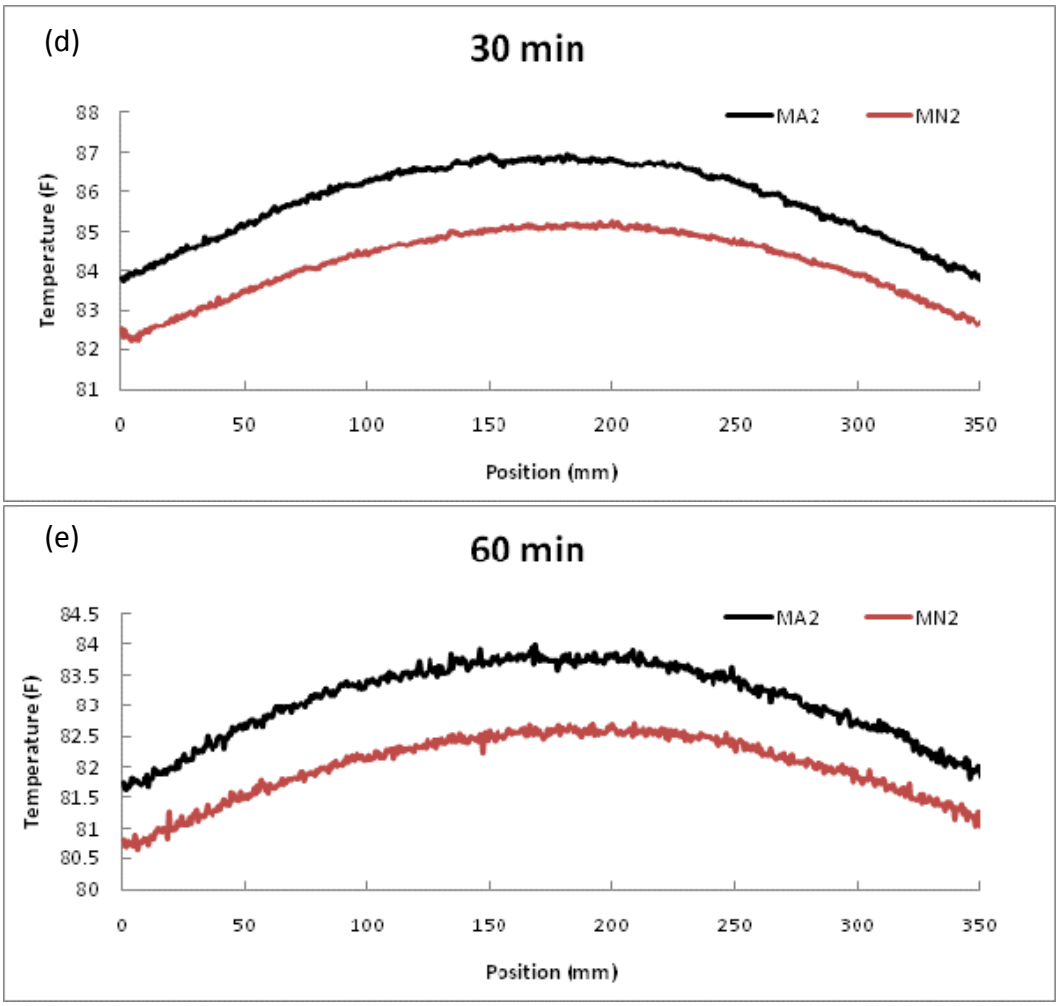

Figure 2.42 (continued). Spatial thermal gradient along line 1 for hardened MA2 and MN2 concrete after heat source was removed for (a) 1 min, (b) 5 min, (c) 10 min, (d) 30 min, (e) 60 min

2.4.5.1 Additional Observations

It is conceivable that thermal imaging could be used to characterize the air void system in fresh concrete without an external heat source based on the exothermal hydration reaction. Figure 2.43 shows the temperature increase associated with the heat of hydration for the first 10 hours after placement. Temperatures were measured by thermocouples located in the center and on the surface of the slab. There is a thermal spike on the concrete surface of 10-20 °F between 2-3 hr that could potentially be useful for thermal imaging.

It was earlier stated that thermal imaging is an excellent method for detecting defects. This is demonstrated in Figure 2.44, which shows thermal images of a concrete slab. Within this slab a spherical air void (~30 mm diameter) was located 12 mm below the top surface. The first image (Fig. 2.44a) was taken during the fresh state without an external heat source. The second image (Fig. 2.44b) was taken during the cool-down process after heating the surface for 30 min with a halogen lamp. In both images, the air void is clearly visible, suggesting that thermography could be used to identify entrapped air voids near the surface of a freshly placed slab.

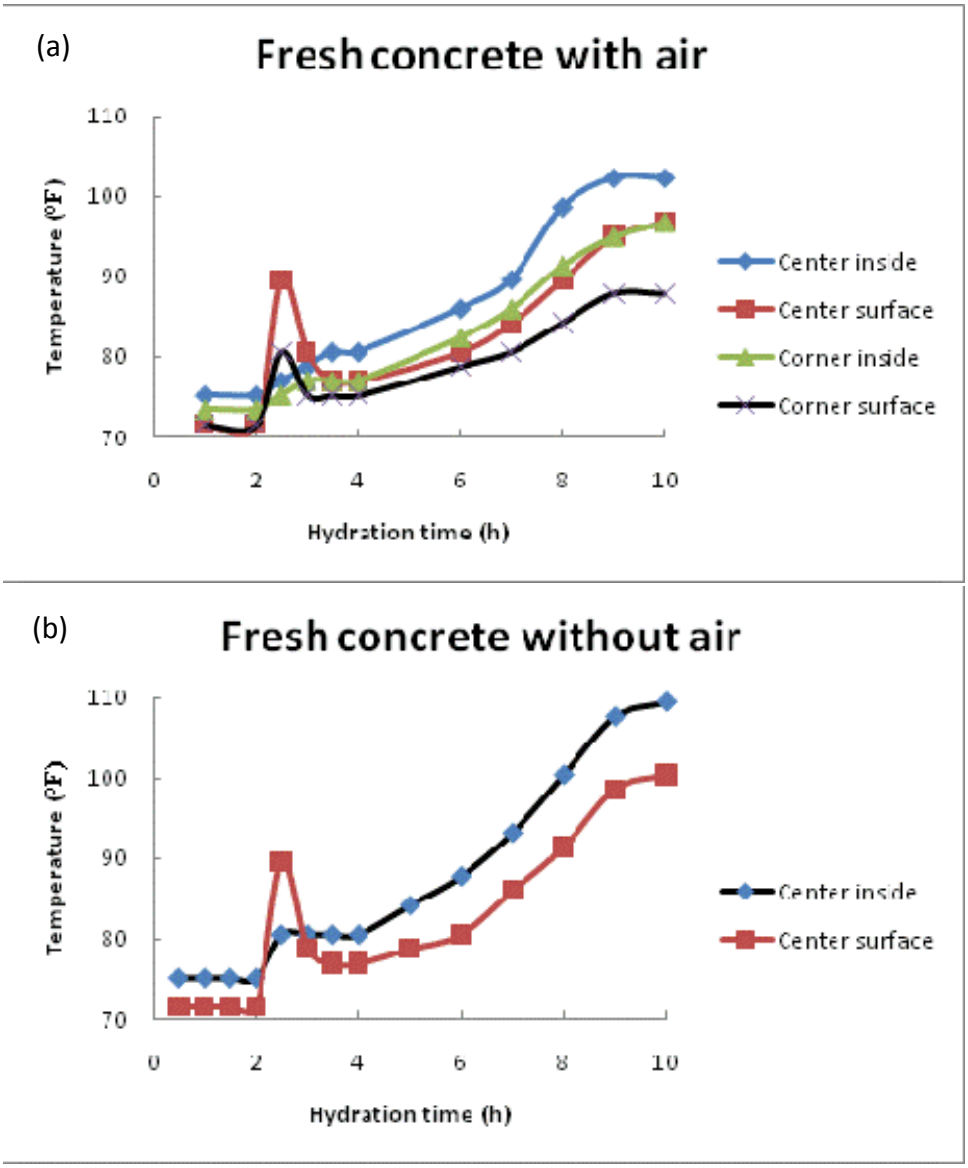

Figure 2.43. Heat of hydration measured by thermocouples for (a) NA2 and (b) NN2 concrete

(a)

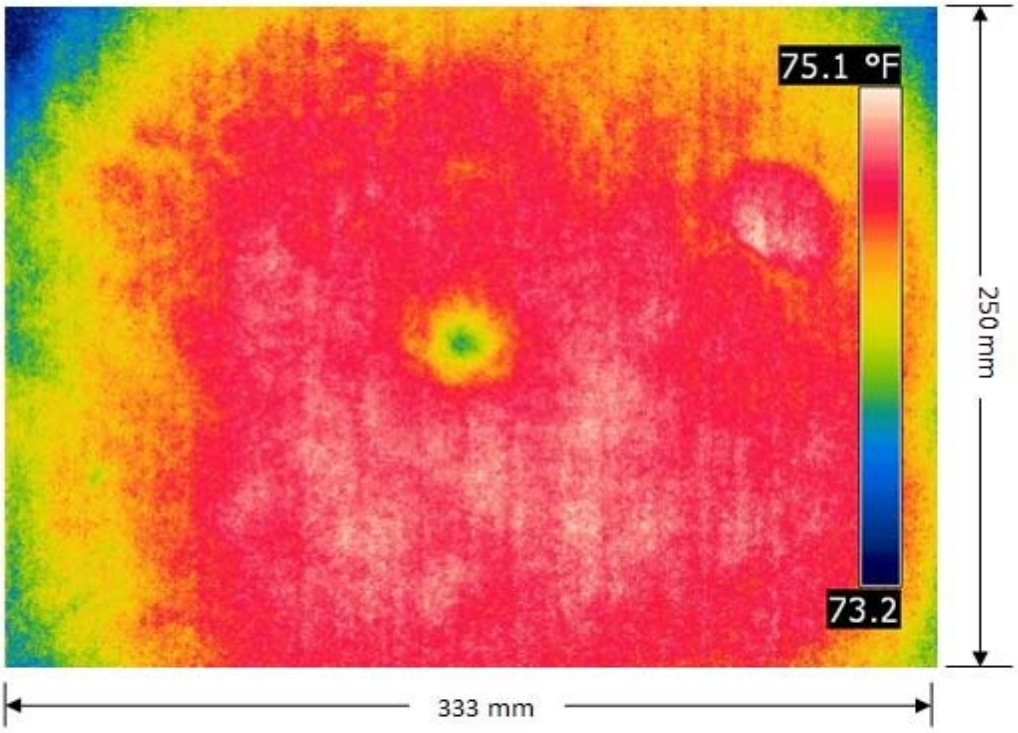

(b)

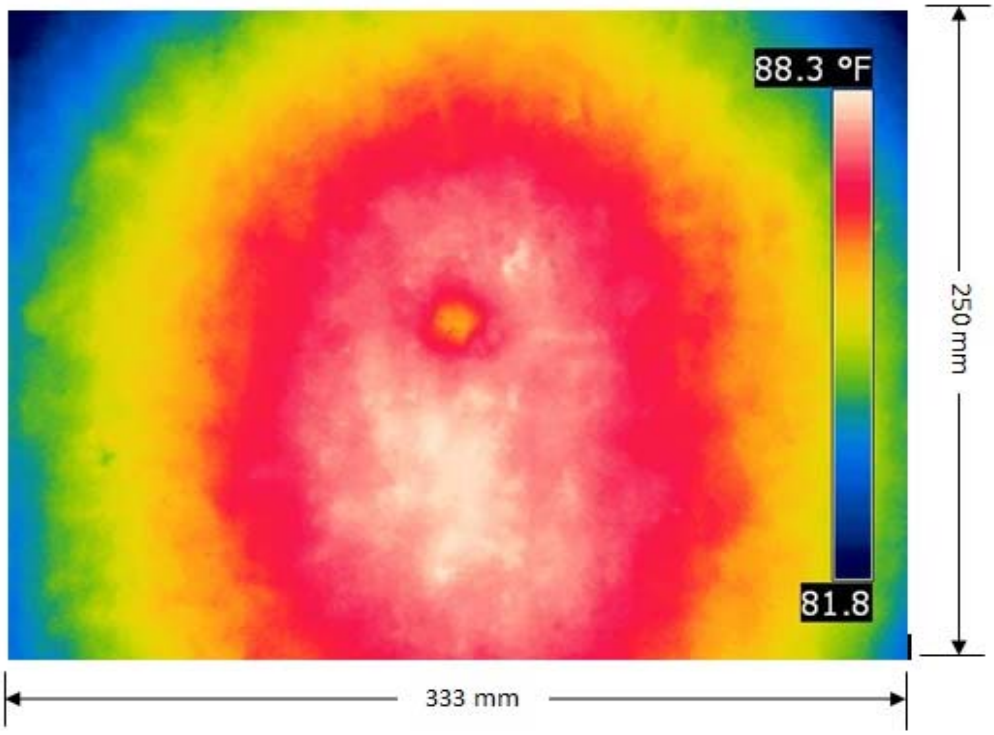

Figure 2.44. Thermal images of subsurface air void, (a) under ambient conditions and no external heat source, (b) 1 min after removal of external heat source

2.4.6 Finite Element Simulations: Numerical Results and Analysis

Finite element simulations of heat conduction in concrete were conducted in order to help delineate the potential benefits of thermography for characterization of the air void system in fresh concrete. A number of concrete representative volume elements (RVE) were created based on porosity variations. Use of an RVE enables reasonable run times for models containing air voids, rather than having to smear out the effects of the voids by using a homogeneous model. The RVEs are described below.

RVE1: 2-mm cube of concrete with no air voids, used for comparison to concrete with air voids

RVE2: 0.4-mm cube of concrete with 10 percent air content, ten 0.1-mm spherical air voids

RVE3: 2-mm cube of concrete with 10 percent air content, the air void size distribution is: one 1 mm, eighteen 0.3 mm, six 0.2 mm, and twenty-four 0.1 mm

RVE4: same as RVE3 except the locations of the air voids are different

The air voids are somewhat randomly located within all RVEs and all voids are fully contained within the RVE. Sections through the RVEs containing air voids are shown in Figure 2.45. The thermomechanical properties input to the analysis are: density 2400 kg/m^3, modulus of elasticity 41000 MPa, Poisson ratio 0.21, coefficient of thermal expansion 10x10^{-6} °C^{-1}, specific heat capacity 0.75 kJ[kg °C]$^{-1}$, and thermal conductivity 0.29 W[m °C]$^{-1}$. The ABAQUS/Standard general-purpose, finite-element code was employed with DC3D10 10-node quadratic heat transfer tetrahedron elements to accommodate the irregular geometry surrounding the air voids. The finite element mesh is shown in Figure 2.46. Two different types of thermal loading were applied.

(1) The heat of hydration (an exothermic reaction) is represented by an internal body heat source (25 W m^{-3}) acting in the z-direction. The boundary conditions are that the RVE faces normal to the x- and y-directions are at a constant temperature (0 °C) in order to make the RVE compatible with the surrounding concrete and to demonstrate heat flow in the z-direction. Only RVE1 and RVE3 are analyzed for this loading condition. The largest element edge is 0.1 mm for these models.

(2) An external heat source (heat lamp) is represented by a surface heat flux applied to the center of the positive y-face of the RVE. The thermally loaded surface area is 1 mm x 1 mm square. The transient 900 W m^{-2} heat flux is applied for 40 minutes and then removed, at which time a convection boundary condition is applied to the entire positive y-face surface for 60 minutes. The convection coefficient is 50 W [m^2 °C]$^{-1}$. An initial temperature of 18 °C is prescribed on all four faces having normals in the x- and z-directions. The boundary condition on all faces of the RVE except the positive y-face is a heat flux of -5 W m^{-2} in order to maintain compatibility with the surrounding concrete. The concrete surface temperature is output as a

function of time at the midpoint of the surface on which the heat was applied. Additionally, the surface temperature is output during cooldown along a line on the surface that was heated.

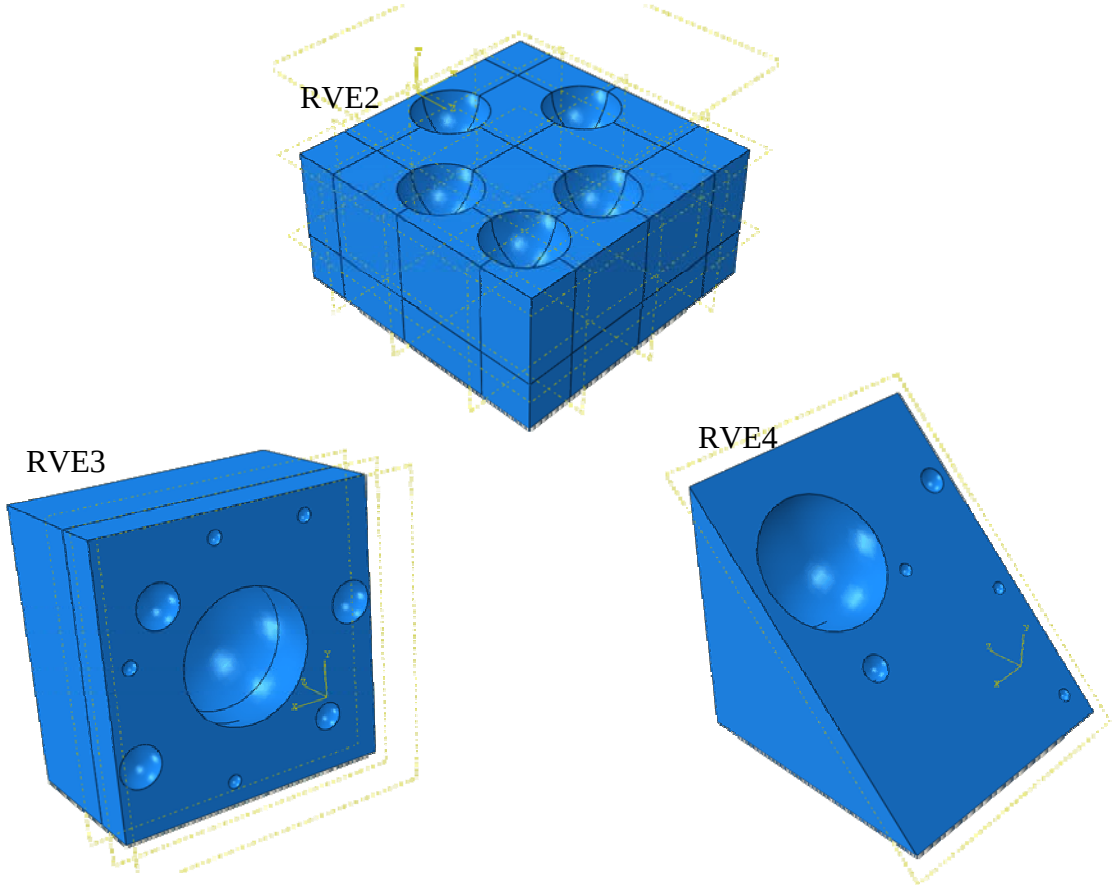

Figure 2.45. Porous concrete RVEs for finite element

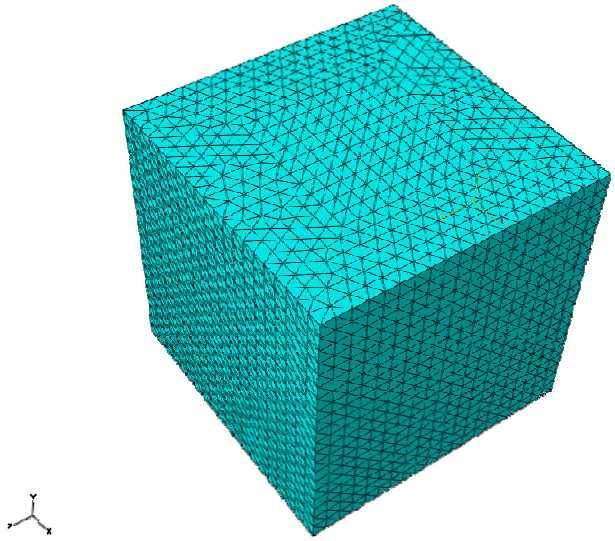

Figure 2.46. Finite element mesh with tetrahedron

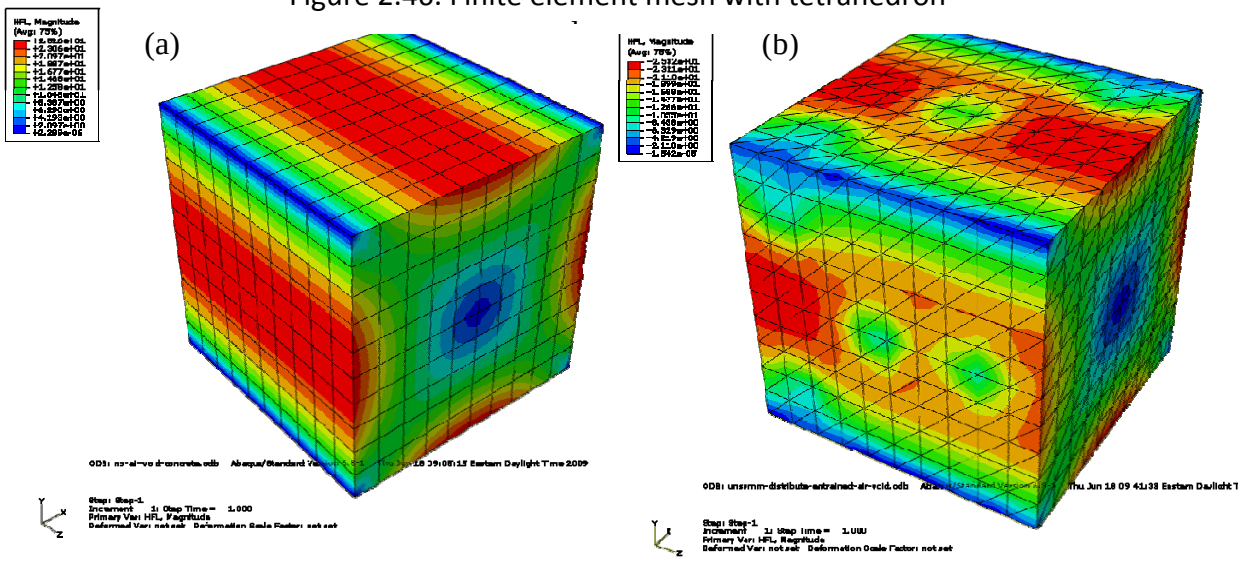

Figure 2.47. Thermal loading case 1 heat flux magnitude contours for (a) concrete RVE with no air voids, (b) concrete RVE with 10% air voids

2.4.6.1. Finite Element Simulation Results

Thermal Loading Case 1:

The purpose of this simulation is to investigate the potential of using the heat of hydration to thermally load fresh concrete in order to thermographically image the effects of the air void system. A comparison of concrete with no air voids and concrete with 10 percent air voids

(RVE2) is shown in Figure 2.47, where contours of the heat flux magnitude are shown on the surface of the RVE. The analogous results for RVE3 are shown in Figure 2.48, where a section through the RVE is also shown. Clearly the void structure affects the heat generation. However, with this simplified model and the boundary conditions applied in this case, it is difficult to ascertain whether there are sufficient thermal fluctuations on the surface to use thermographic imaging based on the heat of hydration.

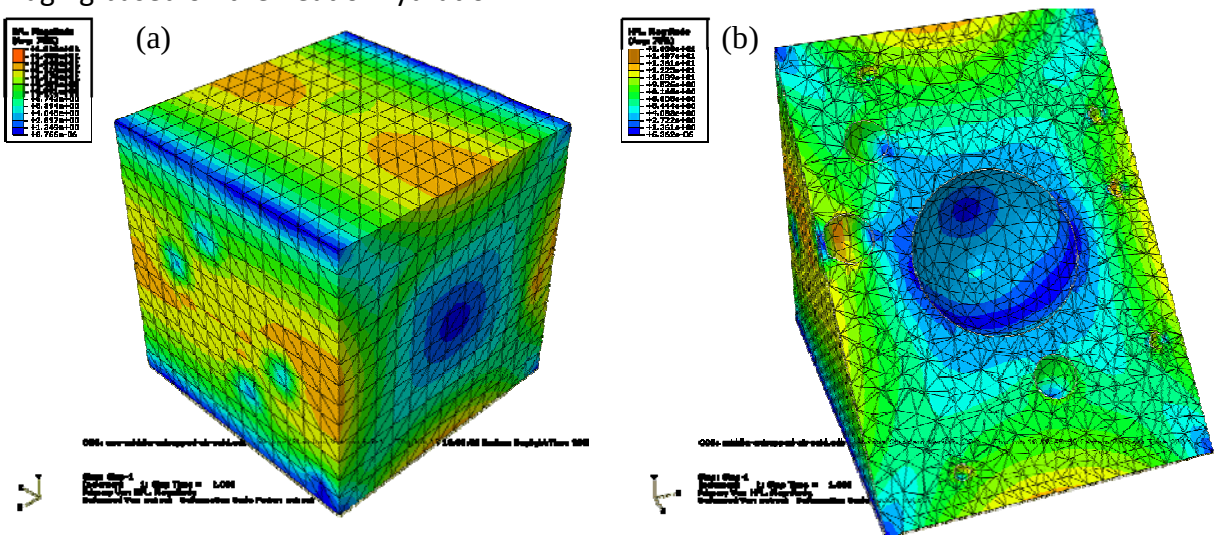

Figure 2.48. Thermal loading case 1 heat flux magnitude contours for RVE3, (a) on RVE surface, and (b) on diagonal section cut through RVE

Thermal Loading Case 2:

Thermal loading is applied to the center of the RVE's top surface for 40 minutes and then the heat flow (heat flux and temperature) is monitored for 60 minutes after that to replicate the laboratory experiment. Of course, both the RVE and the heated zone are significantly smaller than what was done in the laboratory. Figures 2.49 through 2.54 present comparisons of concrete with air voids (RVE1) and without air voids (RVE4) for heat flux (HFL) and temperature (NT11) for 0.5, 1, 5, 30, and 60 minutes after the heat source was removed. The surface of the concrete with no air voids cools more rapidly than concrete with air voids. In addition, there is significantly more fluctuation in both the surface temperature and the heat flux for concrete with air voids. The cooldown of the surface midpoint is shown in Figure 2.55 for concrete with and without air voids. Again, concrete without air voids is seen to be a better heat conductor. The thermal gradient along a line across the center of the RVE surface is shown in Figure 2.56 for both types of concrete (RVE1 and RVE4).

These finite-element simulations indicate that thermal imaging has good potential for air void characterization in fresh concrete. It is likely that flash thermography will be more effective.

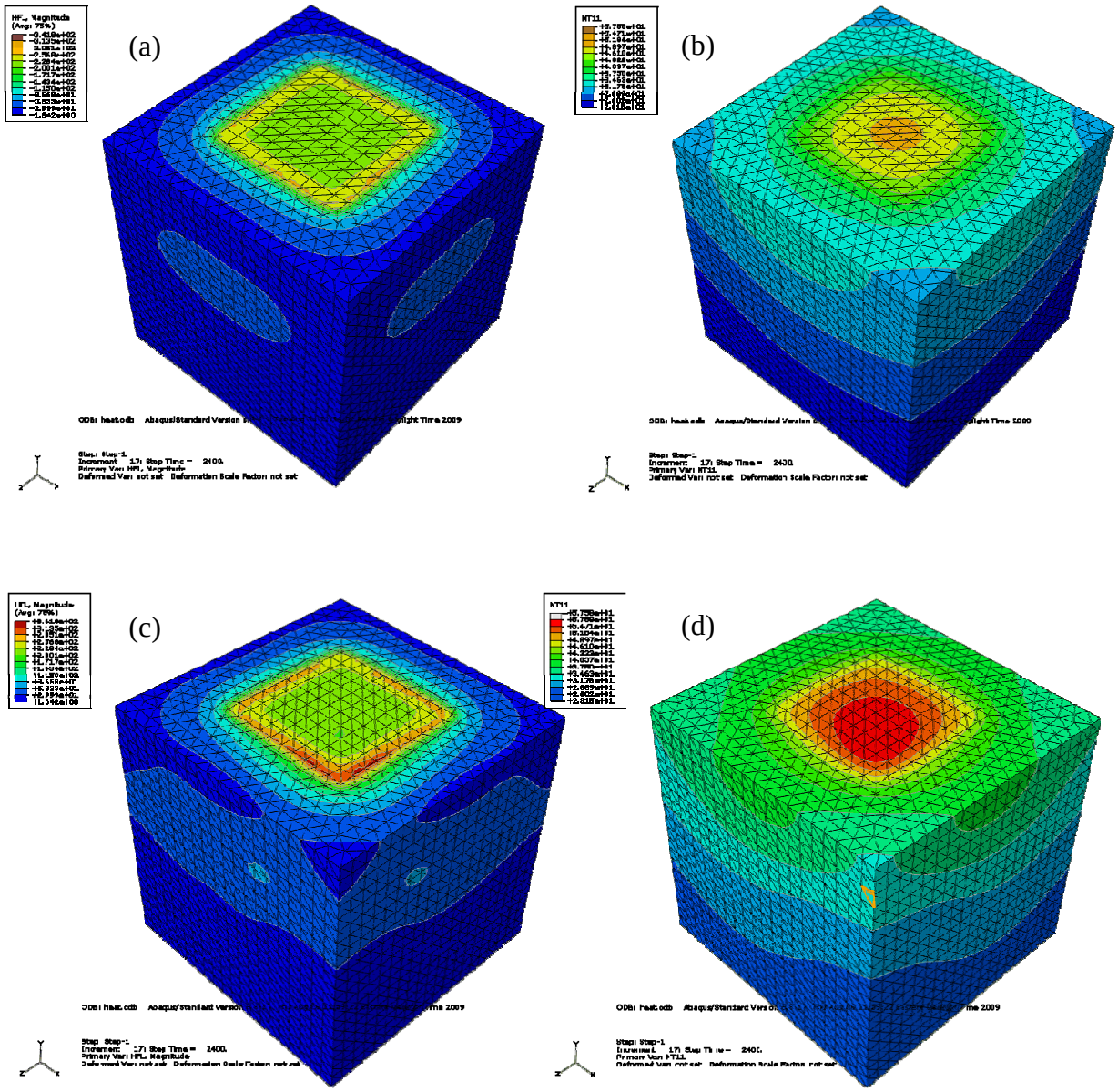

Figure 2.49. Thermal loading for 40 min followed by cooldown. After 0.5 min; concrete with no air voids, (a) heat flux and (b) temperature; concrete with air voids - RVE4 (c) heat flux and (d) temperature

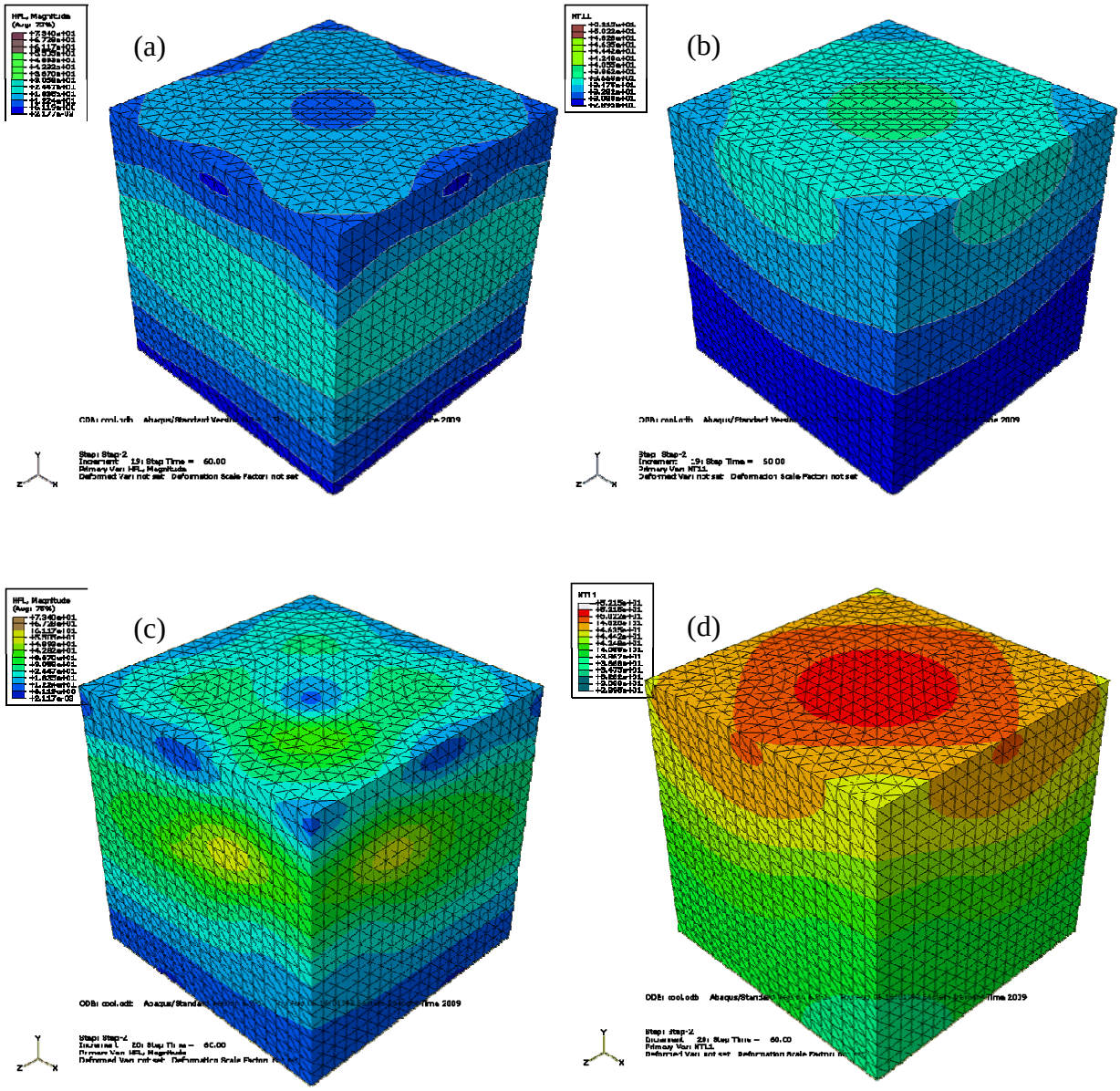

Figure 2.50. Thermal loading for 40 min followed by cooldown. After 1 min; concrete with no air voids, (a) heat flux and (b) temperature; concrete with air voids - RVE4 (c) heat flux and (d) temperature

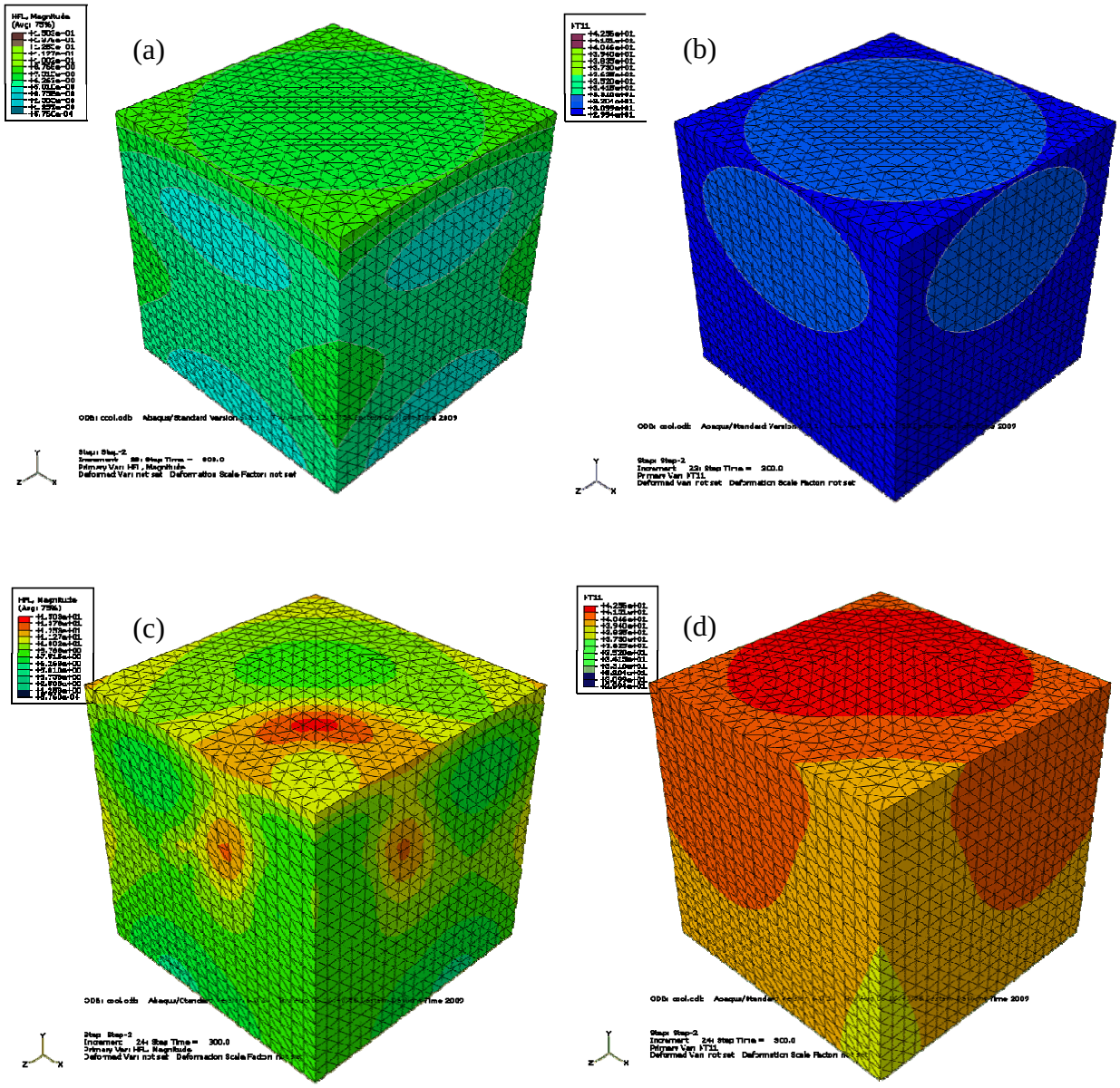

Figure 2.51. Thermal loading for 40 min followed by cooldown after 5 min; concrete with no air voids, (a) heat flux and (b) temperature; concrete with air voids - RVE4 (c) heat flux and (d) temperature

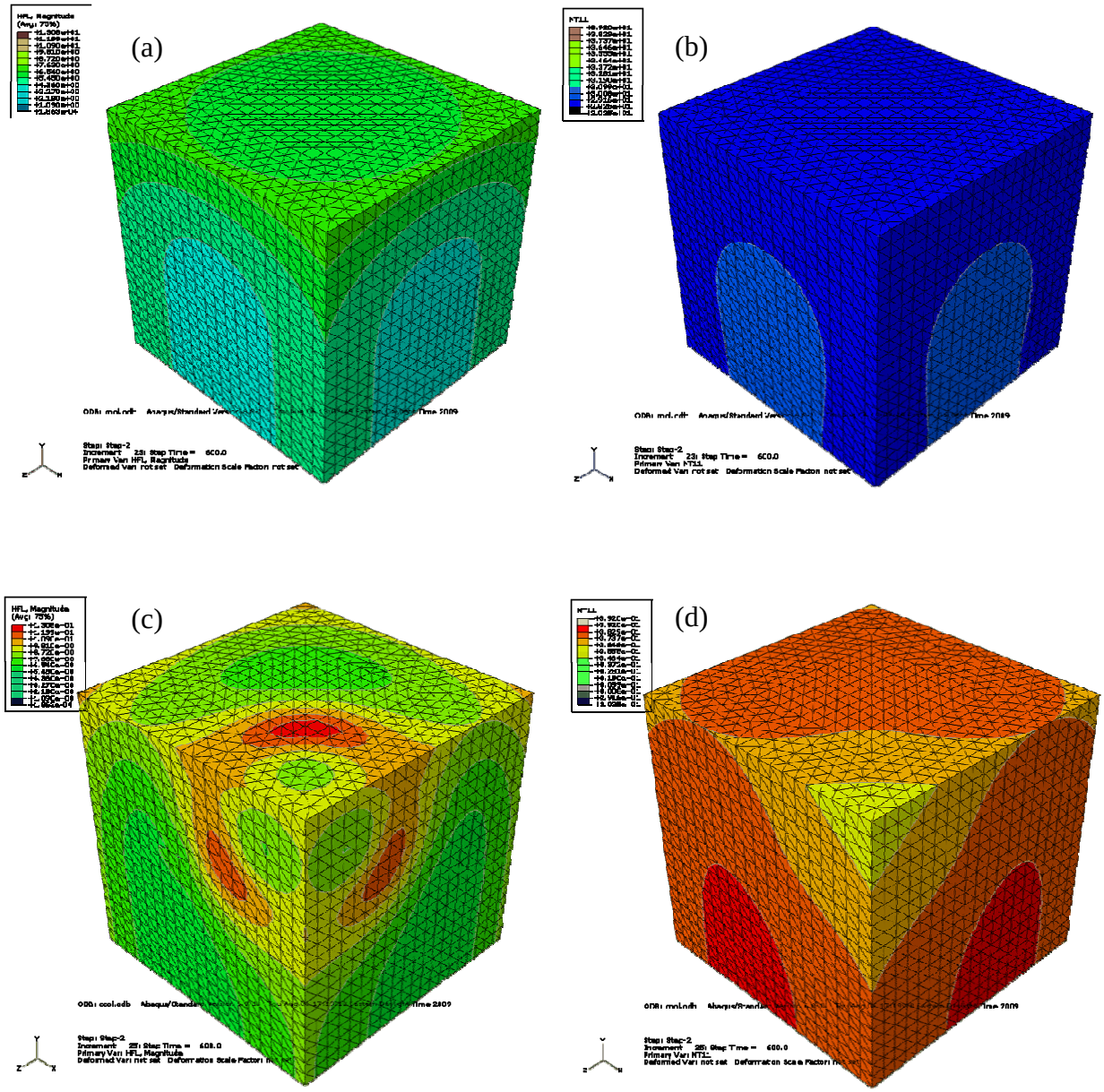

Figure 2.52. Thermal loading for 40 min followed by cooldown after 10 min; concrete with no air voids, (a) heat flux and (b) temperature; concrete with air voids - RVE4 (c) heat flux and (d) temperature

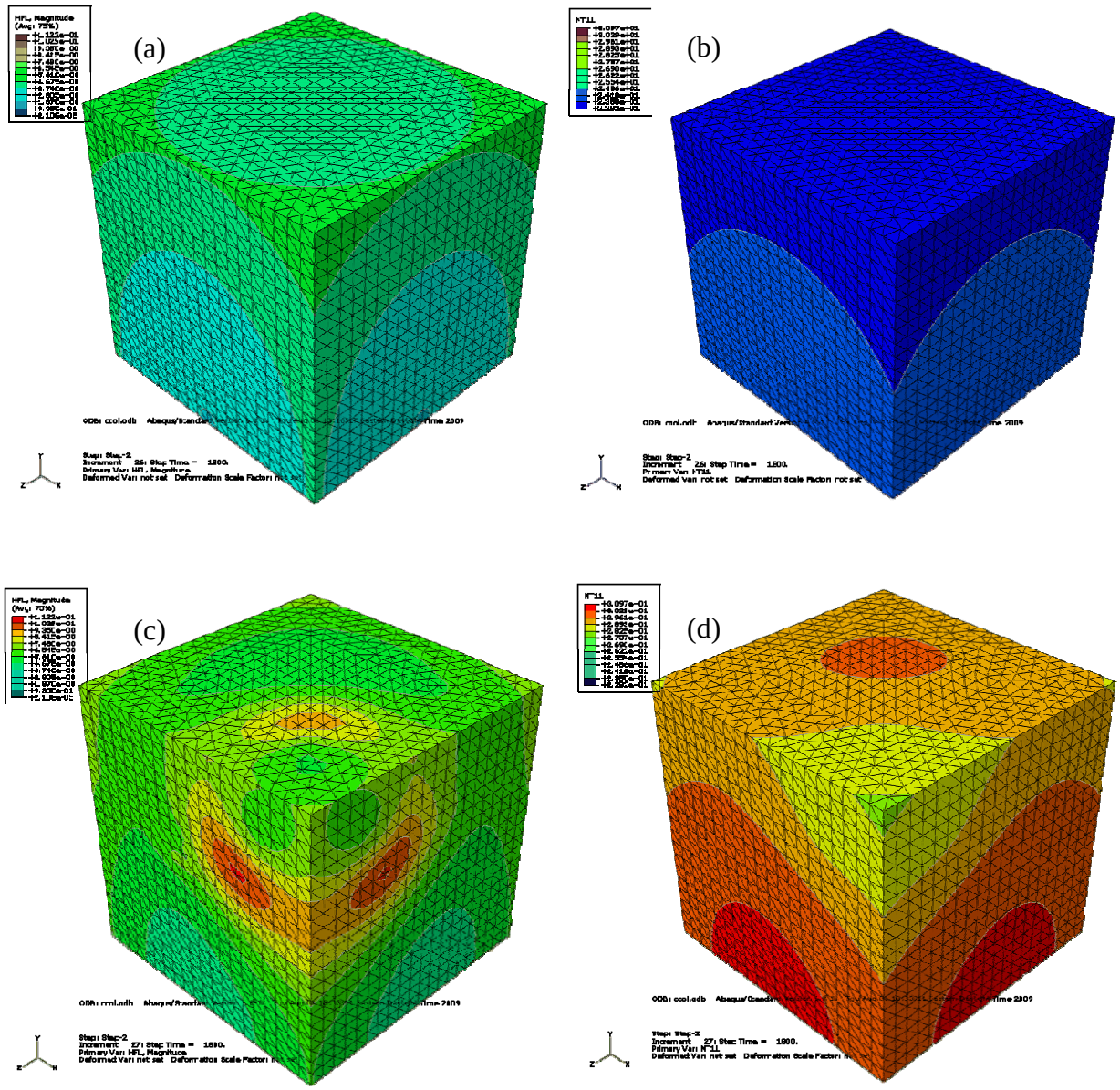

Figure 2.53. Thermal loading for 40 min followed by cooldown after 30 min; concrete with no air voids, (a) heat flux and (b) temperature; concrete with air voids - RVE4 (c) heat flux and (d) temperature

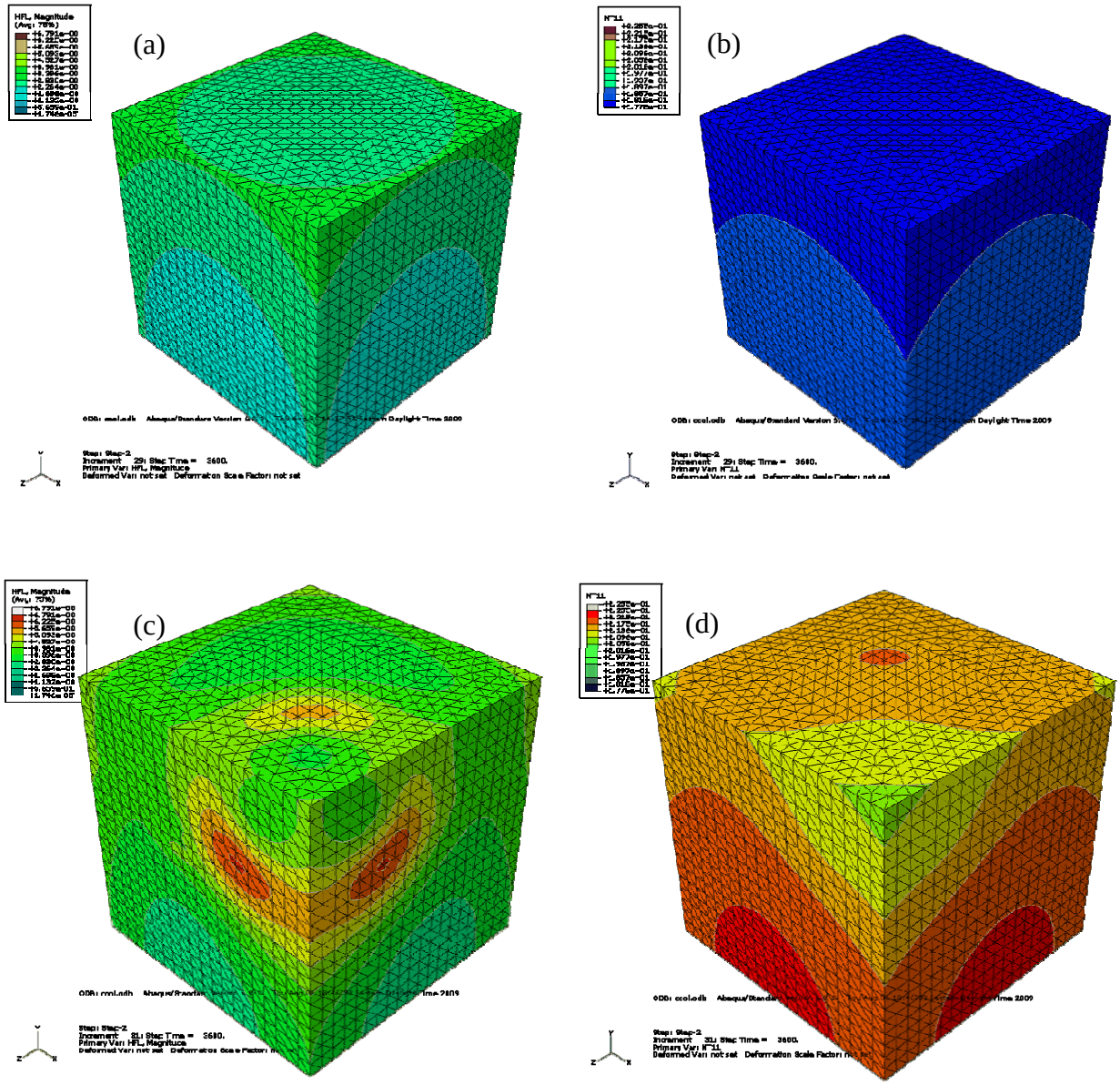

Figure 2.54. Thermal loading for 40 min followed by cooldown after 60 min; concrete with no air voids, (a) heat flux and (b) temperature; concrete with air voids - RVE4 (c) heat flux and (d) temperature

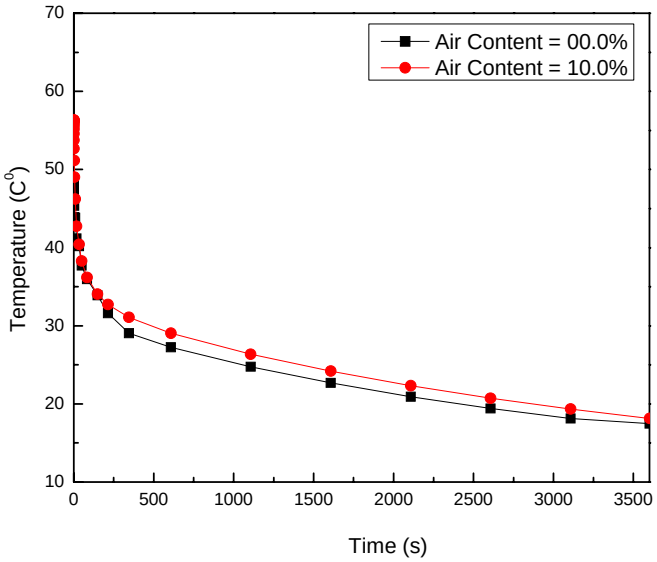

Figure 2.55. Cool down of RVE surface midpoint for first hour after removing the heat source

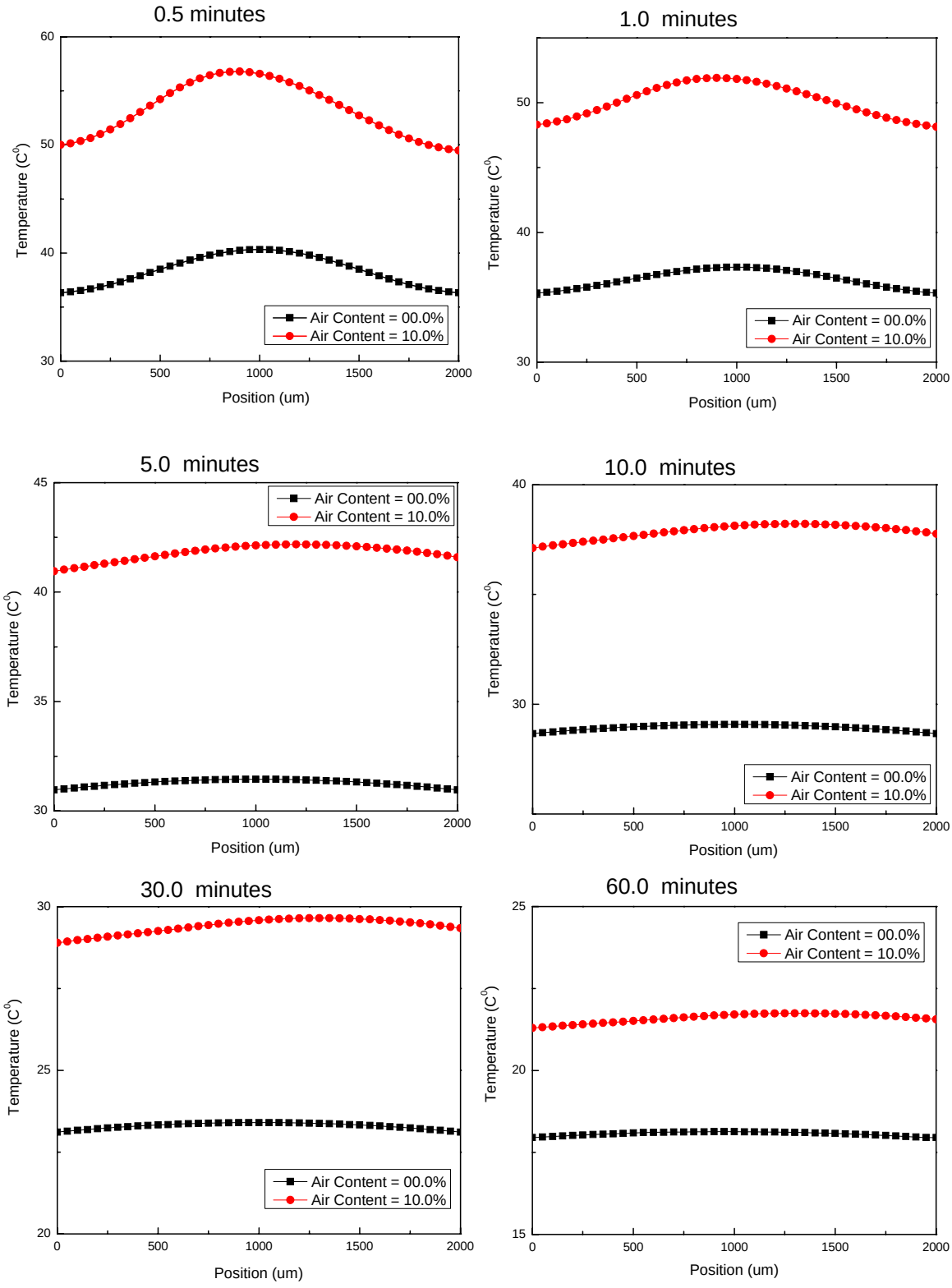

Figure 2.56. Thermal gradients along the midlength of the surface for concrete without air voids and with air voids 0.5, 1, 5, 10, 30, and 60 min after removing the heat source

2.4.7 Discussion

The results presented in this section indicate that thermography can be used to identify thermal field features that have a significant difference in concrete with and without air entrainment. This important observation was confirmed for both the fresh and hardened states. Data were collected as early as 2 hr after concrete placement. Surface temperature data, acquired by an infrared camera for concrete with and without air entrainment, showed that cooldown measurements over time at a single point are insufficient for air void system characterization. However, when spatial thermal gradients are determined on the concrete surface, it is found that there is an observable difference, which appears to be attributable to the air void system. The temperature gradient along a straight line on the concrete surface was found to be as follows:

Normal concrete mix with air entrainment (NA2) 5 min after removing the heat source,

$$T(x) = 0.0633\,x - 0.000180\,x^2$$ (T in degrees F and x in mm)

Normal concrete mix without air entrainment (NN2) 5 min after removing the heat source,

$$T(x) = 0.0532\,x - 0.000147\,x^2$$ (T in degrees F and x in mm)

The results of finite-element simulations clearly show that these features are dependent on the rates of heat transfer at the concrete surface, which can be strongly affected by the air void structure. The thermography test setup used in this study is fairly portable and therefore suitable for use in field applications. Additional experimental observations indicate that large-size air voids located near the surface of concrete are clearly visible in the infrared image by using the hydration heat of fresh concrete as the only heat source.

3. SUMMARY AND CONCLUSIONS

The objective of this project was to evaluate current technologies that have the capability of characterizing the air void system in concrete within the first several hours of placement. This objective was met by developing a comprehensive technology assessment and literature review, and conducting a laboratory evaluation of two selected technologies: ultrasound and thermography. Experimental results showed that both technologies can capture physical features that are significantly affected by the air void system in concrete.

3.1 Summary of Literature Review

The literature review assessed eight technologies that are currently used to characterize air voids in concrete or that have the potential of characterizing the air void system in concrete. For each technology, its capabilities and limitations for use in fresh concrete (defined as concrete within the first 24 hours of placement) and hardened, as well as field application were determined.

Two technologies currently under development were found to be well suited for field applications: ultrasound and thermography.

Nondestructive ultrasound techniques are currently being used to characterize the air void structure of fresh cement paste. A qualitative study in fresh mortar conducted by Aggelis and Philippidis (2004) indicated promising results. Two research groups (at Georgia Tech and Northwestern Universities) are currently conducting experiments using different ultrasonic features to evaluate specific properties of the cement paste. These efforts are still in progress. The literature review found that more progress has been made on the characterization of hardened cement paste using ultrasonic techniques. Work done by Biwa (2001) and Punurai et al. (2007) indicated that the attenuation results can be used to predict the entrained air void size and content and the volume fraction of the cement paste.

Thermography uses heat transfer and infrared imaging science to detect defects in structures. In concrete structures, it has been successfully used to characterize shallow voids or surface cracks. Two sources of heat are used: impulse and flash. Researchers have found that impulse-thermography is suitable for detecting shallow voids (Maihofer et al., 2003); however, the resolution of the camera may limit the maximum size of void that can be detected. Flash thermography could give a better resolution. Sham et al. (2008) were able to detect surface concrete cracks of 0.1 to 0.5 mm width using flash thermography. It could be envisioned that detection of shallow voids in hardened concrete is within the capabilities of this technology. In order to be implemented in fresh concrete, development of a correlation between surface radiation and air void system parameters needs to be established.

3.2 Summary of Laboratory Evaluation

The laboratory evaluation of two selected technologies - ultrasound and thermography - was based on experiments aimed at demonstrating the feasibility of ultrasound and thermography technologies to characterize the air void system of fresh concrete, with an eye toward field implementation.

Two different concrete mixtures were used in the laboratory evaluation: with and without entrained air. These concrete mixtures were characterized in the fresh and hardened state. Obtained characteristics include total air content using pressure air tests and workability using slump tests. Hardened concrete properties such as compression strength at 3, 7, and 28 days were obtained, as well as air void parameters (paste content, air content, specific surface and spacing factor) determined using a linear transverse analysis. Concrete slabs were used for ultrasound and thermography tests. Laboratory tests were obtained from both small (2-ft-square and 6-in-thick) and large (6-ft-square and 6-in-thick) slabs. Measurements were taken using ultrasound and thermography equipment within the first 24 hours after concrete placement.

The ultrasound tests involved transmitting and receiving Rayleigh surface waves with piezoelectric transducers, Plexiglas wedges and steel mediators. The wedges and mediators were fabricated specifically for this project. The test setup enables determination of Rayleigh wave speed (dependent upon elastic properties), attenuation (dependent on wave scattering and material damping), and whether there are gradients in elastic properties near the concrete surface. Results show that ultrasound is able to penetrate fresh concrete as early as 4 hr after placement and that the Rayleigh wave speed is significantly influenced by the air void system. Attenuation measurements had too much scatter to be useful. The scatter is believed to be due to variable contact pressure between the mediator and the concrete surface from test to test. A spring-loaded mounting fixture is expected to correct this. The key result is that the Rayleigh wave speeds in normal concrete mix with air entrainment (NA2) and in normal concrete mix without air entrainment (NN2) are 1017 and 1213 m/s, respectively, 5 hours after placement. The difference of 16 percent is large enough to give Rayleigh waves strong potential to characterize the air void system in addition to quantifying the air content. Some (inexpensive) adjustments to the laboratory equipment should enable much improved attenuation measurements.

Surface temperature data, acquired by an infrared camera, for concrete with and without air entrainment, showed that cooldown measurements over time at a single point are insufficient for air void system characterization. However, when spatial thermal gradients are determined on the concrete surface, it is found that there is an observable difference, which appears to be attributable to the air void system. The key result is a comparison of the temperature gradient along a straight line on the concrete surface:

Normal concrete mix with air entrainment (NA2) 5 min after removing the heat source,

$T(x) = 0.0633\ x - 0.000180\ x^2$ (T in degrees F and x in mm)

Normal concrete mix without air entrainment (NN2) 5 min after removing the heat source,

$$T(x) = 0.0532\,x - 0.000147\,x^2$$ (T in degrees F and x in mm)

These temperature profiles were obtained during cooldown after localized surface heating with a lamp. The coefficients have been regressed to a quadratic polynomial and appear to depend on the air void system. It is envisioned that thermal imaging could be used to characterize the air void system in fresh concrete without an external heat source based on the exothermal hydration reaction. Finite-element simulations conducted in this study clearly show that the air void structure affects the heat conduction.

3.3 Conclusions

The ultrasound tests were able to show that the Rayleigh wave speed is influenced by the air void system in fresh concrete. A significant difference was found on the measured Rayleigh wave speeds for concrete with and without entrained air. These measurements were made as early as 4 hr after concrete placement; thus, they reflect properties of the fresh concrete state. The equipment used is portable and therefore can be implemented in field evaluations.

Thermography tests were able to effectively recognize concrete with and without entrained air by comparing measured spatial thermal gradients. These differences were consistent both at the fresh and hardened state and indicate a possible correlation with the air void system. Finite element simulations confirmed that the concrete air void structure affects the heat conduction. Experimental measurements were successfully taken as early as 2 hr after concrete placement but could be taken immediately, proving that fresh concrete can be characterized. In addition, the portable features of the equipment used are suitable for field applications.

4. REFERENCES

AASHTO (2002). “An apparatus that measures the air-void characteristics of fresh concrete.” <http://www.transportation.org> (September, 2008).

Aggelis, D. G., and Philippidis, T. P. (2004). “Ultrasonic wave dispersion and attenuation in fresh mortar.” *NDT and E International*, 37(8), 617-631.

Ansari, F. (1990). “New method for assessment of air voids in plastic concrete.” *Cement and Concrete Research*, 20(6), 901-909.

Ansari, F. (1994). “Fiber-Optic Air Meter.” Strategic Highway Research Program, National Research Council, Washington, DC.

ASTM C39 (2005). “Standard Test Method for Compressive Strength of Cylindrical Concrete Specimens.” American Society for Testing and Materials, West Conshohocken, Pennsylvania.

ASTM C143 (2008). “Standard Test Method for Slump of Hydraulic Cement Concrete.” American Society for Testing and Materials, West Conshohocken, Pennsylvania.

ASTM C138 (2008). “Standard Test Method for Unit Weight, Yield, and Air Content (Gravimetric) of Concrete.” American Society for Testing and Materials, West Conshohocken, Pennsylvania.

ASTM C173 (2008). “Standard Test Method for Air Content of Freshly Mixed Concrete by the Volumetric Method.” American Society for Testing and Materials, West Conshohocken, Pennsylvania.

ASTM C231 (2008). “Standard Test Method for Air Content of Freshly Mixed Concrete by the Pressure Method.” American Society for Testing and Materials, West Conshohocken, Pennsylvania.

ASTM C457 (2008). “Standard Test Method for Microscopical Determination of Parameters of the Air void System in Hardened Concrete.” American Society for Testing and Materials, West Conshohocken, Pennsylvania.

Biwa, S. (2001). “Independent scattering and wave attenuation in viscoelastic composites.” *Mech. Mater.*, 33(11), 635–647.

Carlson, J., Sutter, L., Van Dam, T., and Peterson, K. R. (2006). “Comparison between flatbed scanner and RapidAir 457 System Parameters of Hardened Concrete.” *Transportation Research Record*, 1979, 54-59.

Catexol 1000N Specification Sheet (2009), Axim Italcementi Group, Middlebranch, Ohio, USA.

Catexol AE260 Specification Sheet (2009), Axim Italcementi Group, Middlebranch, Ohio, USA.

Clark, M.R, McCann, D. M., and Forde, M. C. (2003). "Application of infrared thermography to the non-destructive testing of concrete and masonry bridges." *NDT&E International*, 36(4), 265–275.

Corr, D. J., Juenger, M. C. G., Monteiro, P. J. M., and Bastacky, J. (2004). "Investigating Entrained Air Voids and Portland Cement Hydration with Low-temperature Scanning Electron Microscopy." *Cement and Concrete Composites*, 26(8), 1007-1012.

Corr, D. J., Lebourgeois, J., Monteiro, P. J. M., Bastacky, S. J., and Gartner, E. M. (2002). "Air Void Morphology In fresh Cement Pastes." *Cement and Concrete Research*, 32(7), 1025-1031.

Desai, D. H., Tikalsky, P. J., and Scheetz, B. E. (2007). *Hardened Air in Concrete Roadway Pavements and Structures*, Report No. FHWA-PA-2007-002-510401-06, Pennsylvania Transportation Institute, University Park, PA.

Distlehorst, J. A., and Kurgan, G. J. (2007). "Development of Precision Statement for Determining Air Void Characteristics of Fresh Concrete with Use of Air Void Analyzer." *Transportation Research Record* 2020, 45-49.

Elsen, J. (2001). "Automated air void analysis on hardened concrete - Result of a European intercomparison testing program." *Cement and Concrete Research*, 31, 1027-1031.

FLIR P660 Specification Sheet (2008), FLIR Systems Inc., Billarica, MA, USA.

Germann Instruments, Inc. (2008). < http://www.germann.org > (October 7, 2008)

Grove, J., Steffes, R., and Wilk, M. A. (2006). "Using the Air Void Analyzer for Real-Time Quality Control Adjustment in the field." CP Tech Center, Iowa State University, Ames, IA.

Halverson, C., White, D. J., and Gray, J. (2005). "Application of X-Ray CT Scanning to Characterize Geomaterials Used in Transportation Construction." *Proceedings of the 2005 Mid-Continent Transportation Research Symposium*, Ames, Iowa.

Han, X., Lub, J., Islam, S., Lia, W., and Zenga, Z. (2005). "Sonic infrared imaging NDE." *Proceedings of the SPIE*, Bellingham, WA, Vol. 5765.

Hover, K. (2002). "Air in Concrete: How Come and How Much?" *Concrete Construction-World of Concrete*, 47(12), 57-61.

Jakobsen, U. H., Pade, C., Thaulow, N., Brown, D., Sahu, S., Magnusson, O., De Buck, S., and De Schutter, G. (2006). "Automated air void analysis of hardened concrete - a Round Robin study." *Cement and Concrete Research*, 36, 1444-1452.

Kosmatka, S. H., Kerkhoff, B., and Panarese, W. C. (2002). *Design and Control of Concrete Mixtures*. 14th edition, Portland Cement Association, Skokie, Illinois, USA.

Krautkramer, J., and Krautkramer, H. (1990). *Ultrasonic Testing of Materials*. 4th edition, Springer Verlag.

Lane, D. S. (2006). *Laboratory Investigation of Air-Void Systems Produced by Air-Entraining Admixtures in Fresh and Hardened Mortar*. VTRC 06-R27, Project No. 72807, Virginia Transportation Research Council, Virginia Department of Transportation.

Landis, E. N., and Corr, D. J. (2008). "Three Dimentional Analysis of Air Void Systems in Concrete." *Measuring, Monitoring and Modeling Concrete Properties*, 517–524.

Litvan, G. G. (1978). "Freeze-Thaw Durability of Porous Materials," *Durability of Building Materials and Components: Proceedings of the First International Conference*, ASTM STP 691, 455-463.

Maierhofer, C., Brink, A., Rolling, M., and Wiggenhauser, H. (2003). "Detection of shallow voids in concrete structures with impulse thermography and radar." *NDT&E International*, 36, 257–263.

Maierhofer, C., Arndt, R., and Rollig, M. (2007). "Influence of concrete properties on the detection of voids with impulse-thermography." *Infrared Physics & Technology*, 49, 213–217.

Miana, A., Han, X., Islam, S., and Newaz, G. (2004). "Fatigue damage detection in graphite epoxy composites using sonic infrared imaging technique." *Composites Science and Technology*, 64, 657–666.

Mindess, S., Young, J. F., and Darwin, D. (2003). *Concrete*. 2nd edition, Upper Saddle River, NJ: Prentice Hall.

PennDOT Publication 35, Bulletin 15, "Approved Construction Materials" (2009). Commonwealth of Pennsylvania Department of Transportation, Harrisburg, Pennsylvania, USA.

PennDOT Publication 408/PennDOT Specifications (2007). Commonwealth of Pennsylvania Department of Transportation, Harrisburg, Pennsylvania, USA.

Pigeon, M., and Pleau, R. (1995). *Durability of Concrete in Cold Climates*. London: E & FN Spon.

Popovics, S., and Popovics, J. S. (1998). "Ultrasonic testing to determine water-cement ratio for freshly mixed concrete." *Cement, Concrete, and Aggregates* 20:262-268.

Punurai, W. (2006) "Cement-based materials characterization using ultrasonic attenuation." Ph.D. dissertation, Georgia Institute of Technology, Atlanta, GA.

Punurai, W., Jarzynski, J., Qu, J., Kurtis, K. E., and Jacobs, L. J. (2006). “Characterization of entrained air voids in cement paste with scattered ultrasound.” *NDT&E Int*., 39, 514-524.

Punurai, W., Jarzynski, J., Qu, J., Kim, J.-Y., Jacobs, L. J., and Kurtis, K. E. (2007). “Characterization of Multi-scale Porosity in Cement Paste by Advanced Ultrasonic Techniques.” *Cement and Concrete Research*, 37, 38-46.

Rose, J.L. (1999). *Ultrasonic Waves in Solid Media*. Cambridge.

Sham, F. C., Chen, N., and Long, L. (2008). “Surface crack detection by flash thermography on concrete surface.” *Insight: Non-Destructive Testing and Condition Monitoring*, 50(5), 240-243.

Shin, S. W., Yun, C. B., Popovics, J. S., and Kim, J. H. (2007). “Improved Rayleigh wave velocity measurement for nondestructive early-age concrete monitoring.” *Research in Nondestructive Eval*., 18, 45-68.

Simon, M. J. (2005). *An Interlaboratory Evaluation of Variability in the ASTM C 457 Linear Traverse Method*. RI 98-006B, Missouri Department of Transportation, Federal Highway Administration.

Sutter, L. L. (2007). *Evaluation of Methods for Characterizing Air Void Systems in Wisconsin Paving Concrete*. WisDOT SPR# 0092-03-16, WHRP 07-05, Michigan Technological University, Wisconsin Department of Transportation, Federal Highway Administration.

Thomas, M. (2002). “A New Vision for Air Void Analysis.” *Concrete Technology Today*, 23(1), 6.

Zalocha, D., and Kasperkiewicz, J. (2005). “Estimation of the Structure of Air Entrained Concrete Using a Flatbed Scanner.” *Cement and Concrete Research*, 35(10), 2041-2046.

Zhang, S., and Wang, K. (2005) "Effects of Materials and Mixing Procedures on Air Void Characteristics of Fresh Concrete." *Proceedings of the 2005 Mid-Continent Transportation Research Symposium*, Ames, Iowa.